

Received 25 July 2025, accepted 9 August 2025, date of publication 14 August 2025, date of current version 21 August 2025.

Digital Object Identifier 10.1109/ACCESS.2025.3599112



Planar Microwave Sensors: State of the Art and Applications

CARLOS G. JUAN[®]¹, (Senior Member, IEEE), KATIA GRENIER[®]², (Senior Member, IEEE), MOHAMMAD H. ZARIFI[®]³, (Senior Member, IEEE),

AMIR EBRAHIMI¹⁰4, (Senior Member, IEEE), AND FERRAN MARTIN¹⁰5, (Fellow, IEEE)

Neuroengineering Biomedical Research Group, Institute of Bioengineering, Miguel Hernández University of Elche, 03202 Elche, Spain

Corresponding author: Carlos G. Juan (carlos.juan01@umh.es)

This work was supported in part by MCIN/AEI/10.13039/501100011033, Spain, through ERDF European Union under Project PID2022-1391810B-I00; and in part by the AGAUR Research Agency, Catalonia Government, under Project 2021-SGR00192 and Project 2024 ICREA 00114. The work of Carlos G. Juan was supported in part by MICIU/AEI/10.13039/501100011033 under Grant RYC2022-036257-I, and in part by ESF+.

ABSTRACT This review paper focuses on the latest advances and applications of planar microwave sensors contributed by the most prominent researchers in the field. The paper presents the different working principles, design approaches, fabrication technologies, materials, and applications of a wide variety of planar sensors operating at microwave and millimeter-wave frequencies, including contact and contactless sensors, wired and wireless sensors, microfluidic sensors, "green" sensors, wearables, biosensors, physical sensors, chemical sensors, and more. Advanced techniques for sensor performance optimization (e.g., sensitivity, resolution, selectivity, etc.), based on artificial intelligence, active feedback loops, microwave spectroscopy, losses engineering, etc., will also be discussed in the paper.

INDEX TERMS 3-D printing, active sensors, artificial intelligence, biosensors, chemical sensors, coupled resonator sensors, dielectric characterization, differential sensors, functional films, green sensors, liquid sensors, loss engineering, microfluidics, microwave sensors, microwave spectroscopy, permittivity sensors, physical sensors, planar technology, resonant sensors, RFID sensors, sensitivity/resolution/selectivity optimization, substrate integrated waveguide (SIW), textile-based sensors, wearables, wireless sensors.

I. INTRODUCTION

The research in planar microwave sensors has experienced an exponential growth in recent years, mainly pushed by today's paradigms of the Internet of Things (IoT), the Fourth Industrial Revolution (also known as Industry 4.0), and the Digital Transformation (or Smart World). Thus, there is an increasing demand for cost-effective, small-sized, and smart sensors and sensor networks, to be applied in a wide diversity of scenarios, such as smart cities, smart health, smart agriculture, civil engineering, structural health

The associate editor coordinating the review of this manuscript and approving it for publication was Ali Karami Horestani.

monitoring, biosensing, agrifood industry, security, motion control, automotive industry, space, etc.

There are many sensing technologies (e.g., optics/photonics, acoustics, electrochemical, etc.), but RF/microwaves (extending the spectrum from UHF up to THz frequencies) offer a series of unique advantages aligned with the requirements of the above-cited paradigmatic concepts [1]. In general, this technology features easy and cost-effective manufacturing processes and ease of integration with further electronic equipment. Conversely, the required driving electronics may become costly for certain applications, and these devices must face other drawbacks such as increased conductor and radiation losses, impact of parasitic effects and fabrication non-idealities or

²LAAS-CNRS, Université de Toulouse (UT), 31000 Toulouse, France

³School of Engineering, The University of British Columbia, Kelowna, BC V1V 1V7, Canada

⁴School of Engineering, Royal Melbourne Institute of Technology (RMIT) University, Melbourne, VIC 3001, Australia

⁵CIMITEC, Departament d'Enginyeria Electrònica, Universitat Autònoma de Barcelona, 08193 Bellaterra, Spain



susceptibility to electromagnetic interference. Nonetheless, their high operation speed, compactness, reproducibility, scalability and robustness, among other advantageous characteristics, make microwave devices an interesting option for many applications, including sensing contexts.

Thus, besides their low cost and size, microwave sensors, and particularly planar sensors, can be implemented in flexible substrates, including plastics, organic substrates, and even fabric, by means of subtractive (etching) or additive (printing) processes, and they are also compatible with other technologies of interest for sensing, such as microfluidics, micromachining, 3-D printing, etc. Additionally, microwaves are very sensitive to the electromagnetic properties of the materials they interact with. Thus, microwave sensors are very useful for the dielectric characterization of materials (solids or liquids), and for the measurement of many physical, chemical, and biological variables related to material permittivity. Planar microwave sensors can operate by contact or contactless with the material under test (MUT), or analyte, and can be wirelessly connected to the reader (of interest in many IoT applications), in schemes based on the so-called sensing tags (which act as a "smart skin", able to provide information of the material or sample under study).

Another important aspect of planar microwave sensors is that the necessary associated electronics for signal generation, processing, and communication purposes can be seamlessly integrated within the sensor's substrate, representing a reduction in system costs and complexity. In summary, planar microwave sensors constitute an enabling technology for the deployment of the IoT, Industry 4.0, and Smart World, where sensing is necessary to obtain information of the system under consideration, in order to gain insight on its current state and take appropriate decisions and actions (either through human intervention or autonomously) when necessary.

Within this framework, this review paper is intended to provide the reader an up-to-date state of the art on planar microwave sensors, including the main working principles, materials and technologies, performance optimization techniques (mainly focused on sensitivity, resolution and selectivity), and applications. Applications of planar microwave sensors cover a wide range of scenarios, in fields as diverse as biosensing [2], [3], [4], [5], [6], [7], [8], [9], [10], [11], smart health care [12], [13], [14], physical sensing (e.g., temperature and humidity sensors [15], [16], [17], [18]), chemical sensing (e.g., gas sensors [19], [20], [21]), structural health monitoring (SHM) [22], [23], [24], [25], automotive and space industry [26], [27], [28], motion control [29], [30], [31], agrifood industry (e.g., for edible oil deterioration by usage [32], [33], [34], [35], or for the detection of adulterated food or beverages [36], [37]), smart agriculture [38], etc. To ease the readability, Table 1 lists the main nomenclature with the associated definitions, in alphabetical order.

The paper is organized as follows. Section II is devoted to briefly reviewing the main sensing principles of planar

microwave sensors, mainly (although not exclusively) determined by the considered output variable. Section III reviews the main technologies and materials useful for sensing using microwaves. The main approaches for sensor performance optimization are the subject of Section IV. This section mainly considers strategies for sensitivity, resolution, and selectivity optimization. Section V is focused on wireless and radiofrequency identification (RFID) sensors, of increasingly growing interest within the framework of IoT. Section VI reports some representative applications of planar microwave sensors. Finally, Section VII highlights the main relevant conclusions.

II. WORKING PRINCIPLES

Planar microwave sensors can be categorized according to various classification criteria, such as the operating frequency (i.e., RF, microwave, mm-wave, or THz sensors), or their application (e.g., physical, chemical, and biological sensors), among others. There are also several binary classification schemes, including contact/contactless sensors, wired/wireless sensors, differentialmode/single-ended sensors, non-resonant/resonant sensors, reflective-mode/transmission-mode sensors, invasive/noninvasive sensors, intrusive/non-intrusive sensors, singlefrequency/broadband sensors, etc. However, probably the most convenient classification of planar microwave sensors is by their working principle [1]. Thus, according to such categorization criterion, planar microwave sensors can be divided into frequency-variation sensors, frequencysplitting sensors, magnitude-variation sensors, and phasevariation sensors. Essentially, the considered output variable determines the working principle. Nevertheless, there are sensors where several output variables simultaneously can be used for sensing. Although differential sensing is a mode of operation, rather than a working principle, we will also include planar differential sensors in the classification scheme of the present section (a typical output variable in such sensors is the cross-mode transmission or reflection coefficient). The main relevant feature of differential sensors is their robustness against cross-sensitivities caused by changes in ambient factors (temperature and humidity).

Planar sensors based on the previous principles have been applied to the measurement of many types of variables, mainly correlated with material permittivity, including also material permittivity itself (dielectric characterization). It should be noted that, in these cases, signal acquisition is very simple and it can be achieved with usual RF detection components, without need for sophisticated processing. Nevertheless, it should be mentioned that, for dielectric characterization, most previous sensors are able to provide the dielectric properties of materials in specific frequency bands (narrowband dielectric characterization). By contrast, there are planar microwave sensors devoted to the broadband characterization of materials, based on the so-called dielectric spectroscopy, a technique able to provide the real and the imaginary part of the complex permittivity of materials



TABLE 1. Nomenclature.

Term	Succinct Definition
3-D print	Three-Dimensional print.
Agrifood	Related to agricultural production, food
_	processing, distribution and consumption.
AI	Artificial Intelligence.
Biosensing	Sensors devoted to biological and medica applications.
ВЈТ	Bipolar Junction Transistor.
CELC	Complementary Electric-LC.
CMOS	Complementary Metal Oxide Semiconductor.
CMPA	Circular Microstrip Patch Antenna.
CNN	Convolutional Neural Network.
CPW	Coplanar Waveguide.
CSRR	Complementary Split-Ring Resonator.
DEP	Dielectrophoresis.
Differential-mode	Sensor consisting of two independent sensors
sensor	one of them devoted to a reference load.
DNA	Deoxyribonucleic Acid.
ECT EMI	Electrochemotherapy.
Frequency-splitting	Electromagnetic Interference. Sensor for which the sample breaks the
sensor	symmetry between two resonators.
Frequency-variation	Sensor for which the canonical output variable
sensor	is the resonance frequency.
FSS	Frequency Selective Surface.
C	Sensor produced with environmentally friendly
Green sensor	materials and techniques.
IDC	Inter-Digital Capacitor.
IMP	Intermodulation Products.
IoT	Internet of Things.
JFET	Junction Field-Effect Transistor.
LTCC	Low Temperature Cofired Ceramic.
LUT Magnituda maintina	Liquid Under Test.
Magnitude-variation sensor	Sensor for which the canonical output variable is the magnitude of the scattering parameters.
MEMS	Microelectromechanical Systems.
MLMS	Machine Learning.
MMIC	Monolothic Microwave Integrated Circuit.
MUT	Material Under Test.
NDT	Non-Destructive Testing.
PCB	Printed Circuit Board.
PDMS	Polydimethylsiloxane.
PEDOT:PSS	Poly(3,4-ethylenedioxythiophene) polystyrene sulfonate.
Phase-variation	Sensor for which the canonical output variable
sensor	is the phase of the scattering parameters.
	Pseudomorphic High Electron Mobility
рНЕМТ	Transistor.
PTFE	Polytetrafluoroethylene (Tefllon®).
Q _u -based sensor	Sensor for which the canonical output variable
_	is the unloaded quality factor.
REF	Reference.
RF	Radiofrequency.
RFID PS(G)	Radiofrequency Identification.
<i>RS(G)</i> SAR	Relative Sensitivity to Glucose. Specific Absorption Rate.
SHM	Structural Health Monitoring.
SIR	Stepped-Impedance Resonator.
SIW	Substrate-Integrated Waveguide.
SMA	SubMiniature version A.
SNR	Signal-to-Noise Ratio.
SRR	Split-Ring Resonator.
TDOA	Time Difference of Arrival.
TDR	Time-Domain Reflectometry.
Textile sensor	Sensor, either flexible or embroidered
TNT	integrated into the fabric of a certain garment. Titanium Dioxide nanoTube.
UHF	Ultra-High Frequency.
UV	Ultraviolet.
VCO	Voltage-Controlled Oscillator.
VNA	Vector Network Analyzer.
VOC	Volatile Organic Compounds.

(solids, liquid, bio-samples, etc.) over a broad band of frequencies. These sensors are also included in this section, even though dielectric (microwave) spectroscopy is a specific measurement technique, rather than a working principle.

It should also be mentioned that in certain classification schemes of planar microwave sensors that obey their working principle, wireless and RFID sensors are also included (e.g., in [1]). Nevertheless, these sensors exhibit so many particularities that bespeak to consider them in an independent and extended section (Section VI). Next subsections will briefly review the different sensor types classified by their working principles, including those based on microwave spectroscopy, emphasizing their strong and weak points, as well as their pros and cons.

A. FREQUENCY-VARIATION SENSORS

Frequency variation is probably the most extended working principle in planar microwave sensors [39], [40], [41], [42], [43], [44], [45], [46], [47], [48], [49], [50], [51], [52], [53], [54], [55], [56], [57], [58], [59], [60], [61], [62], [63], [64], [65], [66], [67], [68]. Frequency-variation sensors are based on resonant sensing elements. Their canonical output variable is the resonance frequency. This parameter is highly dependent on the dielectric properties of the environment surrounding the sensing resonator. Some examples are a solid or liquid sample, or a functional film with dielectric properties highly correlated with the physical, chemical or biological variables to be measured (measurand), see [1], Section 7.3, and references therein. Such a resonant element can be an electrically small semi-lumped resonator, or a distributed resonator. On the other hand, the sensor can be implemented by means of a transmission line (the driving element) loaded with (or coupled to) such sensing resonator (or a set of sensing resonators), either operating in reflection or in transmission (see for example, [40], [41], [42], [43], [44], [45], [46]), or it can be implemented in a wireless configuration [16], [17], [18], [37], [69], [70], [71], [72], [73], [74], [75], [76], [77], [78], [79], [80], [81]. In the latter case, the sensing element can be a resonator, or a set of resonators, separated from the driving element, the reader, and operating typically in backscattering (e.g., [16], [17], [18], [74]). In such wireless sensors, the reader uses typically a broadband planar or a horn antenna fed by a frequency sweeping signal. An alternative is to consider the antenna as sensing element (see, e.g., [82], [83], [84], [85]), the output variable typically being the resonance frequency of the transmission coefficient between such antenna and a wideband receiver. In transmission-line based and wireless resonant frequency-variation sensors, a frequency varying signal covering the required input dynamic range of the sensor is needed. Figure 1 depicts various configurations of resonant frequency-variation sensors.

There are cases where more than one variable needs to be measured. For example, fully characterizing a dielectric



material requires the knowledge of both the dielectric constant and the loss tangent of such material (or the real and the imaginary part of its complex permittivity). In such cases, at least two output variables are needed. Most frequency-variation sensors consider as an additional output variable either the magnitude of the resonance peak or notch, or the quality factor, mainly related to the loss factor of the sample under study, or analyte [2], [43], [46], [86]. The resonance frequency mostly correlates with the dielectric constant of the material under test (MUT) or environment surrounding the sensing element. Nevertheless, cross-sensitivities between the output variables (resonance frequency and magnitude/quality factor) and the input variables (dielectric constant and loss tangent in the considered example) are unavoidable. Such cross-sensitivities are mainly manifested when high-loss materials are involved.

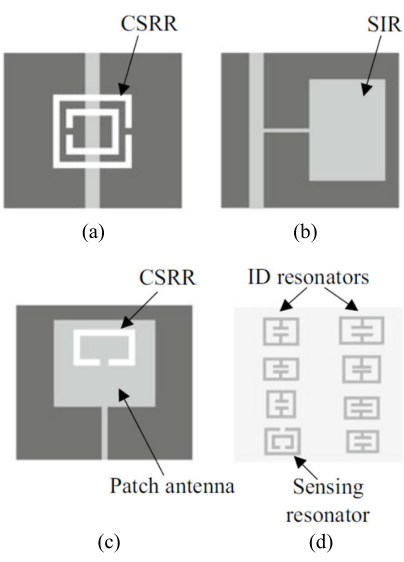


FIGURE 1. Topologies of some possible configurations of resonant frequency-variation sensors. (a) Transmission line coupled to a semi-lumped resonant element (complementary split ring resonator, CSRR); (b) transmission line loaded with a semi-lumped resonator(stepped-impedance resonator, SIR); (c) patch antenna loaded with a resonant element (CSRR); (d) back-scattered chipless-RFID sensor based on a set of resonators for identification, and one resonator for sensing. The upper metal level is depicted in soft grey, whereas the lower metal level is depicted in dark grey.

Frequency-variation sensors are robust against electromagnetic interference (EMI) and noise, as far as such sensors are based on frequency measurements (the canonical output variable is the resonance frequency of the sensing element). However, broadband signals (at least covering the output dynamic range) are needed for sensing. If a vector network analyzer (VNA) is used, this aspect does not represent a limitation. However, even though low-cost VNAs are commercially available nowadays, there are situations where their cost is prohibitive. In such cases, a voltage-controlled oscillator (VCO), or an array of VCOs, typically managed by a microcontroller, is required, and this increases the cost of the associated electronics, at least when compared to the cost of the electronics in the so-called single-frequency sensors

(mainly phase-variation and magnitude-variation sensors), to be discussed later.

B. FREQUENCY-SPLITTING SENSORS

Frequency-splitting sensors are a variant of frequencyvariation sensors [87], [88], [89], [90], [91], [92], [93], [94], [95], [96], [97]. Such sensors consist of a transmission line loaded with (or coupled to) a pair of identical sensing resonators [see Figures 2(a) and (b), where stepped-impedance resonators (SIRs) are considered]. The resonators can be located at the same transverse plane in the line [88], [89], [91], [94], or in a cascaded configuration [90]. The operating principle is frequency splitting, generated when the resonators are asymmetrically loaded. Namely, when the resonators are identical (same load), a single resonance arises (manifested as a single notch or peak). However, when the symmetry in resonator loading is truncated, two different resonances appear, and the frequency separation (and magnitude difference) between such resonances is a measure of the difference in the dielectric loads of both sensing resonant elements. Typically, one of the resonators is considered as reference (REF). whereas the other one is affected by the measurand. Such sensors are similar to differential-mode sensors and are used, e.g., as comparators. However, frequency-splitting sensors are not "true" differential sensors, since a single sensor, rather than two independent sensors, is used. Nevertheless, frequency-splitting sensors share some advantages with differential-mode sensors, particularly, they are insensitive to common-mode stimuli, typically caused by changes in environmental factors.

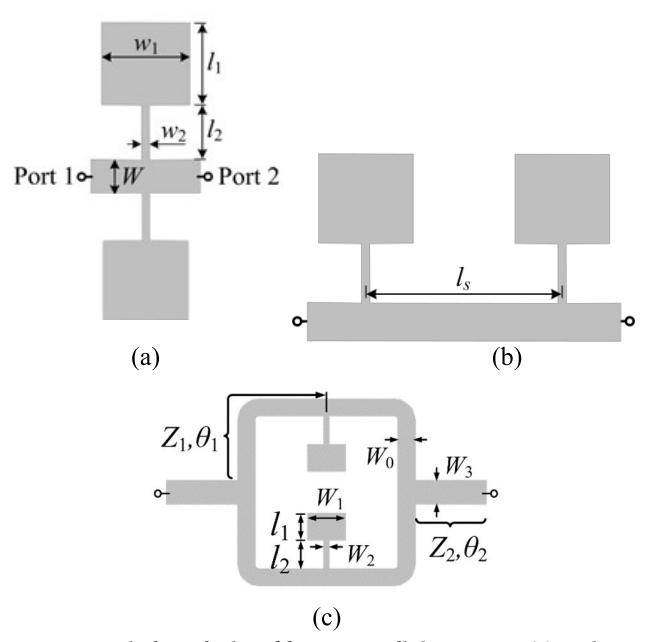


FIGURE 2. Typical topologies of frequency splitting sensors. (a) Device with the sensing resonators (SIRs) located at the same transverse position; (b)device with the sensing elements (SIRs) separated a half wavelength(cascaded configuration); (c) device based on the splitter/combiner configuration.



A limitative aspect of frequency-splitting sensors based on resonators located at the same transverse plane is inter-resonator coupling, which degrades the sensitivity as, discussed in [91]. For example, in the specific configuration of Figure 2(a), negative inductive coupling between the SIRs arises. To circumvent this issue, the cascaded configuration, with the resonant element separated enough, is a solution [90]. Another solution is the so-called splitter/combiner configuration of Figure 2(c) [91], [93]. With such topology, inter-resonator coupling is prevented, provided the resonators are separated enough. However, in this case, the notches in the transmission coefficient are due to signal interference and, due to this fact, sensitivity is degraded, unless the separation between the resonator's position and the T-junctions is adequately chosen. In particular, it is convenient to translate a virtual ground at the T-junctions at the resonance frequency of the SIRs, and this is achieved by choosing the electrical length θ_1 , see Figure 2(c), as $\theta_1 = 180^{\circ}$ at that frequency [91]. Additional solutions to prevent inter-resonator coupling have been reported in [94] and [96].

Frequency-splitting sensors, like frequency-variation sensors, need wideband interrogation signals for sensing (a limitative aspect), but are robust against EMI and noise. Nevertheless, the solutions to circumvent sensitivity degradation (mainly inter-resonator coupling) either increase the overall sensor size or add complexity to the sensor. Thus, the use of such sensors is justified when comparison to a REF measurand is needed, or when measurements under severe variations in ambient factors are expected.

C. PHASE-VARIATION SENSORS

In phase-variation sensors, the canonical output variable is the phase of either the transmission (transmission-mode) or reflection (reflective-mode) coefficient of a transmission line, or a transmission line-based structure (e.g., loaded or coupled to a resonant element), measured at a certain (operating) frequency [98], [99], [100], [101], [102], [103], [104], [105], [106], [107], [108], [109], [110], [111], [112], [113], [114], [115], [116], [117], [118], [119], [120], [121], [122], [123], [124], [125], [126], [127], [128], [129], [130], [131], [132], [133], [134], [135], [136], [137], [138], [139]. Thus, unlike the previous sensors, phase-variation sensors are singlefrequency devices, where the electronics for sensor feeding is as simple as an RF/microwave oscillator (or a VCO tuned at the operating frequency). This reduces the overall sensor cost in operative environment. Additionally, phase measurements, like frequency measurements, are robust against EMI and noise. These aspects, combined with the highly achievable sensitivities and resolutions of these sensors (an aspect to be discussed later), make them very suitable in scenarios where tiny variations of a measurand in the vicinity of a certain REF value should be detected.

Both non-resonant and resonant phase-variation sensors have been reported [107], [108], [109], [110], [111], [112], [113], [114], [115], [116], [118], [119], [120], [121], [122], [123], [124], [125], [126], [127], [128], [129], [130], [131],

[132], [133], [134], [135], [136], [137], [138], [139]. For sensitivity optimization, the maximum possible phase slope of either the reflection or the transmission coefficient at the operating frequency must be achieved, see Figure 3 [135]. Concerning non-resonant sensors, highly sensitive devices have been reported by considering long (meandered) sensing lines [100], [102] or artificial lines (with controllable dispersion diagram) [98], [101], [103], [104], [106]. Nevertheless, these non-resonant phase variation sensors tend to exhibit large sensing regions, or their designs are relatively complex (designing composite right/left-handed lines [98], slow-wave transmission lines [103], [104], [106], or electro-inductive wave transmission lines [101] with the required dispersion is not absent of certain difficulty).

Alternatively, high phase slopes can be achieved by considering resonant phase-variation sensors tuned to the resonance frequency of the sensing resonator when it is loaded with the REF sample or affected by the REF measurand. Such sensors can operate either in reflection [107], [108], [109], [110], [111], [112], [113], [114], [115], [116], [117], [118], [119], [120], [121], [122], [123], [124], [125], [126], [127], [128], [129], [130], [131], [132], [134], [136], [137], [139] or in transmission [98], [99], [100], [101], [102], [103], [104], [105], [106], [133], [138], and the relevant aspect to boost up the sensitivity is to adequately design the sensing resonator. For example, in one-port reflective-mode phasevariation sensors merely consisting of the access lines and the sensing resonant element (either distributed or semi-lumped), the strategy for sensitivity optimization is to increase the L/C(inductance to capacitance) ratio in series-type resonators, or to reduce it in parallel-type resonators (this enhances the phase slope at resonance) [1], [111], [112]. If the resonators are distributed, particularly, open-ended quarterand half-wavelength sensing resonators, the characteristic impedance must be high and low, respectively [108]. Note that a high impedance is equivalent to a high L/C ratio, the required condition to boost the phase slope (and the sensitivity) in a series type resonator, like the open-ended quarter-wavelength resonator. Thus, it is obvious that in an open-ended half-wavelength resonator (parallel type) the required impedance to enhance the sensitivity must be low. Efficient strategies to boost up the sensitivity in phase-variation sensors will be later discussed.

D. MAGNITUDE-VARIATION SENSORS

Magnitude-variation sensors are also single-frequency sensors. In this case, the output variable is the magnitude of the transmission or reflection coefficient of the sensing structure at the operating frequency. Nevertheless, by using an envelope detector, the magnitude of the transmission or reflection coefficient can be converted to a voltage.

In these sensors, two categories can be distinguished. On the one hand, there are magnitude-variation sensors based on coupling modulation between a host line and a (typically movable) resonant element. Such sensors are mainly devoted to the measurement of linear or angular displacements and

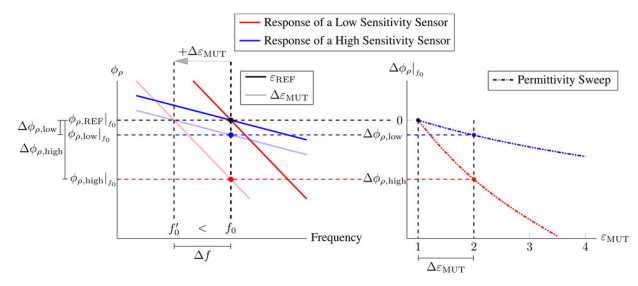


FIGURE 3. Illustration of sensitivity enhancement in a reflective-mode phase-variation sensor related to the increase in the phase slope at the operating frequency. The variation of the phase of the reflection coefficient at the operating frequency, f_0 , as consequence of an overall shift in the phase response, increases with the phase slope. When the dielectric constant of the MUT changes a quantity Δe_{MUT} , the variation experienced by the phase of the reflection coefficient at f_0 for the high-sensitivity sensor (higher phase slope), $\Delta \varphi_{\rho,\text{high}}$, is larger than for the low-sensitivity sensor, $\Delta \varphi_{\rho,\text{low}}$.

velocities [29], [30], [31], [141], [142], [143], [144], [145], [146], [147], [148], [149], [150], [151], [152], the stator (i.e., the static part of the sensor) being the host line. Both, short-range displacements [140], [141], [142], [143], [144], [145], [146], [147], [148], as well as moderate-to-long range displacements [29], [30], [31], [149], [150], [151], [152] can be measured with these sensors.

In the first case, symmetry disruption between the host line and the resonant element has been used as the canonical sensing mechanism, and the sensitivity is mainly determined by the shape of the sensing resonant element. For example, if a transmission line exhibiting a magnetic wall in its axial symmetry plane (i.e., a microstrip line or a CPW) is symmetrically loaded with a symmetric resonator (etched in an independent movable substrate) exhibiting an electric wall in its symmetry plane at the fundamental resonance, line-to-resonator coupling at that frequency is prevented, see Figure 4 [1], [153]. The reason is the different nature of the (aligned) symmetry planes of the line and resonator (one a magnetic wall and the other one an electric wall). However, by disrupting the perfect symmetry, line-to-resonator coupling is activated, and a notch in the transmission or reflection coefficient is generated. The magnitude of such a notch depends on the level of coupling and hence on the relative displacement (linear or angular, or both) between the line and the resonator.

For moderate and long-range displacements, electromagnetic encoders constitute a good solution [29], [30], [31], [149], [150], [151], [152]. In this case, a chain of resonators (linear in linear encoders and circular in rotary encoders) etched in a dielectric substrate (a disc in rotary encoders) constitutes the movable part of the sensor, whereas the stator is a transmission line fed by means of a harmonic signal. By encoder motion over the stator at short distance, the magnitude of the transmission coefficient is modulated, generating an amplitude-modulated (AM) signal at the output port of the stator line. Such signal contains the relevant information relative to the velocity (inferred from the time lapse between adjacent pulses in the envelope function of

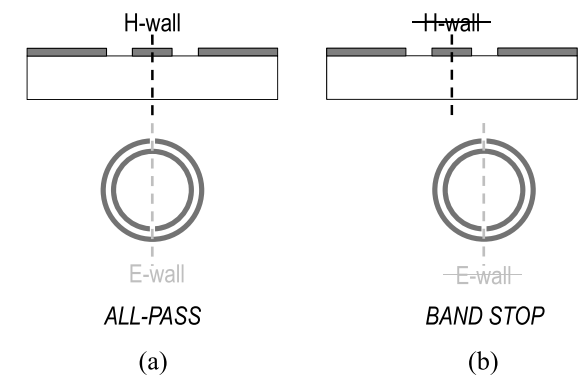


FIGURE 4. Sketch showing the effects of symmetry disruption in a CPW transmission line loaded with a SRR etched in the backside of the substrate. (a) Perfect symmetry, preventing line-to-resonator coupling; (b)symmetry truncation by means of a lateral displacement of the SRR, thereby activating coupling. The CPW and the SRR (etched in the back substrate side) are depicted in cross-sectional and bottom views, respectively, for better understanding.

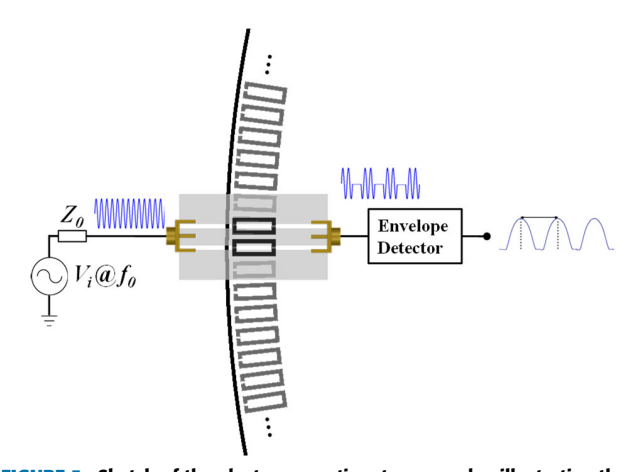


FIGURE 5. Sketch of the electromagnetic rotary encoder, illustrating the working principle.

the AM signal) and displacement (determined from the cumulative number of pulses from a reference position). Figure 5 depicts a sketch of an electromagnetic rotary encoder.

Besides the previous coupling-modulation sensors, mostly devoted to motion sensing, there are also magnitude-variation sensors useful for the dielectric characterization of materials, or for the measurement of variables related to material permittivity [154], [155]. In this case, the sensing mechanism is similar to that in phase-variation sensors. When the dielectric properties of the medium surrounding the sensing element (typically, but not necessarily, a resonator) change, there is an overall shift in the frequency response, which translates into a variation in the magnitude of the transmission or reflection coefficient at the operating frequency. A high slope in the magnitude response at the operating frequency is useful to boost up the sensitivity (similar to phasevariation sensors), and, for this purpose, structures that provide closely spaced transmission and reflection zeros are convenient [154], [155]. Figure 6 illustrates this aspect.



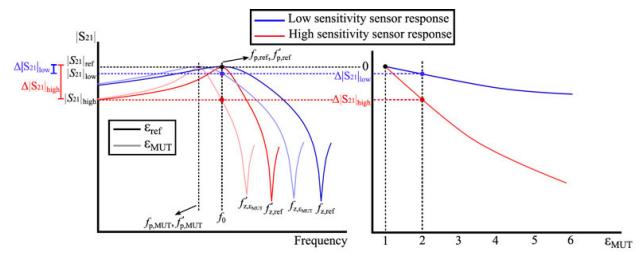


FIGURE 6. Sketch showing the strategy for sensitivity optimization in a magnitude-variation sensor (particularly, a transmission-mode sensor). A strong variation of the magnitude of the transmission coefficient with frequency of the operating frequency, f_0 , generates an important variation of the magnitude of the transmission coefficient at that frequency when the dielectric constant of the MUT, ε_{MUT} , varies. A pole and a transmission zero in the magnitude response, closely spaced (as depicted in the figure), contribute to boost the sensitivity.

There are also magnitude-variation sensors devoted to the dielectric characterization of materials and to the measurement of related variables that exploit symmetry disruption in symmetric devices like directional couplers [156], [157]. Sensor feeding in magnitude-variation sensors is simple, since a single-tone (harmonic) signal suffices for that purpose (an advantageous aspect shared with phase-variation sensors). Moreover, a simple envelope detector can be used to monitor the output signal (thereby avoiding a vector network analyzer) [154]. Nevertheless, the magnitude of the transmission or reflection coefficient (or, equivalently, the generated voltage, provided an envelope detector is used) is more prone to the effects of EMI and noise than the phase.

E. DIFFERENTIAL-MODE SENSORS

Differential-mode sensors consist of two independent (singleended) sensors, one devoted to the so-called reference (REF) material, and the other one devoted to the material (or measurand) under test (MUT) [4], [5], [10], [158], [159], [160], [161]. As compared to single-ended sensors, differential sensors exhibit major robustness against cross-sensitivities related to environmental factors, i.e., caused by changes in temperature, humidity, or atmospheric pressure. Namely, environmental variables are seen as common-mode stimuli by differential sensors, provided that, at the typical scale of the sensors, such variables are uniform. Therefore, the effects of ambient factors, or other undesired common-mode stimuli, are minimized in differential-mode sensors. This robustness against potential cross-sensitivities caused by ambient factors is also an attribute of frequency-splitting sensors, but, as mentioned in Section II-B, frequency-splitting sensors are not "true" differential sensors, since they are not composed by two independent (single-ended) sensors (but rather by two sensing elements, typically resonators, that share one or two single-ended ports).

The output variable in a differential microwave sensor can be the differential resonance frequency between the two sensors constituting the composite device, the differential phase (measured at a certain frequency), or the differential magnitude (also measured at a certain frequency). In applications where two variables should be measured,

e.g., the dielectric constant and the loss tangent of a MUT, two differential output variables are used, for example, the differential resonance frequency and the differential resonance magnitude (provided the two sensors constituting the differential pair are resonant).

In differential-mode resonant sensors, the sensing elements are typically two transmission lines, each loaded with a planar resonator, either a metallic or a slot resonator. In many reported implementations of such resonant differential sensors operating in transmission, the cross-mode transmission coefficient is the considered output variable (e.g., in [4], [5], [159], [160]). If the sensing elements of the composite pair are uncoupled, the cross-mode transmission coefficient is simply:

$$S_{21}^{cd} = S_{21}^{dc} = S_{21,\text{MUT}} - S_{21,\text{REF}},$$
 (1)

where $S_{21,\mathrm{MUT}}$ and $S_{21,\mathrm{REF}}$ are the transmission coefficients of the single-ended sensors devoted to the MUT and to the REF sample, respectively. There are various examples in the literature where the maximum in the magnitude of the cross-mode transmission coefficient and, eventually, the frequency of such maximum, have been the considered output variables. Very good sensitivities and resolutions in such sensors have been reported [4], most of them devoted to the accurate measurement of solute content (e.g., glucose, or electrolytes) in aqueous solutions (nevertheless, the measurement of total electrolyte concentration in biological samples, particularly, horse urine, has also been demonstrated [5]).

The most important limitative aspects of differential-mode sensors are their size and potential imbalances that might be caused by fabrication-related tolerances or by imperfections in the fabrication process. Such imbalances might generate a non-negligible differential output signal in the absence of a differential input signal, representing a false reading, or limiting sensor resolution. One possibility to alleviate sensor imbalances in differential sensing is to perform two consecutive measurements (one with the REF material and the other one with the MUT) in a single-ended sensor. This is not a real-time measurement, but it is reasonable in situations where changes in the input variable proceed at a temporal scale much larger that the time lapse between subsequent measurements (and, of course, if the environmental variables do not vary during measurement).

F. MICROWAVE SPECTROSCOPY-BASED SENSORS

As indicated at the beginning of this section, microwave dielectric spectroscopy is a measurement technique devoted to determining the complex permittivity of samples over a broad frequency band, rather than a working principle [162], [163], [164], [165], [166], [167]. Many materials, especially liquids and biological entities, exhibit strong frequency dispersion, and therefore, gathering information regarding the dependence of their dielectric properties with frequency is of interest. Moreover, microwave spectroscopy can provide dielectric signatures that can be useful to identify samples,



to determine material composition, etc. Figure 7 presents an example of dielectric spectra obtained for two liquids, deionized water and ethanol in aqueous solution. It illustrates the impact of adding ethanol to water on the permittivity. Such dielectric responses may then be mathematically modeled in a more or less complex manner, such as through the Cole–Cole representation, or the Debye, Cole–Davidson or Havriliak–Negami models [168]. The physical behavior of matter is therefore made accessible.

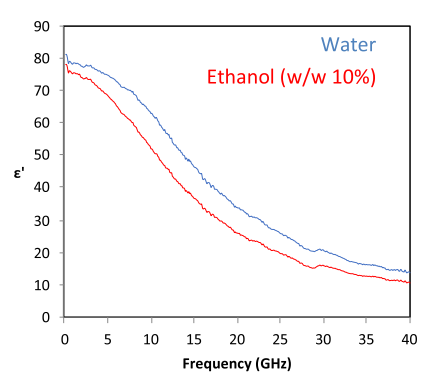


FIGURE 7. Example of dielectric spectra of de-ionized water and ethanol in aqueous solution obtained with a miniature microwave coplanar waveguide.

Most planar sensors based on microwave spectroscopy are non-resonant and use transmission line sections for sensing. The idea behind such technique is to infer the complex propagation constant of the sensing line (dependent on the dielectric properties of the considered analyte) over the considered frequency band from the measurement of the Sparameters, and, from it, obtain the complex permittivity of the sample [162], [163], [164]. Analytical methods for retrieving the complex propagation constant have been reported [163], [164], [169], [170]. Dealing strictly with microwave dielectric spectroscopy, the variation of the complex permittivity should only be considered, as illustrated in Figure 7. However, beyond theory, electrical parameters such as capacitor and conductance are also taken into consideration, while the dimension of the object under test is not defined. This is notably the case of biological materials in liquids, such as single cells or microtissues in their culture medium [171], [172].

Moreover, there are also planar resonant sensors devoted to the broadband dielectric characterization of samples [166], [167]. These sensors utilize the effects of the dispersive dielectric constant of the MUT on the multiple resonances that the sensing resonator exhibits. Namely, the sensor is based on the changes generated by the analyte at the fundamental resonance frequency and at its harmonics, and such strategy has been designated as discrete microwave spectroscopy in [166]. A clear advantage of this latter resonant method over the previous non-resonant microwave dielectric spectroscopy approach is simplicity. The reason is that, by using a sensing resonator, recording the changes in the resonance frequency and magnitude of the different

harmonics suffices to retrieve the dielectric information of the sample over the considered frequency band.

III. NEW MATERIALS AND TECHNOLOGIES

Most planar microwave sensors are implemented in printed circuit board (PCB) technology, due to its low cost and easy fabrication. Nevertheless, many microwave sensing devices have been implemented in alternative modern planar technologies, such as substrate integrated waveguide (SIW), fabric/textiles, monolithic microwave integrated circuit (MMIC) technology, and flexible substrates, including new polymeric and organic substrates (e.g., paper), among others. Moreover, there are many examples of microwave sensors implemented in planar form that include additional elements, such as fluidic channels, liquid holders, or micropipes, usually fabricated by means of specific up-to-the-minute technologies (microfluidics, 3-D printing, micromachining, etc.). All these technologies are the subject of the present section, where the main aim is to highlight their benefits for microwave sensing. The section also includes a discussion on advanced materials for microwave sensing (e.g., graphene, liquid metals, and liquid crystals), as well as on the need to use functional films (sometimes called smart films), in order to enhance the sensitivity with certain variables (typically such films exhibit a high dependence of their permittivity with the variable of interest).

A. FUNCTIONAL AND SMART FILMS

Functional and smart films are increasingly gaining attention in the microwave structures, where they are being explored both as interface layers and as integral components of fabricated designs [173], [174], [175], [176], [177]. These advanced films are poised to replace traditional materials such as carrier substrates and metallic traces, offering unique advantages in terms of performance and sustainability. By leveraging their tunable electrical, mechanical, and thermal properties, these materials open new pathways for the design of high-performance, lightweight, and environmentally friendly microwave devices [178], [179]. Furthermore, their compatibility with novel fabrication techniques, such as printing and additive manufacturing, enables cost-effective production processes and greater design flexibility [180], [181], [182], [183], [184].

While metals like copper offer excellent electrical conductivity, their rigidity and weight limit their use in emerging applications such as satellite and wearable communications. MXenes, particularly Ti_3C_2 films, have emerged as promising alternatives due to their exceptional conductivity (1.8 \times 10⁵ S/m [185]), tunable surface chemistry, and mechanical flexibility, offering a compelling replacement due to their superior conductivity and flexibility. Large-flake MXenes demonstrate superior electrical conductivity and reduced inter-flake resistance due to fewer junctions, resulting in higher quality factors and lower losses. In cyclic humidity tests, large-flake Ti_3C_2 films outperformed their small-flake counterparts, showing more stable resonant



frequencies ($\approx 1.7\%$ shift) and enhanced quality factors (150 unloaded, 35 loaded), underscoring their robustness in variable environmental conditions. Additionally, MXene circular membranes were used to fabricate lightweight microwave devices, demonstrating comparable performance to metal-based systems in sub-6 GHz bands, with operation frequencies tunable via membrane size and a significant reduction in thickness and weight [185], [186], [187].

B. ADVANCED MATERIALS

TiO₂ nanotube membranes stand out as free-standing, semiconducting, and self-organized nanostructures, uniquely suited for advanced sensing applications. Unlike other metal oxides, these membranes can be delaminated from their native substrates and adapted to various surfaces, enabling smooth integration into diverse sensing systems, at the expense of more costly and difficult manufacturing. Recently, Noothongkaew et al. [188] showcased their potential by employing TiO2 nanotube membranes as UV (UltraViolet) photoconductors, successfully transferring them from anodized foil to a transparent ITO substrate. This flexibility and adaptability highlight TiO2's promise for non-contact microwave sensing, especially in UV detection where material options are often constrained. Their integration with planar microwave resonators has already been demonstrated for light detection using microwave resonator sensors [189].

Wide-band-gap semiconductors such as TiO2, ZnO, and SnO2 are highly sensitive to UV irradiation and offer customizable structures suited for various applications. Several notable advancements by Zarifi et al. introduced a low-cost, robust integration of self-organized anodic titanium dioxide nanotube (TNT) membranes with microwave split ring resonators (SRRs) to detect UV light. Operating on changes in permittivity and conductivity induced by UV illumination, the TNT membrane absorbs light and generates charge carriers, which alter its dielectric properties. These variations are tracked via changes in the resonator's transmission gain [190], [191], [192]. Building on this concept, further studies demonstrated the effectiveness of UV-excited TNT-integrated microwave resonators in detecting humidity, volatile organic compounds, and self-assembled monolayers. In a more recent advancement, UV-excited TNT-based sensors were used for liquid mixture characterization, showing the ability to detect changes in materials beyond the electric-field sensing region by analyzing the UV light transmitted through the sample, highlighting the sensor's extended range and versatility [193].

Alijani et al. have investigated the microwave photoconductivity of titanium dioxide nanotube (TNT) layers of varying thicknesses for potential applications in sensing and wireless communication. TNT layers were integrated with a custom-designed planar microwave resonator to evaluate their performance under UV illumination. Changes in resonant frequency, amplitude, and quality factor were monitored over time, revealing a clear dependence on layer thickness. The analysis showed that an intermediate TNT thickness yielded the most effective microwave photoconductivity response, balancing light absorption and electromagnetic interaction. Experimental findings were supported by theoretical modeling and structural analysis, which confirmed the relationship between crystallite size, layer thickness, and photoconductive efficiency. This insight is valuable for designing high-performance microwave sensors and components for future wireless and photonic systems [194].

In microwave sensing applications, split ring resonators (SRRs) are widely employed to detect variations in the dielectric properties of materials by monitoring shifts in their resonant frequency and amplitude. However, most studies focus on single-resonator systems targeting specific molecular signatures, which underutilizes the rich information available across the broader frequency spectrum. One promising solution involves the use of liquid metals like Galinstan and EGaIn, which provide passive, continuous tuning without requiring complex fabrication or power consumption. Liquid metal can alter the electromagnetic coupling within a resonator, enabling frequency shifts up to 800 MHz [68], [189]. Liquid metals like Galinstan, an alloy of gallium, indium, and tin, are room-temperature conductive fluids known for their high electrical and thermal conductivity, low toxicity, and excellent deformability. Unlike mercury, Galinstan is non-toxic and remains liquid below freezing, making it ideal for flexible electronics, stretchable circuits, and thermal interface applications [195].

Rafi et. al. have proposed a novel architecture for characterizing liquid mixtures with similar dielectric properties, which are difficult to distinguish using conventional single-frequency microwave sensors. The proposed sensor features a planar, resonant-based design with a tunable frequency range from 2.1 to 2.8 GHz, achieved by injecting variable volumes of liquid metal into an integrated fluidic channel. While traditional dielectric probe measurements at a fixed 2.82 GHz frequency failed to differentiate between two test materials, the new sensor successfully distinguished them by tuning the frequency to 2.72 and 2.68 GHz. This tunable sensing approach addresses misidentification issues in materials with overlapping dielectric properties and offers advantages over noise-prone broadband techniques like dielectric probes and spectroscopy. Additionally, it holds potential for more stable performance under temperature variations. However, the current frequency tuning range is limited, which constrains overall sensitivity. Further research is needed to expand this range and enhance the sensor's performance and reliability [68].

C. MICROFLUIDIC SENSORS

One of the prominent applications of radiofrequency (RF) and microwave sensors is in biomedical and biological monitoring and characterizations [196]. In contrast to the optical techniques such as fluorescence tagging, microwave sensors do not require any time-consuming sample preparation and are capable of detecting materials in a label-free and



non-invasive manner [4]. Furthermore, microwave planar sensors are inherently compatible with electronic integration technologies such as complementary metal oxide semiconductors (CMOS), Microelectromechanical Systems (MEMS), low temperature cofired ceramic (LTCC), etc. Thus, microwave planar sensors can be designed and fabricated in miniaturized and compact forms suitable for integration within the lab-on-a-chip platforms suitable for biological detections. However, a major challenge in bio-sample detection is usually, the small amount of the sample (blood, saliva, sweat, etc.) available for sensing and experiments. Nowadays, such a challenge can be addressed by the advent of microfluidic technology. In such technology, the liquids can be accurately processed in micro and even nano scales and guided to the most sensitive area of the planar microwave sensors for accurate and high-sensitivity characterization [197], [198].

On the other hand, the advent of metamaterials in the last decades opened new avenues for the development of high-sensitivity microfluidic sensors. In fact, metamaterialsinspired resonators such as split-ring resonators (SRRs), complementary split-ring resonators (CSRRs), and electric-LC (ELC) resonators produce resonances with highly dense and concentrated electric fields (E-field) within a small area that is ideal for deployment of microfluidic channels required for microfluidic dielectric sensing [199]. The initial designs of metamaterials-inspired microfluidic sensors were simply composed of SRRs coupled to planar transmission lines such as microstrip as shown in Figure 8(a). The SRR produces a highly dense E-field in the capacitive gap area making in the hot spot for dielectric sensing. Thus, a microfluidic channel was realized within the gap area as shown in Figure 8(c) for sensing purposes. Applying the dielectric liquid under test (LUT) into the channel modifies the resonance frequency and the quality factor (Q) as indicated in the measured transmission response ($|S_{21}|$) for the water-ethanol samples of various concentrations. Such variations are then used to develop a mathematical sensing model for retrieving the complex permittivity of the unknown liquids.

The most important factor in any type of sensor is, typically, sensitivity. The sensitivity in frequency-variation-based microwave microfluidic sensors is defined as:

$$S_{\varepsilon_r} = \frac{f_{\varepsilon_r} - f_{empty}}{f_{empty}(\varepsilon_r - 1)} \times 100, \tag{2}$$

where f_{ε_r} is the resonance frequency for the LUT, f_{empty} is the resonance frequency of the sensor with empty channel, and ε_r is the relative permittivity of the LUT. According to the above equation, the sensitivity is directly proportional to the frequency shift produced by each liquid sample. Various strategies were developed in literature to improve the frequency shift leading to sensitivity enhancement. An example is the design in [39], where a CSRR was used instead of the SRR. The CSRR is etched out of the ground plane below the microstrip transmission line as shown in Figure 9(a). The electric fields produced by the microstrip

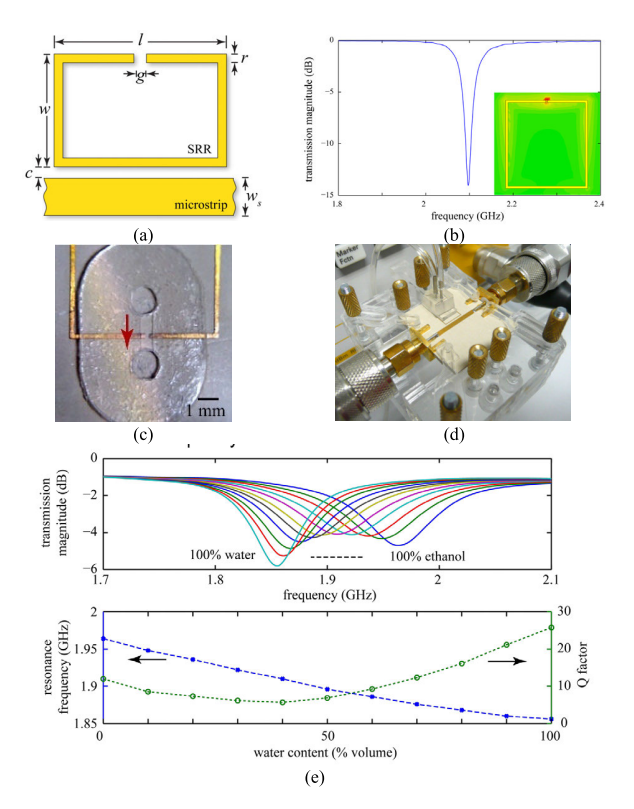


FIGURE 8. A metamaterial-inspired microfluidic sensor in [199]. (a) A SRR coupled to a microstrip line. (b) Full-wave simulated transmission response of the bare sensor together with the E-field distribution at resonance. (c) The microfluidic channel realized in the SRR gap area. (d) The fabricated sensor together with the measurement setup. (e) Measured responses of the sensor for water-ethanol solutions of various water volume fractions. Reprinted under CC-BY license from [199].

line excite the CSRR in the ground plane. The circuit model of such a circuit is also presented Figure 9(a), where the L_cC_c and R_c model the CSRR, the L stands for the inductive behavior of the microstrip section above the CSRR, and C models the coupling capacitance between the microstrip and the CSRR. At the resonance frequency defined by (3), the combination of C, L_cC_c is short circuited to the ground producing a zero in the S_{21} response of the sensor.

$$f_z = \frac{1}{2\pi\sqrt{L_c(C + C_c)}}. (3)$$

Loading any dielectric sample onto the CSRR modifies the value of C_c capacitance leading to a frequency shift from which the dielectric sample can be characterized. In comparison with the SRR, the CSRR offers a larger capacitive effect since the whole slot area around the resonator acts as a capacitive gap between the inner metallic patch of the resonator and the surrounding ground plane. At resonance, there is a highly dense E-field concentration at the lower side of the CSRR slot, which is ideal for microfluidic dielectric sensing. Thus, a microfluide channel made of Polydimethylsiloxane (PDMS) is fabricated and mechanically attached to the sensor aligned with the lower side of the CSRR for microfluidic dielectric sensing. The fabricated and assembled sensor is presented in Figure 9(c).



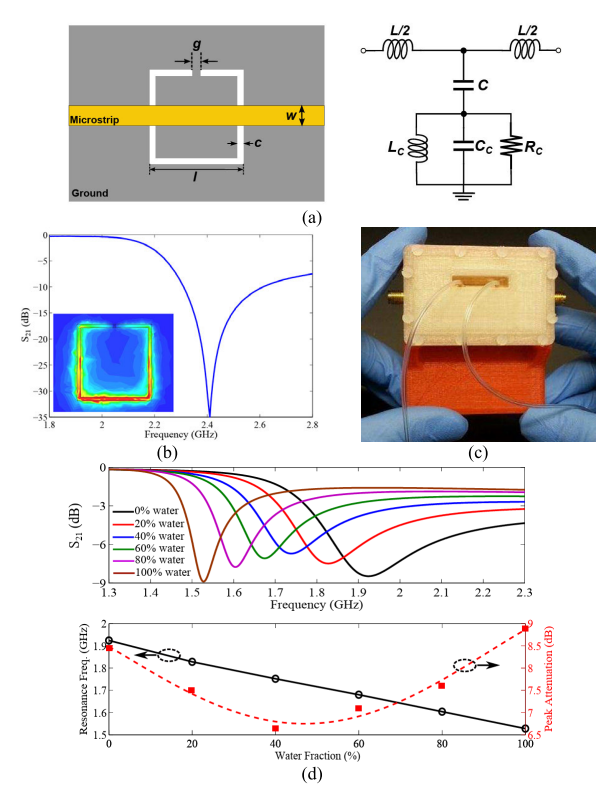


FIGURE 9. CSRR-based microfluidic sensor in [39]. (a) Sensor layout and the circuit model. (b) Full-wave simulated transmission response of the bare sensor together with the E-field distribution at resonance. (c) The fabricated sensor prototype. (d) Measured responses of the sensor for water-ethanol solutions of various water volume fractions. Reprinted with permission from [39]; copyright 2014 IEEE.

For verification of microfluidic dielectric sensing, water-ethanol solutions of different water fractions were used. As shown in the measured results, injection of different samples to the channel modifies the resonance frequency and depth of $|S_{21}|$ at resonance and such variations were used to develop a mathematical model for complex permittivity measurements. According to the measured results, the maximum frequency shift produced by the CSRR-based sensor is four times larger than the one of the SRR-based sensor in [199], while the bare sensor resonance frequency and the test samples (water-ethanol solutions) are the same for both of the sensor. This means that the CSRR-based sensor offers a fourfold sensitivity improvement compared with the SRR-based sensor mainly due to the larger effective sensing area in the CSRR compared with the SRR.

According to the circuit model of the CSRR-based sensor in Figure 9, and (3), two capacitors (C_c and C) contribute to the resonance frequency however, only the C_c capacitor is modified by loading the microfluidic LUTs onto the channel. Such a characteristic poses a limit to the frequency shift and as a result the sensitivity of the CSRR-based sensor. In order to address such a challenge, a new sensor was proposed in [56] using a microstrip transmission line loaded with a step impedance resonator (SIR) as demonstrated in Figure 10(a) together with its circuit model. In the circuit

model, the C_R capacitance models the edge capacitance between the rectangular patch of the SIR and the ground metallization realized on the top surface, which is electrically connected to the bottom ground plane using metallic via holes. Furthermore, the L_R stands for the inductive behavior of the narrow metallic strip that connects the microstrip line to the rectangular patch.

At the resonance frequency described by:

$$f_r = \frac{1}{2\pi\sqrt{L_R C_R}},\tag{4}$$

the combination of L_RC_R is short circuited to the ground resulting in a bandstop notch in the $|S_{21}|$ response of the sensor [Figure 10(b)]. There is a high concentration of E-field in the gap area around the capacitive patch of the sensor that is ideal for microfluidic dielectric sensing. Based on the circuit model, there is only one capacitor in the sensor (C_R) , which contributes to the resonance frequency and this capacitor is directly affected by implementing a microfluidic channel in the gap area of the sensor and injecting LUTs into the channel. Thus, it is expected that the SIR sensor offers a higher sensitivity compared with the CSRR-based sensor. This is verified through the measurement of the SIR sensor with water-ethanol solutions. According to the measured results in Figure 10, the SIR-based sensor produces larger frequency shift compared to the CSRR-based sensor, while the resonance frequency for the empty channel is almost the same for the two and the sensors were tested with identical LUTs. The average sensitivity of the SIR sensor is 1.7 times larger than the CSRR-based sensor.

This section studied microwave-based microfluidic sensors and some methods for improving the overall frequency shift and sensitivity in such sensors. A more detailed study of the sensitivity enhancement in microwave-based planar sensors will be discussed in Section IV of this article.

D. 3-D PRINTING

Additive manufacturing methods are drawing an increased attention among the researchers and electronic designers due to the low-cost manufacturing and offering additional freedom degrees in realization of complex structures that are not realizable using conventional fabrication methods [200]. Likewise, microwave engineering and sensor technology are also benefiting from the recent advances in threedimensional (3)-D) printing fabrication methods. Such technology led to the development of various novel microwave components and antennas with novel geometries that are challenging to implement using the other existing fabrication technologies [200]. More importantly, new generation of 3-D microwave sensors have recently been designed and developed offering fast and cheap alternatives to sensors used for various health care and IoT applications [199], [201], [202], [203], [204], [205], [206], [207].

One of the most prominent advantages of the 3-D printing fabrication is in the design and realization of microfluidic sensors. As discussed in the previous section, in microfluidic



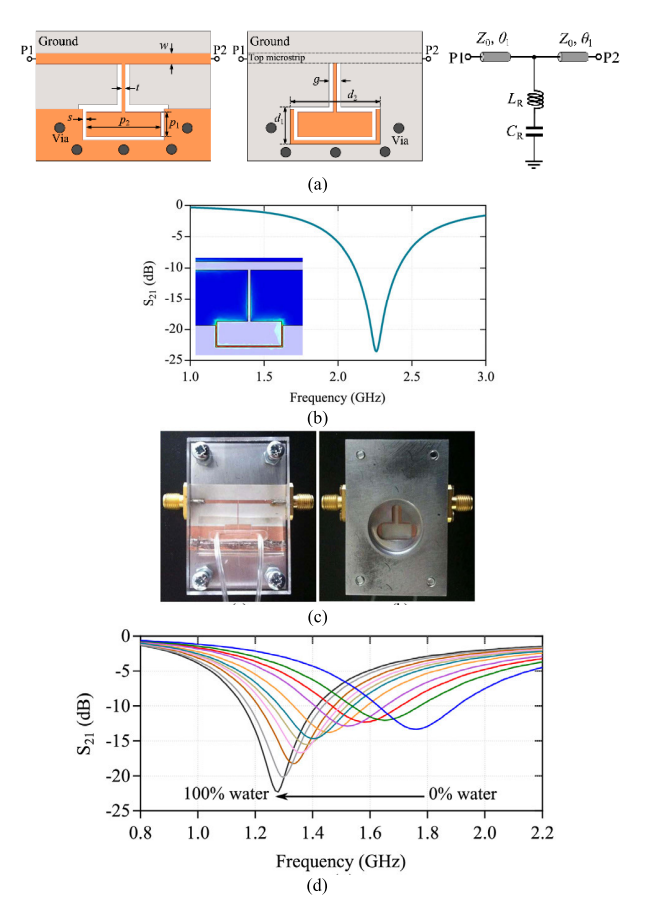


FIGURE 10. SIR-based microfluidic sensor in [56]. (a) Sensor layout and the circuit model. (b) Full-wave simulated transmission response of the bare sensor together with the E-field distribution at resonance. (c) The fabricated sensor prototype. (d) Measured responses of the sensor for water-ethanol solutions of various water volume fractions. Reprinted with permission from [56]; copyright 2019 IEEE.

sensors, a dedicated fluidic network is required to manipulate and guide the microfluidic test samples to the most sensitive area of the sensor. In conventional technologies, the microfluidic network is fabricated on PDMS or other biocompatible materials and then attached to the main microwave sensor circuit. In the majority of microfluidic sensors, a mechanical fixture is required to push the microfluidic network against the microwave circuit substrate and keep it in place to enhance consistency of the measurements. However, the addition of the fixture increases the total profile of the device and this is not desired specially for the integrated applications, where there is high necessity to have compact sensor for deployment within a small electronic package. 3-D printing can be of high advantage here since it allows the design and fabrication of both microwave circuit and microfluidic sections of the sensor within a single compact structure.

A sample prototype of the 3-D printed microwave microfluidic sensor is the one designed in [206] that is based on a SIW cavity resonator. A schematic view of this sensor is presented in Figure 11 together with the fabricated sensor prototype. The fundamental structure of the

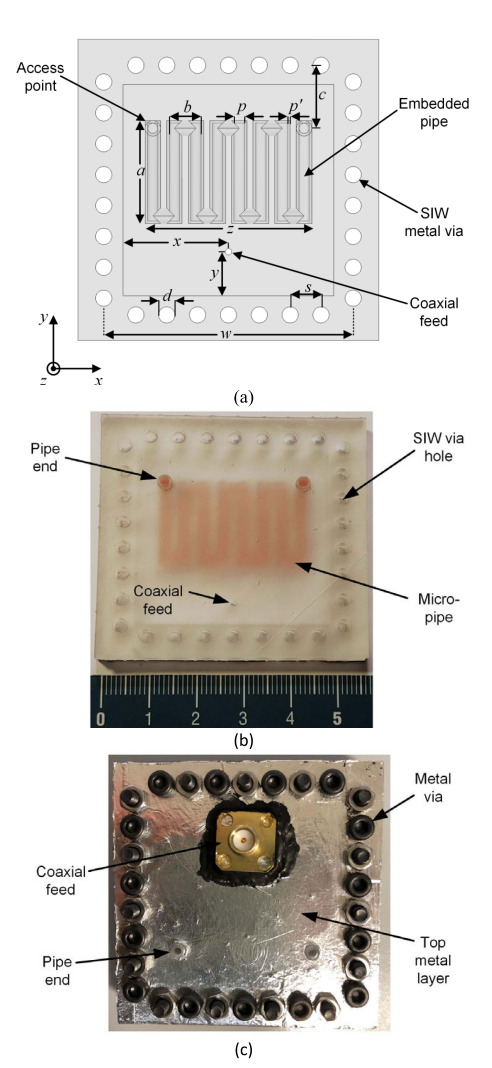


FIGURE 11. (a) Schematic view of the 3-D printed SIW-based microwave microfluidic sensor in [206]. (b) The 3-D printed substrate with the integrated microfluidic channel. (c) The final sensor prototype after adding the metallization layers, metallic vias, and the SMA port. Reprinted with permission from [206]; copyright 2020 IEEE.

sensor is a rectangular SIW resonator, where the multifolded microfluidic channel is integrated within the main dielectric substrate of the SIW using 3-D printing technology as shown in Figure 11(a) and (b). As seen, using such a design, the microfluidic network is directly integrated within the sensor structure alleviating the need for additional mechanical package to hold the microfluidic and the microwave resonator together. In fact, the microfluidic liquid-under-test (LUT) fills part of the SIW cavity and thus, the complex permittivity of the LUT contributes to the total effective permittivity of the SIW cavity and, in this way, the resonance frequency and the quality factor of the resonance is affected by the complex permittivity of the LUT. Such an effect is used in [206] for retrieving the complex permittivity of the unknown LUTs by measuring the resonance frequency and unloaded quality factor (O_u) .

3-D printing technique has also been used for the design of microwave sensors for complex permittivity of microfluidic



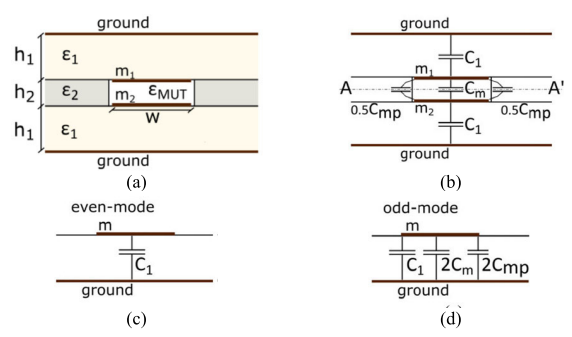


FIGURE 12. Conceptual schematic of the 3D printed microwave sensor in [207]. (a) Side view of the broad side coupled strip lines together with the 3D printed micro-cavity for microfluidic samples. (b) Representing the distributed capacitive network of the sensor. (c) The capacitive network under even-mode excitation. (d) Capacitive network under odd-mode excitation. Reprinted with permission from [207]; copyright 2020 IEEE.

samples over broadband. An example of such application was presented in [207], where broadside coupled strip lines were used for complex permittivity measurements. As shown in the conceptual view of the sensor in Figure 12(a), The LUT is sandwiched in between the two coupled strip lines using a 3-D printed insert layer, while the strip lines on the top and bottom layers are fabricated using conventional printed circuit board (PCB) technology. Plastic ports are attached to the 3-D printed insert acting as the in/outlets for the dielectric LUT as shown in Figure 13(d). By inserting the LUT in the channel between the strip lines, the sensor response can be analyzed under the even and odd-mode excitations. For the even mode, the pair of strip lines are excited symmetrically meaning that the magnitude and phase of the voltage distribution along the strip lines are the same. In this case, the symmetry line between the lines acts a magnetic wall and the total even-mode capacitance is:

$$C_e = C_1, (5)$$

where C_1 is the distributed capacitance between each of the strip lines and the ground plane. On the other hand, for the odd mode, the two strip lines are excited with equal magnitude but with 180° phase difference. This means that the symmetry line in between the strips acts as an electric wall and the total odd-mode capacitance is:

$$C_o = C_1 + 2(C_m + C_{mp}),$$
 (6)

where the C_m capacitance is attributed to the dielectric LUT and C_{mp} is attributed to the electric field fringing into the 3D-printed insert on the sides of the LUT. The relation between the complex permittivity of the LUT (ε_{LUT}) and the C_m is described as:

$$C_m = \frac{\varepsilon_0 \varepsilon_{LUT} w}{h_2}. (7)$$

This means that the ε_{LUT} has direct effect on the odd-mode characteristic impedance (Z_o) of the broadside coupled transmission lines. Therefore, the frequency dependent ε_{LUT} has been obtained by even and odd-mode analysis of the coupled strip pairs. The fabricated and assembled sensor

prototype is shown in Figure 13 presenting the top, bottom, the 3-D printed middle layer as well as the assembled sensor. This sensor was used to measure complex permittivity of various liquids such as Ethanol, Methanol, Isopropanol, etc. The measurements in [207] prove a high precision of the sensor in wideband complex permittivity measurements up to 3 GHz.

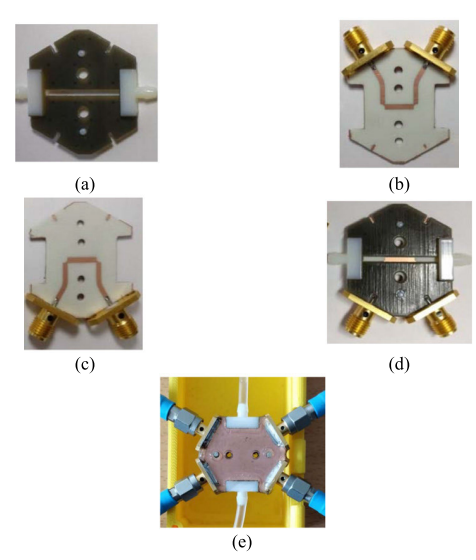


FIGURE 13. The fabricated broadside coupled strip line sensor in [207].

(a) 3D printed middle insert with plastic liquid in/outlets. (b) Top layer stripe line PCB. (c) Bottom strip line PCB. (d) The 3D printed insert placed on top of the bottom strip line PCB. (e) The final assembled sensor prototype. Reprinted with permission from [207]; copyright 2020 IEEE.

E. SUBSTRATE INTEGRATED WAVEGUIDE (SIW) SENSORS

When designing microwave sensors, most of the strategies to attain the desired sensitivity focus on the optimization of the topology of the sensor and its electrical characteristics, as shown in prior sections. While important, these factors are not the only ones impacting the final performance of the device. The sensing structure, including the position of the MUT and its influence on the response of the sensor plays also a crucial role. Indeed, this is often a limiting aspect for general microstrip sensors, characterized by an electric field chiefly confined into the substrate. When the MUT is placed in the upper volume of the sensor, as usual, its presence has a moderated influence on the weak radiated fields (fringing fields), thereby posing a limit for the sensitivity.

Trying to overcome this issue, other technologies were researched. Part of the scientific community placed their interest on the so-called substrate-integrated waveguide (SIW) configurations. A SIW structure is achieved with two copper-clad planes (top and bottom) and side rows of metallized vias, overall forming an effective cavity or waveguide inside the substrate [208], [209]. This configuration yields field distributions and responses akin to rectangular waveguides, including high Q factors, while considerably reducing the cost [208], [210]. As it will be shown in the next



paragraphs, the unique characteristics of these structures can be used for intriguing sensing purposes [211].

Indeed, SIW structures can be strategically conceived in order to generate considerable fields at interesting points close or next to the MUT, thus increasing the interaction with the sample. An example is the use of SIW sensors with slotted resonators in the sensing region, allowing the field lines to travel across the MUT, being therefore perturbed by the properties of the sample. These sensors are convenient for dielectric characterization of solid small-sized samples placed onto the slots [212]. A square slot was used for broadband characterization of the complex permittivity of small solid samples through the excitation of different TE modes [213]. Custom slotted resonators can be engineered on the top (or bottom) plane of the SIW, such as CSRRs, in order to have a response characterized by transmission zeros highly sensitive to the dielectric permittivity of a sample placed onto the slotted resonators [214]. This use of CSRR-loaded SIW was also proved effective for complex permittivity determination of solid slabs through the associated variations in the resonance frequency and quality factor [215].

This technique has been also used for microfluidic characterization with good sensitivities, placing the microfluidic channel just on top of the slot [216], or soaking the slot region into the liquid [217]. In another approach, two extensions were soldered to the top and bottom copper-clad planes of a SIW in order to have an empty-substrate prolongation of the structure, to be soaked into the liquid under test, providing for liquid characterization [218]. The CSRR-loaded SIW strategy has also found application in other contexts. For instance, a remote high temperature sensor for industry applications was proposed thanks to the microwave scattering read by an interrogating coplanar waveguide antenna [219]. In a different work, the CSRR structure was placed above an embedded sealed cavity inside the SIW, this cavity being sensitive to pressure, for remote pressure detection in hightemperature scenarios [220].

Another possibility of great interest, based on the cavity resonator technique, consists in directly embedding the MUT into the substrate thanks to the modern manufacturing techniques. This technique has been mainly exploited for microfluidic measurements, having the microfluidic channel (or pipes) flowing through the substrate in the SIW [221], as it can be seen in Figure 14. A usual cavity sensor is made of a cavity resonator with a hole drilled through the cavity. This hole is filled with the MUT or with the channel for liquid characterization [222], [223]. The presence of samples with different properties inside the cavity yields a perturbation noticeable enough to be characterized from the changes in the response of the sensor.

This idea has been applied with liquid pipes travelling vertically through the SIW. The integration of a metallic sheath covering the pipe before and after entering the SIW, as shown in Figure 14, was proved convenient for sensitivity improvement in complex dielectric characterization of liquids [221]. A similar approach exploited the propagation of

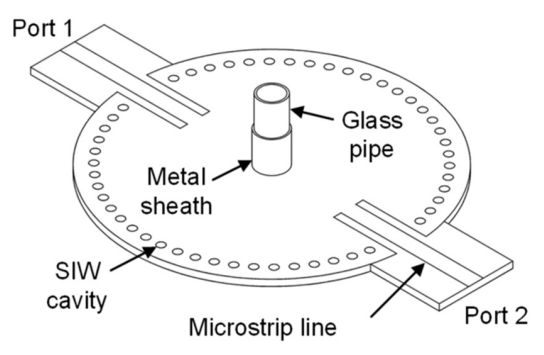


FIGURE 14. Example of a SIW cavity resonator sensor for characterization of permittivity in liquids, including a vertical pipe travelling through the SIW cavity and a metal sheath covering it. Reprinted with permission from [221]; copyright 2018 IEEE.

several TM modes for complex dielectric characterization of liquids applied to solute concentration detection, such as glucose concentration determination in aqueous solutions [224] or water–ethanol volume fraction [225].

In addition to the vertical crossing of the channel through the SIW, other re-entrant configurations have been proposed. This time, the input and output points for the channel lay in the same plane, the top or bottom plane of the SIW. This implies that that channel bends inside the substrate, and it might travel longer distances inside the SIW, thus facilitating a greater interaction with the inner fields, depending on the design. Sophisticated designs based on this concept were used for complex permittivity estimation in liquids [226], [227] and solute concentration detection [228]. Sensitive humidity sensors have also been developed under this scheme [229], [230].

F. TEXTILE SENSORS AND WEARABLES

The advancements in modern implementation techniques have notably pushed the boundaries of fabrication possibilities during the last years, allowing now for new ways of circuitry production that can seamlessly adapt to the requirements of certain applications, hitherto unimaginable. A good example is the recent development of textile and wearable pieces of sophisticated electronics. These devices can be integrated into garments or textile pieces, hence easing their use for specific sensing purposes in certain applications, such as quotidian or biomedical ones.

One of these enabling techniques was the printing of flexible electronics [231], [232]. This development allowed for passive flexible electronics devoted to certain applications, such as signal conditioning [233] or energy harvesting [234], [235], among others, leading to good performances. In addition to material characterization [236], soon these flexible electronic devices found application in wearable contexts [237] since they can be integrated into textiles thanks to its non-rigidity and low size [238]. For example, a wearable button antenna was produced using the fabric itself as substrate, intended for WLAN communications in multi-sensor systems [239]. Indeed,



textile-integrated body area networks are of great interest for advanced healthcare monitoring techniques [240]. The involved sensors can provide valuable information about many health variables and biomarkers, such as breath rate thanks to a wearable flexible spiral resonator tag [13], for example. A recent work proposed the use of a flexible monopole antenna for adaptive ablation in lung cancer treatment [241]. Other approaches used flexible microwave resonators as humidity sensors [242], [243], or sensors integrated into the fabric for detection of sweat and urine leakage [244].

As a complementary technology, the recent years have witnessed the development of directly embroidered microwave circuitry thanks to conductive threads, providing for perfect integration into garments [245]. As these electronic textiles or e-textiles feature seamless integration with clothes, they open the door for new sensing scenarios [246], [247]. The usual technique consists in implementing the layout directly into the fabric with a sewing machine and silver-plated nylon yarn [248]. There are several factors that will have an influence on the final results, such as the properties of the yarn and the fabric or the stitch filling pattern and dimensions, among others [249], [250], [251]. For instance, this technique was applied with a two-layer non-woven 100% polyester textile material (approximate thickness of 1.60 mm, $\varepsilon_r =$ 1.30, $\tan \delta = 0.0045$), covering the bottom layer (plane) with 35 μ m thick adhesive copper tape (conductivity of 5.8×10^7 S/m) [97]. With a resonant frequency-splitting sensing scheme (see Sect. II-B), this e-textile microwave sensor demonstrated effective water absorption detection capabilities with good sensitivity, as shown in Figure 15. Humidity e-textile sensors were proposed based on these principles [252].

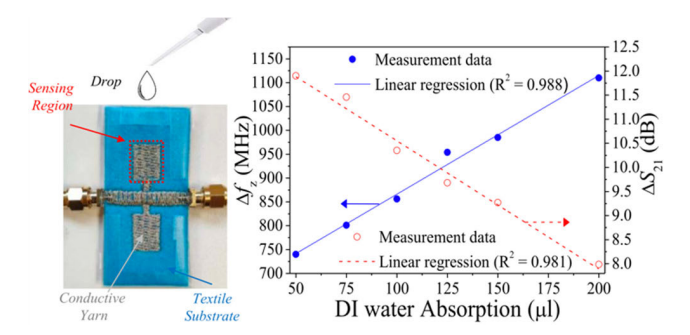


FIGURE 15. Picture (left) and results (right) for the frequency-splitting embroidered e-textile water absorption sensor in [97]. Reprinted with permission from [97]; copyright 2022 IEEE.

Making use of similar techniques, the possibilities of microwave embroidered e-textile sensors have been explored for several contexts in recent publications. A triangular patch broadband antenna loaded with shorting pins was proved effective for communications in the ISM band [253], which could benefit, for example, from an embroidered e-textile microwave bandpass filter [254]. Embroidered antennas for wearable applications based on double ring resonators were

proved to have specific absorption rates (SAR) meeting the strict medical standards [255]. Considering more specific medical applications, an embroidered low-frequency capacitive spiral was shown to have sucrose concentration determination properties when poured with different solutions [256], or an e-textile ultrawideband monopole antenna on cotton substrate was proved to perfectly adapt to any woman's breast shape for microwave imaging and breast cancer screening [257], among others.

Apart from the evident biomedical interest, these sensors have also been shown useful for general material characterization [258]. In general, in addition to their consummate integration into clothes or adaptation to the required shapes, these devices possess other interesting features such as washable or stretchable properties [259], [260]. As a matter of fact, although still facing some challenging limitations such as restricted conductivity in the yarns, lack of absolute robustness or occasional need for "non-embroiderable" elements (connectors, wires...) [261], [262], this technology is definitely positioning itself as an active frontier for microwave sensors in many daily life and biomedical applications.

G. GREEN SENSORS

The current trends on planar microwave sensors show several aspects to put the focus on. Optimization of certain performance metrics, such as sensitivity or resolution is always sought (see Sect. IV), and also implementation techniques adapted to any situation. In the latter sense, a relatively new research line seeks the production of more environmentally friendly microwave sensors, also known as green sensors. The basic principle of these sensors lays on the utilization of paper substrates and organic conductive ink for the layout.

The use of cellulose materials as substrate, besides ecofriendly, also shows some advantages such as low cost and thin implementations, at the expense of a high porosity and roughness [263]. The layout can be achieved by deposition inkjet printing with conductive ink, featuring high accuracy and good adaptation to the material [264], [265]. Instead of a traditional metallic ink, biocompatible organic conducting polymers can be used to obtain organic ink, one of the most common ones being Poly(3,4-ethylenedioxythiophene) polystyrene sulfonate (usually referred to as PEDOT:PSS) [266], [267]. Although PEDOT:PSS-doped inks show lower conductivities than those of metallic inks, they hold other beneficial characteristics such as organic, biocompatible or easy of processing [268]. The marriage of paper substrate and organic ink results in environmentally friendly and fully recyclable sensors, i.e., green sensors.

This concept has been applied chiefly for the production of green RFID sensors [269]. As an example, a green wireless gas sensor was achieved by integrating a flexible RFID tag with a single wall carbon nanotube with these techniques, proved effective for detecting toxic quantities of ammonia or nitrogen oxide [270]. Using similar techniques, carbon



dioxide and humidity RFID sensors were implemented for air pollution detection purposes with good results [271]. In a different approach, although with implementation techniques akin to the ones exposed here, green chipless RFID tags were demonstrated effective for authentication purposes thanks to chains of resonators interrogated by a bespoke reader [272]. It is therefore easy to see the wide possibilities of this technology, while providing undoubted advancement towards a more respectful and eco-friendlier electronics industry [273].

IV. PERFORMANCE OPTIMIZATION TECHNIQUES

Sensor performance optimization is the main target of researchers involved in planar microwave sensors. There are many sensor performance indicators, but those that have been the subject of a more intensive research activity (with researchers pursuing their optimization) are probably sensor sensitivity, resolution, and selectivity.

A. SENSITIVITY OPTIMIZATION

There are several techniques for sensitivity optimization in planar microwave sensors. Most of them are based on the design of the sensor, but there are also strategies related to the specific arrangement of the analyte, or MUT, with respect to the sensitive part of the device. These techniques will be reviewed next.

1) COUPLED RESONATORS

The use of coupled structures has been proved conducive for boosting the sensitivity in certain configurations [274], [275]. The concept comes from the band-pass filter design realm, where the frequency response of the final device is remarkably sensitive to the different couplings between the involved resonators [276]. Contrarily to the filtering applications, where a higher order (larger number of resonators) means a better performance, for sensing purposes usually two coupled resonators are enough (e.g. [116], [278], [279], [280],) since this sensitive effect can still be attained while keeping compactness.

Without loss of generality, let us consider a two-port network composed of two identical lumped-element shunt RLC tanks electrically and magnetically coupled, where the input/output coupling is relatively low in comparison with the inter-resonator coupling, as described in [281] and shown in Figure 16. For a given resonance frequency in the resonators, the S_{21} response, both in magnitude and phase, will depend on the external Q factor (Q_{ext}) , the unloaded Q factor (Q_u) and the coupling factor (k), as analyzed in [282]. As shown in [281] and illustrated in Figure 16(b)-(e), the variations of any of these parameters yield notable changes in the response. If the MUT is placed within the inter-resonator region or in any position so that its presence has an impact on the value of these parameters, in addition to the impact on each isolated resonator, the device can leverage these aggregate effects for a synergic increase of the sensitivity.

Some works have researched these effects with different approaches. Close scrutiny of the plots in Figure 16 reveals that most of the benefits of the coupled structure come from variations in the quality factors, which are of special interest for solute concentration sensing in aqueous solutions [283], as introduced in Sect. II-a. Particularly, the use of a Q_u -based coupled-resonator sensor was demonstrated to outperform the single-resonator analogue case for glucose concentration measurement in water solutions [284], reaching 298% sensitivity increase with a sample volume 5 times smaller [277]. The convenience of this approach has also been acknowledged and exploited for general permittivity sensing in solids [278], [279], [285], [286], [287], [288], including anisotropy measurements [288], [289]. It is worthwhile to mention that the seminal sensor in [277] also demonstrated measurement capabilities by means of the coupling factor (k) variation, as anticipated from Figure 16(b), which could be of interest for certain applications. Indeed, the possibility of having aggregate effects visible through different metrics from the response of the sensor, as shown in Figure 16, places the coupled-resonator sensors as potential candidates for multi-sensing and enhanced selectivity applications [3], [280], [290], [291], [292], [293], as it will be discussed in Sect. IV-c.

The plot in Figure 16(e) also bespeaks the potential of the coupled paradigm for increasing the sensitivity of the phase-variation sensors introduced in Sect. II-c. Particularly, for reflective-mode phase-variation sensors, a good strategy emerges from the use of a weak coupling between the resonators, which yields split-resonances close to each other, experiencing the phase of the reflection coefficient a notable shift (360° neglecting losses) between these frequencies, i.e., a notably sharp phase slope in a relatively narrow frequency span. This aspect effectively boosts the sensitivity for these sensors tuned between the split-resonances. This concept was in-depth analyzed with weakly coupled distributed resonators [116] and with weakly coupled semi-lumped resonators [117], [123], demonstrating high sensitivities of up to 736° and 818° per unit of dielectric permittivity, respectively. As it can be seen, this is an elegant alternative to the impedance inverters cascading technique for sensitivity enhancement that will be described in Sect. IV-A-II, since comparable sensitivities can be achieved while avoiding the overall sensor size increase imposed by that technique [294].

Concerning transmission-mode devices, an interesting technique consists on coupling resonators to a two-port transmission line, with proved sensitivity improvement effect [51], [56], [89], [295]. This results in transmission zeros in the final response, each one associated with a resonant mode. If an extra resonator with a high Q-factor is coupled to one of those low Q-factor resonators, with overlapping frequencies, their strong coupling shifts the original transmission zero into a sharp transmission peak surrounded by a pair of transmission zeros. The variations of the resonance frequency and Q-factor of this transmission peak were proved highly



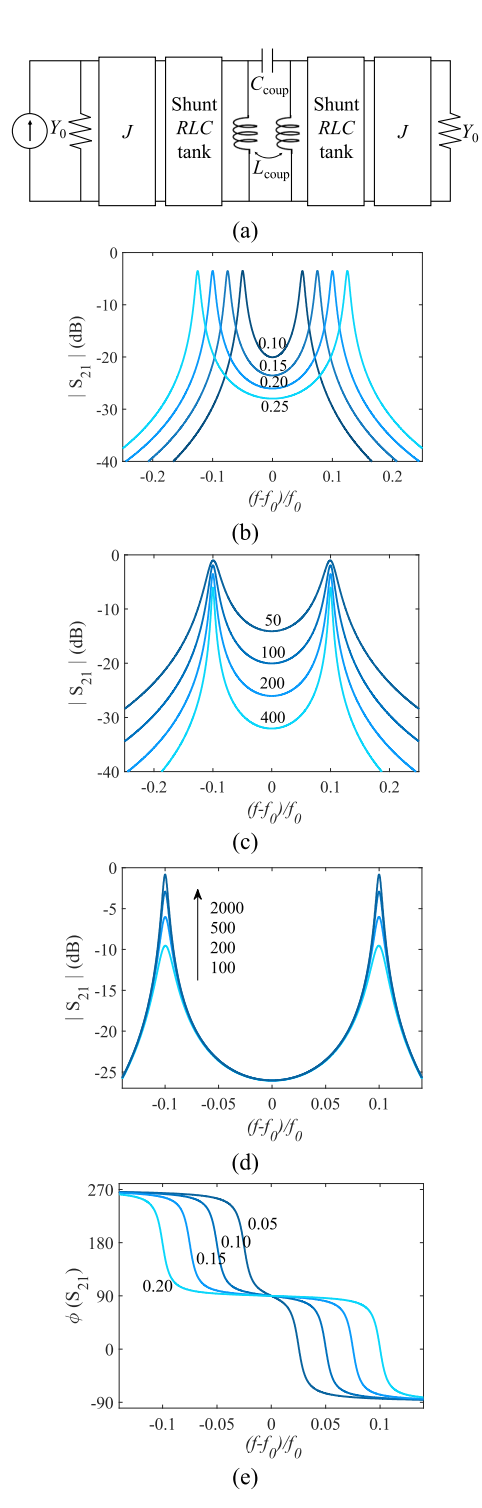


FIGURE 16. Illustration of the interest of coupled-resonator structures for sensitivity boosting. (a) Schematic of a two-port network with two identical lumped-element shunt RLC tanks electrically and magnetically coupled, where Y_0 is the characteristic admittance of the ports, J elements are admittance inverters modelling input/output couplings and C_{coup} and L_{coup} are the lumped elements modelling the electric and magnetic inter-resonator couplings; (b) transmission response for fixed $Q_u=400,\,Q_{ext}=200$ and different values of $k;\,(c)$ transmission response for fixed $Q_{u}=400,\,k=0.20$ and different values of Q_{ext} ; (d) transmission response for fixed $Q_{ext}=200,\,k=0.20$ and different values of $Q_u;\,(e)$ phase of the transmission response for fixed $Q_u=\infty$ (lossless case, for simplicity), $Q_{ext}=100$ and different values of k.

sensitive to the complex permittivity of liquid samples with different configurations [296], [297].

Other approaches have made use of coupled-line sections acting as dielectric permittivity sensor. By putting the sample on the top of the coupled-line section, its dielectric constant can be retrieved from the analysis of certain parameters of the response of the device. A computation method from the differential scattering parameters for differential excitation coupled-line sensors was proved to yield high sensitivity for considerably small solid [298], [299] and microfluidic [207] samples. The isolation level resonance frequency of a high-isolation coupled-line directional coupler was shown to be remarkably sensitive to the changes in the dielectric constant of solid and liquid samples [156].

2) PHASE/MAGNITUDE SLOPE CONTROL

In single-frequency sensors (i.e., phase-variation and magnitude-variation sensors), either the magnitude or the phase of the transmission or reflection coefficient is the typical output variable. As anticipated in Sections II-C and II-D, a high slope in the frequency response of the considered output variable (the magnitude or the phase) is instrumental in achieving a high sensitivity (see Figures 3 and 6). In magnitude-variation sensors, enhancement of the magnitude slope can be achieved through designs that provide closely spaced zeros and poles [154], [155]. In phasevariation sensors, there is typically a significant variation in the phase between a zero and a pole (regardless of whether the sensor operates in reflection or transmission). Thus, designs based on sensing resonators exhibiting closely spaced resonance and antiresonance frequencies have been reported [131], [136]. Nevertheless, there are other strategies for enhancing the phase slope at the operating frequency (and hence the sensitivity), to be briefly discussed next.

One of such techniques is based on the use of a sensing resonator cascaded to a set of impedance inverters with alternating high and low impedances (as compared to the reference impedance of the ports, typically, $Z_0 = 50 \Omega$). Most of these reported sensors operate in reflection [108], [109], [110], [111], [112], [121], [124], [126], but this technique can also be applied to transmission-mode phasevariation sensors [133], [138]. Figure 17 illustrates this sensitivity optimization technique in a transmission-mode sensing structure, based on an openended quarter-wavelength sensing line (in shunt connection) and either one or three inverter stages (implemented by means of quarter-wavelength line sections at the operating frequency) cascaded to it. The sensitivity in the vicinity of the REF dielectric constant is much higher for the sensor that includes three inverter stages since there is a multiplicative effect that depends on the normalized impedances of the inverters, this effect being increased with the number of inverters, as detailed in [133].

Although effective, the previous sensitivity enhancement approach in phase-variation sensors presents a limitation,



namely, the presence of inverters increases the overall sensor size (but not the size of the sensing region). A high phase slope, and hence high sensitivity, can be achieved by merely coupling an identical resonator to the sensing resonator [116], [117], [122], [123], [124], [125], [126], [127], [128], [129], [130], [131], [132], [133], [134]. Typically, this does not significantly increase the sensor size. This phase slope enhancing strategy is illustrated in Figure 18, in regard to a reflective-mode device with coupled resonators described by means of series LC tanks electrically coupled. Due to interresonator coupling, the resonance of the uncoupled resonator splits into two frequencies, f_{-} and f_{+} , with a phase excursion of 360° (provided losses are small) between such frequencies. Therefore, by weakly coupling the sensing resonators, the phase slope is expected to be very high, since closely spaced split resonances will be generated under weak coupling. The frequency of operation must be tuned in between the two resonances, the optimum point being roughly the one where the phase slope is a maximum (approximately f_p , in Figure 18).

A relevant advantage of this technique is that, since inverters are not used, changing the frequency of operation (dictated by the dielectric constant of the REF sample) does not require a sensor redesign. Moreover, such sensitivity optimization technique is very efficient, as illustrated in Figure 19, where a specific sensor based on a pair of coupled resonators, as well as its phase response and sensitivity are depicted [123]. Note that the maximum sensitivity, inferred from the simulated data points (by including losses), is $S_{Lossy} = -818^{\circ}$ per unit of dielectric constant variation, a very high value. Although the reported example is specific of a pair of electrically coupled resonators, described by a series LC tank, a similar behavior is obtained regardless of the coupling mechanism (electric or magnetic) and resonator configuration (series or parallel) [139]. Moreover, highly sensitive reflective-mode phase-variation sensors based on coupled distributed resonators have also been reported [116].

Inspection of Figure 19(c) indicates that the maximum sensitivity inferred from the lossy electromagnetic simulations is superior to that obtained when losses are excluded $(S_{Lossless} = -774^{\circ})$, very similar to the theoretical prediction $(S_{Th} = -775^{\circ})$, see the analytical model by excluding losses that provides such result in [123]). Indeed, with an adequate design, losses help to boost the maximum sensitivity in reflective-mode phase-variation sensors, because losses contribute to enhance the phase slope at resonance, as it was demonstrated in [121], [122], [126], [130], and [137]. Moreover, losses can be engineered, and tuned, to control the sensitivity, as pointed out in [130] and [137], where a junction field effect transistor (JFET) was used as a variable conductance in a reflective-mode phase-variation sensor based on a transmission line terminated with a simple stepped-impedance resonator (SIR). That sensor was applied to submillimeter scale proximity measurements (based on

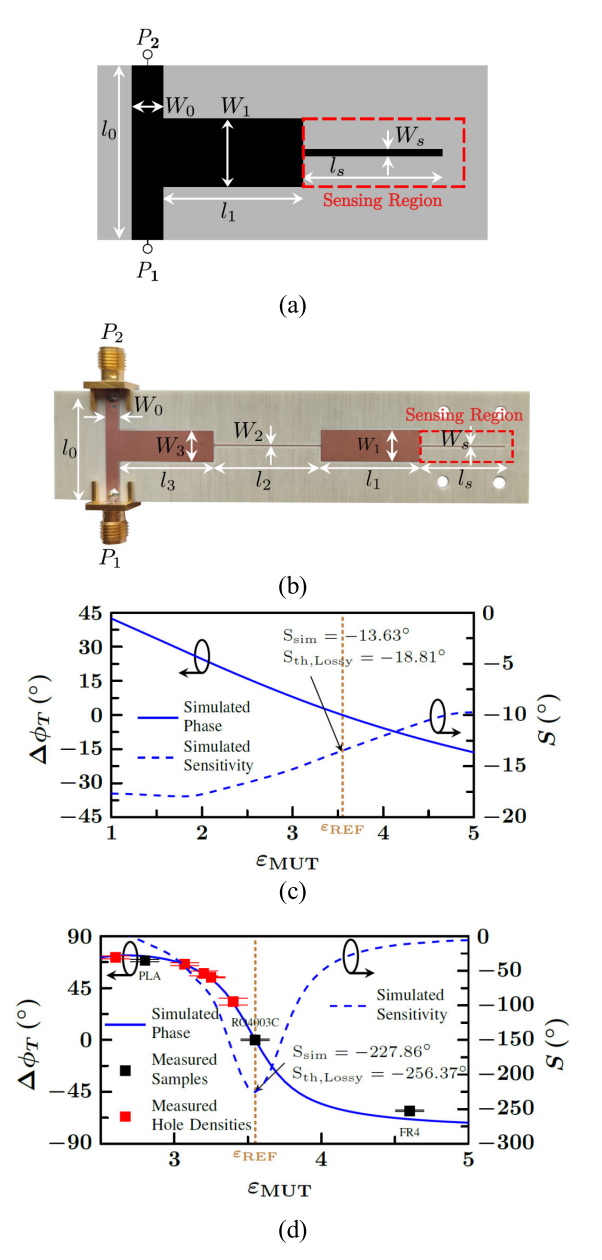


FIGURE 17. Illustration of the sensitivity optimization technique based on cascaded inverters with alternating high and low impedances applied to a transmission-mode phase-variation permittivity sensor. The output variable is the phase of the transmission coefficient at the resonance frequency of the open-ended quarter-wavelength sensing resonator when it is loaded with the REF sample (a semi-infinite MUT with a dielectric constant of 3.55). (a) Layout of the device with a single inverter; (b)photograph of the device with three inverters; (c) Simulated phase response of the sensor in (a) and sensitivity; (d) simulated phase response of the sensor in (b) and sensitivity, as well as measured phases at the operation frequency, for the indicated samples. In (d), the black symbols correspond to the measured phases for specific samples, whereas the red symbols correspond to the phases measured when the sensitive region is coated with the REF sample with different densities of holes(emulating defects). Note that we have actually represented $\Delta\phi_{\rm T}=\phi_{\rm T}-\phi_{\rm T},_{\rm REF}$, where $\phi_{\rm T},_{\rm REF}$ is the phase of the transmission coefficient at the operating frequency for the REF sample (in such a way, the effects of the access lines are eliminated). Dimensions(in mm) are $W_S = 0.2$, $I_S = 19.7$, $W_1 = 7$, $I_1 = 22.09$, $W_2 = 0.2$, $I_2 = 24.339$, $W_3 = 7$, $I_3 = 10.0$ 22.09, $W_0 = 3.36$, $I_0 = 25.64$. Reprinted with permission from [133]; copyright 2025 IEEE.



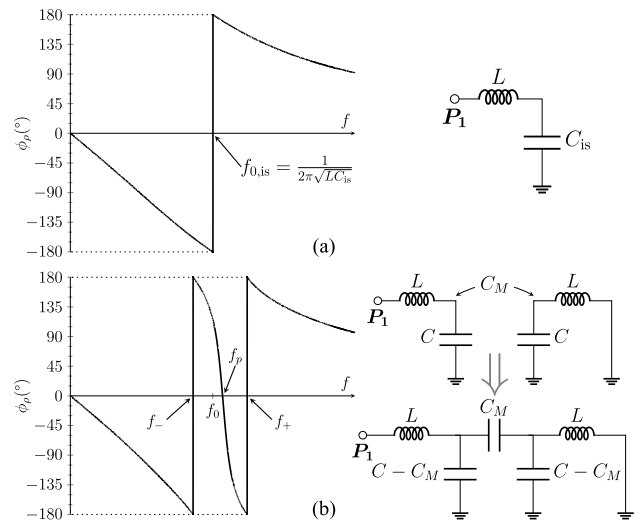


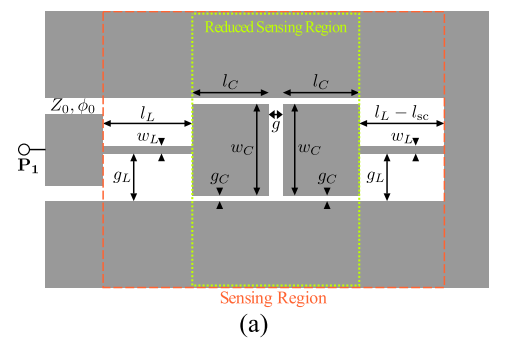
FIGURE 18. (a) Isolated series resonator connected to ground and phase of the reflection coefficient; (b) Two (electrically) coupled resonators and phase of the reflection coefficient. $C_{\rm is}$ is the capacitance of the isolated resonator, C is the self-capacitance of the uncoupled resonator (i.e., with the presence of the other resonator short-circuited to ground), L is the inductance of the resonators, and $C_{\rm M}$ is the coupling capacitance.

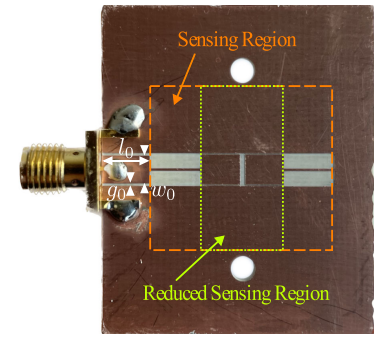
the changes in the effective dielectric constant consequence of separating a dielectric slab from the sensing region), and the maximum achieved sensitivity was as high as $S_{max} = 2291^{\circ}/\text{mm}$. Nevertheless, it should be mentioned that this losses-assisted sensitivity optimization technique does not apply to transmission-mode sensors, where losses tend to degrade the sensitivity, as discussed, e.g., in [133]. The reflective-mode phase-variation sensors reported in [130] and [137], where the sensitivity is enhanced by engineering losses, were designated as lossy sensors in those works.

3) RESONATOR PATTERN OPTIMIZATION

As discussed in Section III-C, in order to enhance the sensitivity in planar microwave sensors, a particular effort was dedicated to increase the effective sensitive area of the sensor or to increase the E-field concentration within the sensing region. A simple and efficient approach that was first proposed in [39] is to use complementary (or slot) resonators instead of the conventional planar resonators. Generally, complementary resonators produce a larger capacitive effect resulting in larger effective sensing areas through which the active sensitive region would be increased resulting in a higher interaction between the fringing E-field at resonance and the material-under-test (MUT) resulting in higher sensitivities.

Over time, resonators with more complicated geometries have evolved to increase the E-field concentration or to further increase the effective sensing area. Examples of such approaches are the integration of interdigital capacitors within the CSRR structure coupled to a microstrip transmission line in [300]. A schematic of this design is presented in Figure 20. As seen, by embedding interdigital capacitor within the CSRR slot, the effective sensitive area (area with large E-field concentration) is increased. This





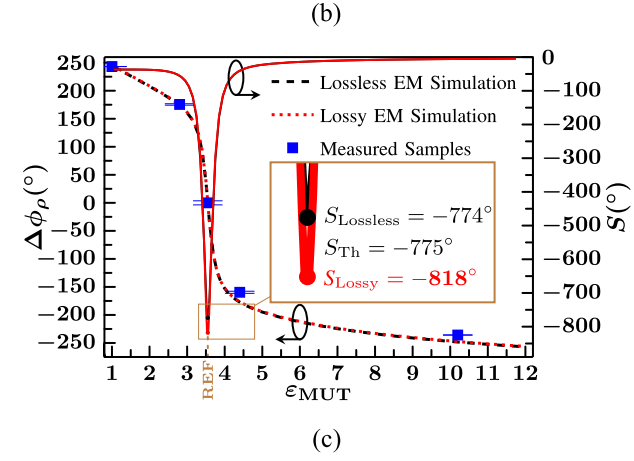


FIGURE 19. Layout (a) and photograph (b) of the fabricated sensor based on a pair of weakly coupled SIRs in CPW technology, and phase dependence of the sensor with ε_{MUT} , and sensitivity (c). The phase is the one in reference to the phase when the sensor is loaded with the REF sample, i.e., $\Delta\varphi_{\rho}=\varphi_{\rho}-\varphi_{\rho,\text{REF}}$. Dimensions (in mm), are: $l_0=6.0$ mm, $w_0=3.39$ mm, $g_0=0.305$ mm, $l_L=6.40$ mm, $w_L=0.3$ mm, $g_L=1.85$ mm, $l_C=4.86$ mm

sensor was used for microfluidic dielectric characterizations by implementing a meandered microfluidic channel along the sensitive slot of the sensor [Figure 20(c)]. The measured results of the sensor with fluidic dielectric samples prove a higher sensitivity compared with the other sensors for a large range of the permittivity values.

Another example of shape optimization for sensitivity enhancement is the microfluidic sensor presented in [301] using a hybrid slot resonator formed by embedding an interdigital capacitor and two CSRRs within a complementary electric-LC (CELC) resonator. As proved in [302] through circuit analysis of the (CELC) resonators coupled

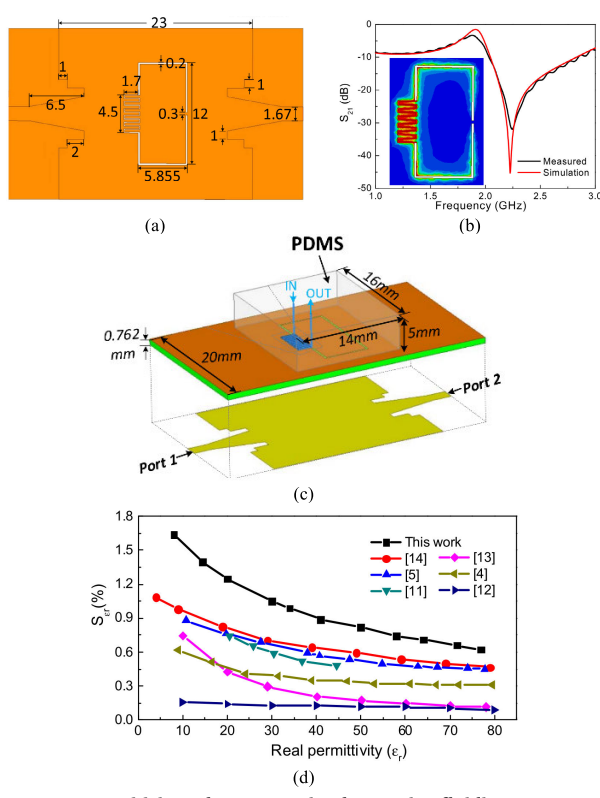


FIGURE 20. Sensitivity enhancement in planar microfluidic sensor through integration of interdigital capacitor with a CSRR resonator [300]. (a) Layout of the sensor. (b) Full-wave simulated |S₂₁| together with E-field distribution at resonance. (c) 3D view of the designed sensor. (d) Sensitivity comparison with the other sensors. Reprinted with permission from [300]; copyright 2020 IEEE.

to microstrip transmission lines, the CELC shows even- and odd-mode resonances, where there is a high concentration of E-field around the middle slot of the resonator in odd-mode resonance as shown in Figure 21(a). By integrating an interdigital capacitor along the middle slot, the effective sensing area is increased with a higher E-field concentration and as indicated in Figure 21(b), the E-field density is further improved by embedding two CSRR slots within the two halves of the CELC resonator. A microstrip line coupled to the final shape optimized resonator was used in [301] for microfluidic dielectric sensing, by integrating a PDMS channel around the interdigital slot of the resonator as shown in Figure 21(b). The sensitivity enhancement for microfluidic dielectric characterization was investigated by performing measurements with water-ethanol solutions. The measurements shown in Figure 21(c) prove significant sensitivity enhancement compared to the other planar microfluidic sensors.

Shape optimization has also been applied to the other non-complementary resonators for sensitivity enhancements. Majority of the designers focused on the design of meandered resonator patterns [303], [304], integration of interdigital shapes within the capacitive part of the resonators [305] and using cross-bridges within the capacitive part of the resonator to form parallel plate capacitances for improving the interaction between the fringing E-field and the MUT [306].

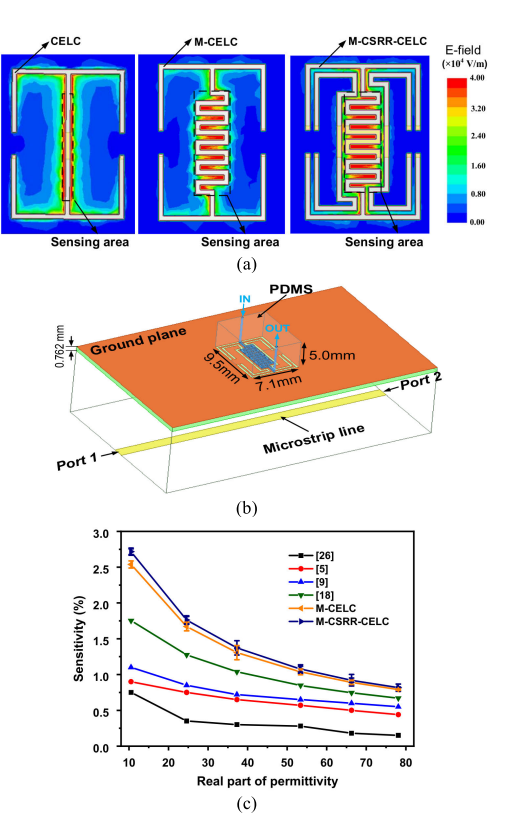


FIGURE 21. Sensitivity enhancement in planar microfluidic sensor Using a modified CELC resonator [301]. (a) E-field enhancement through shape optimization. (b) 3D view of the designed sensor. (c) Sensitivity comparison with the other sensors. Reprinted with permission from [301]; copyright 2021 IEEE.

As explained before, the major goal in these attempts is increasing the effective sensing area and improving the concentration of the fringing E-field at resonance to enhance the sensitivity.

4) EMBEDDED CHANNELS

Another approach for sensitivity enhancement in microwave microfluidic sensors is embedding the channels containing the dielectric liquids into the main sensor substrate. Generally, higher sensitivity can be obtained if a larger part of the electric field from the resonators interacts with the LUT. In conventional designs of the planar resonators, a significant part of the generated E-field is confined within the main dielectric substrate of the sensor especially in the sensors designed in microstrip technology. Such an effect produces parasitic capacitances that do not contribute to sensing and reduce the overall sensitivity. In order to alleviate such challenges, in some designs such as [56] and [155], the ground metallization is removed around the main resonator to remove such parasitic effects. However, the parallel plate capacitance formed between the main metallization of the resonator and the ground plane can be used for sensing if the microfluidic channels are embedded within the sensor substrate.

Implementation of such structures is challenging using conventional printed circuit board (PCB) technology.



In conventional PCB sensors, usually a cavity is milled through the substrate and a capillary is inserted in the cavity to contain and guide the liquid into the sensitive part of the resonator. Such an approach is used in [66] and [307] as shown in Figure 22. However, the realization of more complicated channel geometries such as meandered and spiral structures is challenging using simple milling techniques.



FIGURE 22. Microfluidic channel embedded within the sensor substrate by micro-milling a cavity within the dielectric substrate of the sensor in [66]. Reprinted with permission from [66]; copyright 2022 IEEE.

Recently, by the advent of advanced fabrication technologies such as 3-D printing, and low temperature cofired ceramic (LTCC) the microfluidic channels of arbitrary shapes can be easily embedded within the sensor substrate. An example of meandered microfluidic channel integrated within the 3-D printed SIW cavity sensor for sensitivity enhancement was presented in Section III-D. Another example of embedding the channel within the substrate of a planar sensor through 3-D printing is the sensor in [308], which is based on stub-loaded microstrip transmission line. As shown in Figure 23, the sensor substrate is 3-D-printed with embedded channels using SLA that is water-tight material. Next, the top metallization pattern was dispenser printed on a flexible substrate and then attached to the top surface of the 3-D printed substrate. This sensor can simultaneously characterize three different liquid samples at three different frequency bands using three resonant stubs loaded on a microstrip transmission line.

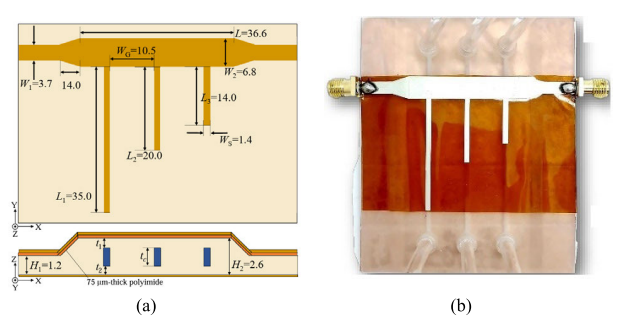


FIGURE 23. Embedding the microfluidic channel within the planar sensor substrate using 3D printing in [308]. (a) Schematic of the sensor and (b) the fabricated and assembled sensor. Reprinted under CC-BY license from [308].

Microfluidic channels can be integrated within the sensor substrate using the LTCC technology as well. In LTCC technology, electronic circuits can be implemented using a multi-layer fabrication of metallic and dielectric materials. Such technology enables the integration of micro-channels together with electronic circuits. A sample realization of

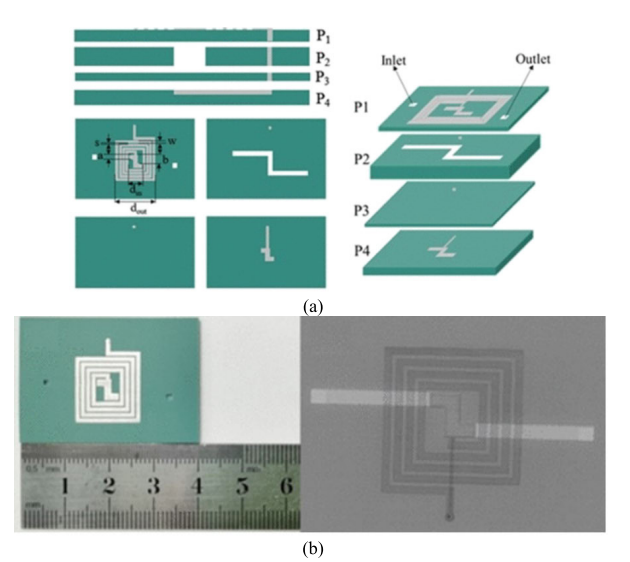


FIGURE 24. Embedding the microfluidic channel within the planar sensor substrate in LTCC technology [309]. (a) Layout and stack up view of the resonator. (b) The fabricated resonator together with X-ray image showing the embedded channel. Reprinted under CC-BY-NCND license from [309].

the microfluidic channels within the main substrate of a microwave sensor was presented in [309], where a semilumped parallel LC resonator (Figure 24) coupled to an inductive loop was used for detection of heavy metal pollutants in drinking water.

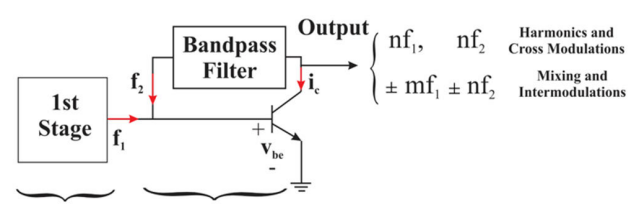
5) INTERMODULATION PRODUCTS

An interesting approach for sensitivity optimization in frequency-variation sensors was proposed based on intermodulation products (IMP), proved able to multiply by an integer number the frequency shift associated to a change in the permittivity of the sample [58], [310]. The idea leverages the non-linearity of active components such as transistors. This non-linearity may yield IMP of two tones, resulting in a more pronounced frequency shift due to permittivity variations in the sample than the one seen in a conventional frequency-variation sensor, as long as at least one of those tones belongs to the signal coming from the sensor.

The mixing capabilities of regenerative active resonators place them as good candidates for the realization of the IMP. To achieve mixer operation, one of the tones (let f_1) is driven from an oscillator, whilst the other one (let f_2) is originated in a feedback oscillator loop including a bandpass filter devoted to tune this second oscillation frequency, as shown in Figure 25. As shown in the figure, the non-linearity of the transistor in the feedback loop makes harmonics and IMP appear. Some of the IMP components are located at $2f_1$ – $f_2 = f_1 - \Delta f$, $3f_1 - 2f_2 = f_1 - 2\Delta f$, $4f_1 - 3f_2 = f_1 - 3\Delta f$,..., where $\Delta f = f_2 - f_1$. Consequently, when a change in the permittivity of the sample leads to a shift in f_1 , this shift is magnified by the IMP index as $2\Delta f_1$, $3\Delta f_1$, $4\Delta f_1$... While the first stage (as sensing element, see Figure 25) shows a shift of only Δf_1 , the 7th IMP (for example) shifts by $4\Delta f_1$. As a result, advantage can be taken from these IMP and mixing



features in order to multiply the frequency shift by an integer number, with undoubted sensing potential.



Oscillator Active Resonator

FIGURE 25. Concept of mixing/intermodulation using double stage active resonator. Reprinted with permission from [58]; copyright 2020 IEEE.

This approach was put into practice with a two-stage sensor, including a sensing oscillator and an active resonator, with double SRRs (dubbed DSRR) as resonators [58], [310]. Signals at $f_2 \approx 5.00$ GHz and $f_1 \approx 4.75$ GHz were generated using the DSRRs as the tank of oscillators. Each DSRR was included in the feedback loop of a regenerative amplifier, its operation being transformed into a feedback oscillator after loss compensation. Mixing stage followed by using the second sensing oscillator as both generator of f_2 and mixing element for the injected f_1 . Wideband high-gain linear antennas were also included for remote sensing capabilities. The concept was proved with measurements of liquids such as ethanol, methanol, acetone and others [58], [310], as well as water-glucose solutions [58]. The results showed effectively multiplied downshifts in the 3^{rd} , 5^{th} and 7^{th} IMP proportional to the IMP index, thus proving the sensitivity enhancement effect.

B. RESOLUTION OPTIMIZATION

Resolution, defined as the minimum amount of input variable, or the minimum change in this input variable, that can be reliably detected, is an important parameter indicator in many applications. Resolution is intimately related to sensitivity. Usually, highly sensitive sensors provide also a good resolution. Nevertheless, in analog sensors, resolution is ultimately dictated by the noise level. In frequency-variation resonant sensors, well defined peaks or notches (related to their quality factor) contribute to improved sensor resolution. To achieve such high-quality factors, loss compensation by using active feedback loops has been proposed, with the result of active sensors. Alternatively, differential techniques, based on the measurement of the cross-mode transmission or reflection coefficient, have been considered for the implementation of a specific type of sensors exhibiting a good resolution. These techniques are succinctly reviewed next.

1) ACTIVE SENSORS

Currently, the resolution of the planar microwave ring resonator sensors is mainly determined by their quality factor. This is while typically ring resonator sensors suffer from moderate quality factors, which will consequently decrease their resolution when exposed to material with similar dielectric properties. The addition of active feedback circuits to a planar ring resonator can drastically improve the quality

factor [311]. In the method of regenerative feedback loop with an active device such as BJT to a passive resonator [Figure 26(a)], a 180° phase shift is created on the output while another 180° phase shift is introduced by the passive resonator. Therefore, constructive feedback compensates the power loss and increases the quality factor. Consequently, the resolution and minimum detectable signal, which are the two main features of a high-quality sensor, are enhanced by orders of magnitude. This concept, due to its ability to significantly enhance sensitivity and resolution, has been explored across various applications of microwave ring resonator sensors, including liquid characterization, microfluidic analysis, gas sensing, and wireless communication [312], [313], [314].

Zarifi et al. demonstrated the implementation of active feedback assisted microwave split ring resonators (SRR) in liquids with different dielectric properties and various concentrations of KOH in water as low as 0.1 mM. The quality factor of the bare resonator structure was measured as 220 while it increased to 22,000 at 1.4 GHz after applying active feedback [Figure 26(b)] [315]. Additionally, in a proposed SRR with active feedback loop, a substrate-embedded microfluidic channel was fabricated with the frequency of operation of 2.63 GHz. The proposed SRR consisted of a gallium arsenide (GaAs) monolithic microwave integrated circuit, pHEMT transistor, operating as a voltage-controlled variable gain amplifier, and a manually tunable phase shifter. In addition, attenuators were used to feed the signal from the network analyzer to the SRR while preventing the amplified microwave signal from returning to the source. A 60% improvement in sensitivity and an increase from 116 to 13,000 in quality factor was reported [Figure 26(c)] [66].

Furthermore, implementing active feedback in microwave SRR sensors is significantly advantageous in gas sensing, particularly where the relative permittivity of the medium shows less variation at low gas concentrations. Zarifi et al. demonstrated active feedback loop assisted SRRs as a non-contact gas sensor for organic vapor detection employing microbeads, beaded activated carbon, and polymer-based beads. The quality factor increased from 200 in no active feedback (i.e. passive) mode to ~1 M when the active feedback loop was enabled, allowing resolution of frequency shifts, in the S₂₁ parameter measurement, as small as 10 kHz in response to 35 ppm of 2-Butoxyethanol at 1.42 GHz [316]. Moreover, CO₂ sensing in the dry CO₂/He mixture media was proposed with active feedback SRR implemented by embedding Zeolite 13X, and two synthesized MOF-199 where a maximum sensitivity of 24 kHz/% CO₂ for MOF-199-M2 and minimum of 10 kHz/% CO2 for Zeolite 13 X Figure 26(d)] was achieved [317].

Besides the conventional metallic SRRs, the concept of integrating active feedback is expanded to non-metallic and organic SRRs where the intrinsic losses further degrade the quality factor. In [67], the quality factor was increased from 1.5 to 600 where, by integrating a manually tunable phase shifter and a wideband LNA, the quality factor of



a polymer-based SRR was continuously tuned to achieve higher values compared to passive metal-based resonators. As shown, the abovementioned advancements demonstrate that active feedback is a practical and effective technique to significantly enhance the performance of SRR sensors.

2) DIFFERENTIAL TECHNIQUES

Differential sensors do not intrinsically provide a good resolution (resolution in differential sensors is related to the imbalance generated by the differential input variable, and by the noise level of the measuring instrument). Nevertheless, it has been found that resonant-type differential sensors devoted to the measurement of electrolytes in liquid (typically water) solutions exhibit excellent resolutions. Electrolytes are present as ions (e.g., Na⁺, K⁺, Ca²⁺, Cl⁻, etc.), thereby contributing significantly to alter the conductivity and the loss factor of the solution. Thus, it has been found that by measuring the magnitude of the cross-mode transmission coefficient in differential sensors based on resonant elements, tiny concentrations of electrolytes, e.g., in aqueous solutions, can be resolved.

Figure 27(a) reports a differential-mode microfluidic sensor, where the sensing resonators are split ring resonators (SRRs), highly sensitive to variation in the complex permittivity of its surrounding [4]. The sensor was devoted to the measurement of KCl concentration in pure deionized (DI) water (see further details concerning sensor fabrication, dimensions, etc., in [4]). One fluidic channel, located on top of one of the SRRs, contains the REF liquid (DI water), whereas the other fluidic channel drives the considered solution in contact with the other SRR (it should be clarified that to avoid liquid absorption by the substrate, a dry film of polyester was deposited on top of the SRRs). Figure 27(c) depicts the measured sensor responses (crossmode transmission coefficient) for different concentrations of KCl, whereas Figure 27(d) depicts the dependence of the maximum value of the cross-mode transmission coefficient with the concentration of KCl. The sensor can detect concentrations as small as 0.25g/L, whereas the maximum sensitivity, achieved in the limit of small concentrations, was found to be $0.032 (g/L)^{-1}$.

3) ELECTIVITY AND ROBUSTNESS OPTIMIZATION BASED ON ARTIFICIAL INTELLIGENCE (AI) AND RELATED TECHNIQUES

The sensors reported here, primarily related to permittivity changes in the MUT, suffer inherent limitations as for selectivity (specificity) or multi-parameter measurement capabilities. When multiple simultaneous changes occur in the MUT, with cross-influences, it is hard to quantify all the specific variables (or even discern a selected one) just from the overall resulting dielectric footprint. Since several phenomena happening at the same time (such as simultaneous change of several components or solutes in the sample) will lead to a single change in the dielectric permittivity, the individual contribution of each phenomenon might be

masked. The capability of the sensor to be selective to a given single phenomenon is therefore undermined. Recent efforts have been made to bypass this limitation for applications requiring the extraction of multiple pieces of information with planar microwave sensors. For example, analytical methods have been proposed for the simultaneous detection of two (complex permittivity) [86], [318], [319] or even three (complex permittivity and thickness) [293] characteristics from solid samples with coupled resonator techniques. Double parameter extraction (complex permittivity) for liquid samples has also been achieved analytically [320], [321], [322], [323], [324], as well as analytical multi-parameter determination with muli-frequency measurement in liquid samples [280], [292], [325].

Despite those efforts, for certain applications and contexts the analytical methods may become intractable. In this regard, the use of artificial intelligence (AI) techniques has been found to be quite useful. The microfluidic applications are a good example, particularly when multiple solutes are involved [326] or when highly accurate characterization is required [327]. A usual case of study is the characterization of alcohol mixtures [328]. An optimal design simultaneously integrating the sensor and the fluidic channel or container is crucial. The use of reinforcement learning techniques has been proved effective for automatic optimization of this design [329]. Neural networks were also proved conducive to sensitivity enhancement [330].

Notwithstanding those progresses, the selectivity remains a significant challenge, being intrinsically limited as simultaneous changes in different solutes are masked beneath the effective permittivity of the solution. Currently under study, some recent advancements have shown the potential of machine learning for complex permittivity characterization in alcohol microfluidics [331] or for multicomponent concentration identification in complex solutions [326], [332].

Due to its intrinsic complexity, the biomedical domain is one of the main fields of application of these techniques, with a special emphasis on glucose concentration sensing. Several approaches have shown resolution and robustness enhancement for glucose detection in binary mixtures with microwave planar sensors and machine learning techniques, such as artificial neural networks, random forest regression or principal components analysis [333], [334], [335], [336], [337]. Other recent approaches addressed the selectivity challenge with these sophisticated techniques, achieving multiple solute concentrations measurement [326] and robust glucose measurement in human trials [338], [339], [340], although with limited number of test subjects, by now. The demonstrated potential has motivated research of these concepts on other biomedical areas, such as oedema severity determination [341], among others [342]. The concept has also raised attention in other realms in addition to biomedical domain, such as quantification of contamination in fuel oil [343] or detection of volatile organic compounds [344], to name a few.



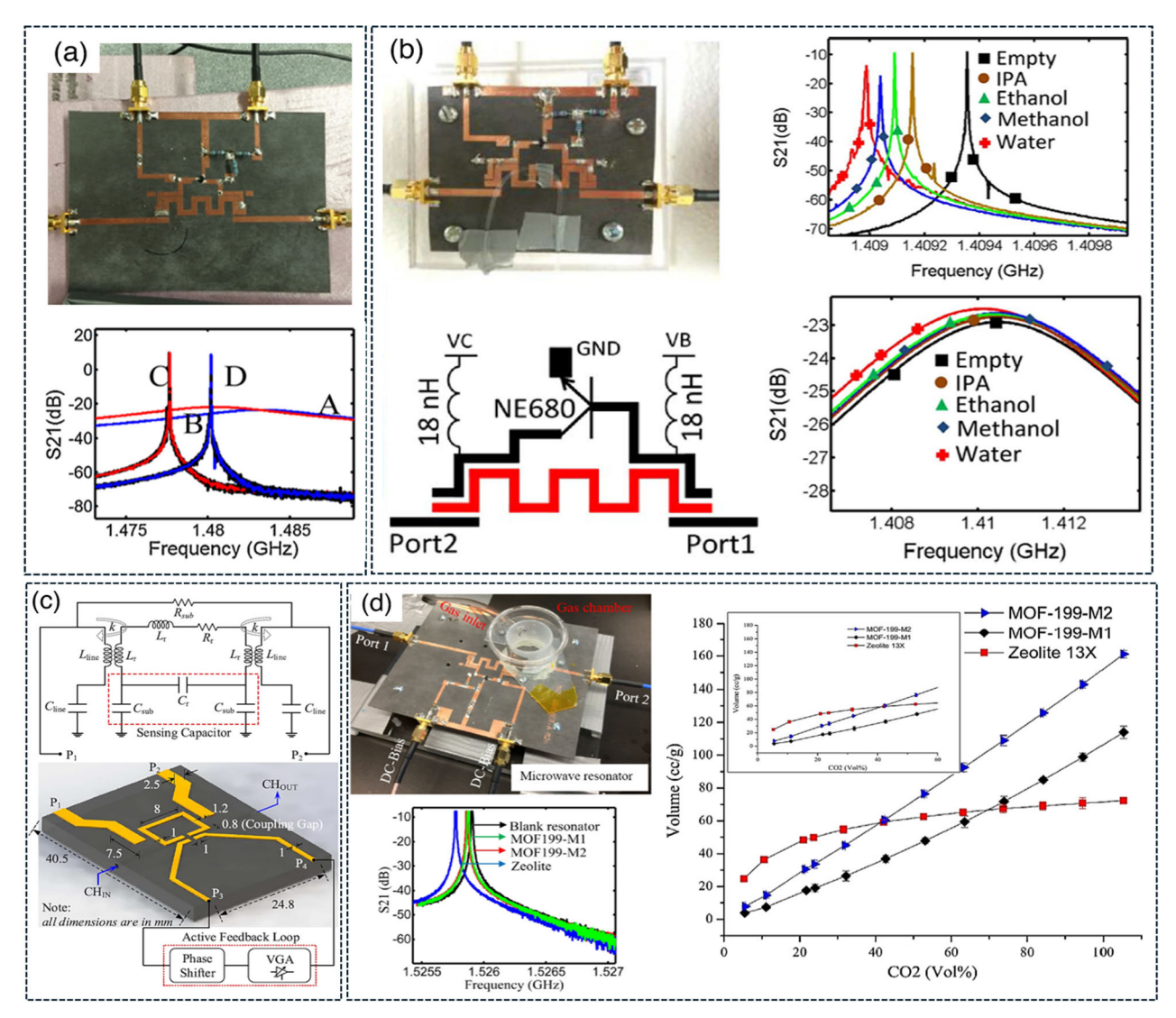


FIGURE 26. Split ring resonators with active feedback loop. (a) The response of the resonator (A) passive SRR, (B) passive SRR with samples, (C) active SRR with sample, (D) active SRR without sample. Reprinted with permission from [311]; copyright 2015 IEEE. (b) Implemented low cost, high precision liquid sensor, S21 parameter of the designed sensor for the different liquids in active mode and passive mode. Reprinted with permission from [315]; copyright 2015 IEEE. (c) Three-dimensional schematic and the electric circuit model of SRR-based proposed microwave sensor using an active feedback loop for characterizing liquids in a substrate-embedded channel. Reprinted with permission from [66]; copyright 2022 IEEE. (d) experimental setup with the microwave active resonator sensor, resonant profile (S₂₁) of the sensor without any material (blank), with MOF and Zeolite while being purged with He at a rate of 200 SCCM at room temperature, CO2 volumetric adsorption of MOF-199 and Zeolite 13X samples, T = 20°C. Reprinted with permission from [317]; copyright 2018 IEEE.

As discussed, achieving high selectivity and robust performance in industrial environments using microwave sensors remains a continuing challenge, limiting their industrial adoption, requiring further research in data processing techniques including AI-based methods [345]. Here, the poor selectivity in microwave sensors arises from the overlapping dielectric properties of materials under test, while limited robustness is primarily due to their susceptibility to environmental effects such as temperature, humidity, and vibrations. As an example, traditional microwave sensors struggle to distinguish between materials in complex mixtures (e.g., water-methanol-ethanol) since their resonant frequency or amplitude depends on the effective permittivity of the entire medium [346], [347].

Similarly, thermal noise and environmental fluctuations further degrade amplitude-based measurements [347].

Selectivity in microwave sensors can be improved either through electromagnetic design modifications to enhance field confinement and sensitivity to specific targets, while the second, more practical approach, uses data processing using AI, which can be applied on existing sensor architectures without the need for hardware redesign. Convolutional neural networks (CNNs) and similar models have been effectively used for complex permittivity estimation, using their ability to learn non-linear relationships from *S*-parameter data with high accuracy [47], [348], [349], [350], [351] (Figure 28). For instance, AI models have demonstrated the capability



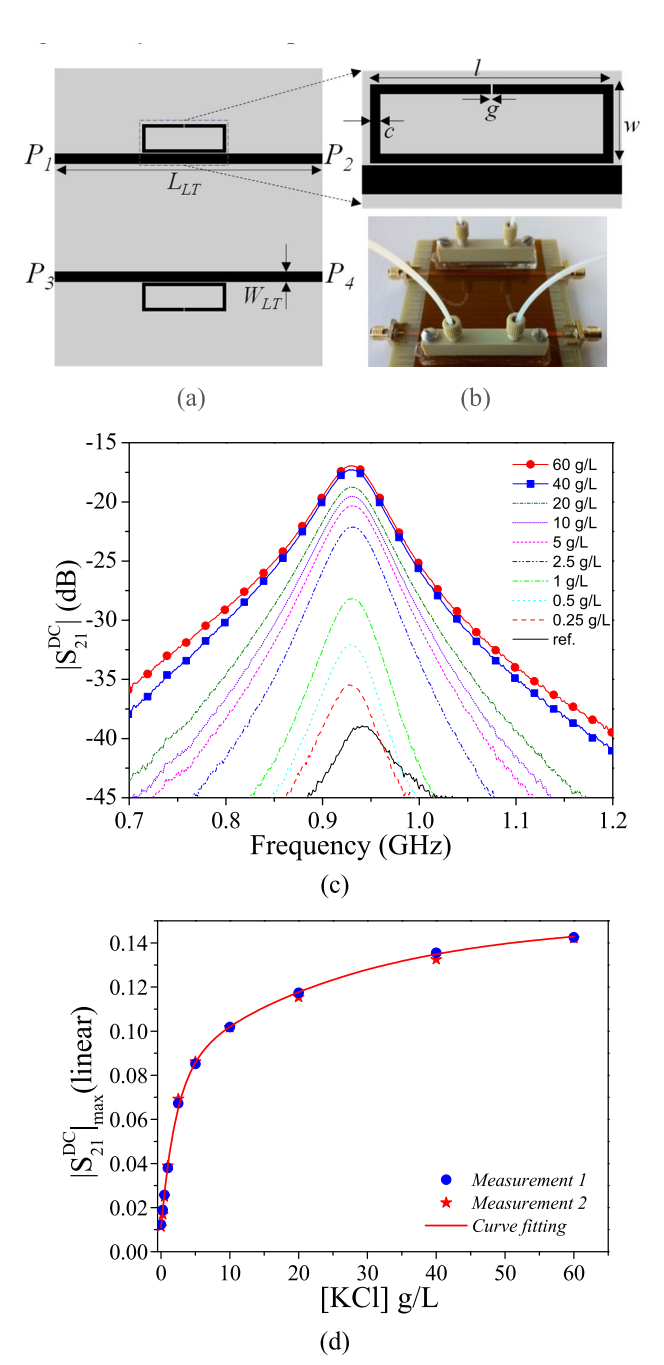


FIGURE 27. Differential-mode fluidic sensor based on a pair of SRR-loaded lines for electrolyte concentration measurements. (a)Topology of the microwave structure; (b) photograph of the sensor, including the microwave structure, the fluidic channels, the mechanical accessories, and connectors; (c) cross-mode transmission coefficient for different values of KCl concentration; (d)variation of $|S_{21}^{DC}|_{max}$ with [KCl]. Dimensions (in mm) are: $L_{LT} = 76.5$, $W_{LT} = 2.79$, I = 24, c = 1, w = 8.17, g = 0.2. The ground plane in (a) is depicted in grey. Reprinted with permission from [4]; copyright 2019 IEEE.

to convert raw *S*-parameters into distinguishable features (frequency, amplitude, and *Q*-factor) [293], wherein sensors with multiple resonances (3.5–5.5 GHz) provide richer data, which CNNs parse to isolate target materials [346], [347], Figure 28(c). However, there exists the threat of low dataset sizes that can underfit the model, for which data augmentation

methods have been used to synthesize AI-generated sensor responses for intermediate values existing between two actual measurement data points [346]. Through the first approach, active sensors with high quality factors ($Q \approx 2700$) have been used, with an improved SNR, enabling CNNs to achieve 0.7 % error [347]. Similarly, neural network-based data processing for microwave sensor data [Figure 28(b)] was used to detect and differentiate between ice, water and air, using 4 frequency points, with an accuracy of 98.8 % [352].

A range of machine learning (ML) models have also been developed to enhance selectivity and robustness, especially in data-limited scenarios. ML-based LightGBM were used to classify different S-parameter responses in real-time [353], for coating damage localization application, Figure 28(a). The same technique was also developed to analyze biofuel mixtures comprising water, ethanol, and gasoline [332]. By processing both magnitude and phase of the S-parameters, the AI model achieved high selectivity, with a low concentration estimation error of just 0.09 %. Similarly, without the need for feature extraction, directly analyzing S₂₁ or S₁₁ magnitude-phase data have been used and deployed for edge devices [354]. Despite these results, the selectivity of planar microwave sensors remains a significant challenge and further research is required to tackle it.

V. REMOTE WIRELESS SENSORS AND ANTENNA-ASSISTED SENSORS

In microwave-based sensing applications, the move towards wireless architecture designs eliminates the need for physical interconnects and wired transmission lines. This enables remote measurement, in addition to easier integration, long distance monitoring, and deployment in inaccessible or harsh environments. Several approaches exist for remote and wireless microwave sensing, including antenna-based sensors, RFID sensors, and waveguide-integrated designs (Figure 29) [353], [355], [356]. These technologies not only support far-field, passive and battery-free operation but also enable remote sensing mechanisms wherein the sensing unit behaves both as the sensor and data transmission, while the excitation unit (antenna or waveguide) behaves as an interrogator or reading device.

A key advantage of wireless microwave sensors is outof-sight monitoring capability, which can be useful in
industrial applications including oil and gas and turbines.
In the past, wireless RFID sensors have been used for
pipeline integrity monitoring wherein the passive sensor was
capable of detecting coating lift-off via resonant frequency
shifts as observed using an interrogating circuitry [357].
However, the reading range in the work was limited to
a few centimeters. For a longer reading distance, active
photovoltaic powered RFID sensors have been developed
with a reading range of tens of meters, making it suitable
for remote IoT applications [358]. Beyond RFID-based
designs, alternative passive antenna structures have also
been explored to enable wireless sensing with improved
sensitivity, mechanical robustness, and greater flexibility



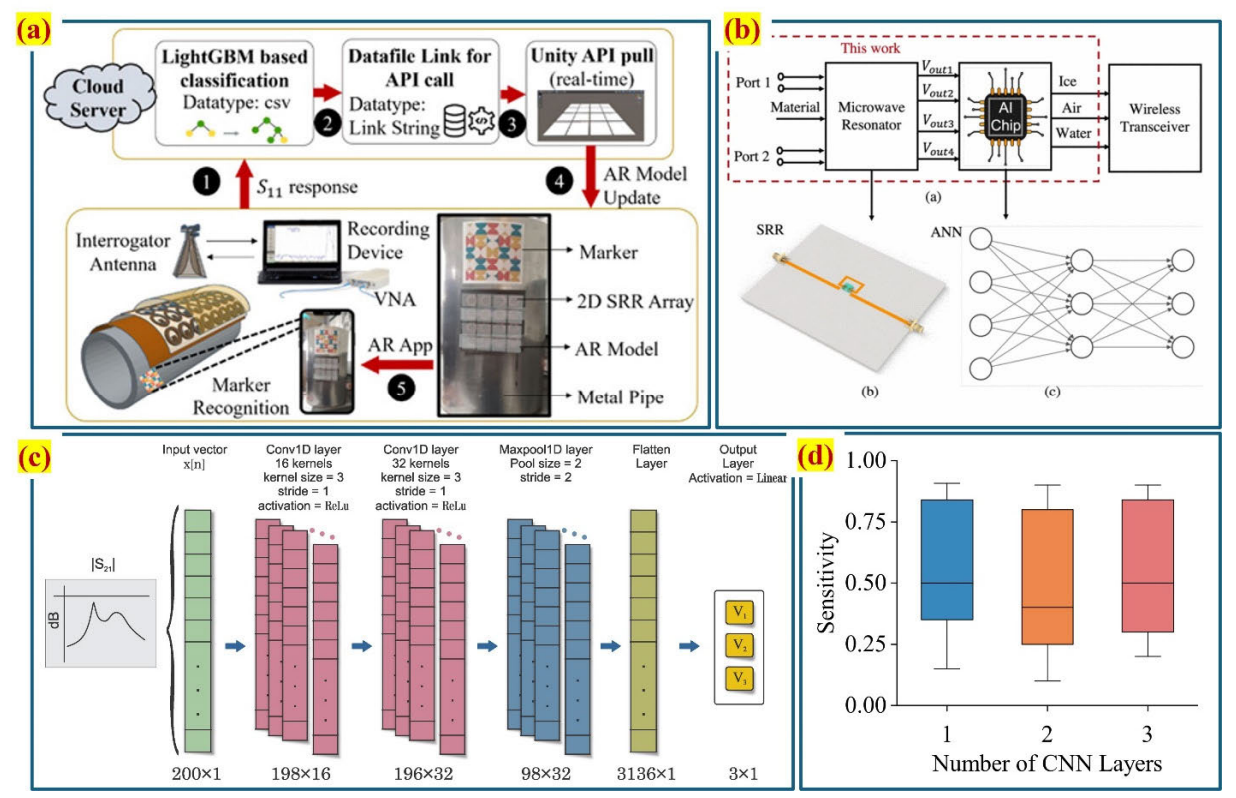


FIGURE 28. Various AI-based data processing techniques to improve selectivity and performance of microwave sensors. Reprinted with permission from [346], [348], [352], and [353]; copyright 2022, 2023, 2018, 2024 IEEE.

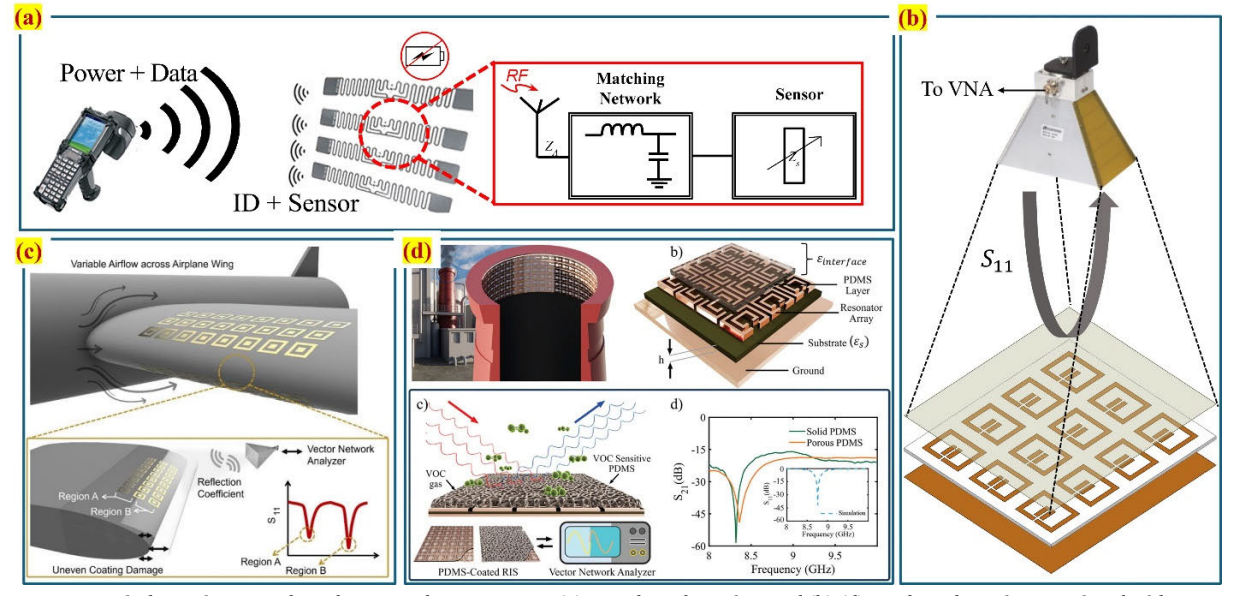


FIGURE 29. Wireless microwave-based sensors that operate on (a) RFID-based sensing, and (b)-(d) FSS-based sensing. Reprinted with permission from [353], [355], and [356]; copyright 2024, 2021, 2024 IEEE.

in integration, particularly in structural health monitoring applications. Folded patch antennas were developed as low-cost, passive, wireless smart sensors for monitoring strain in metallic structures. The antenna's resonance frequency shifted linearly with applied strain and could be wirelessly interrogated [359].

Apart from RFID, frequency selective surface (FSS) based microwave sensors are of particular interest due to their low profile, while exhibiting strong frequency-dependent transmission and reflection characteristics. When used as sensors, FSS structures act as resonant elements whose response shifts with changes in permittivity, conductivity,



or mechanical deformation (like bending, and rotation), which can be used to detect physical parameters such as humidity, strain, or dielectric loading. In the past, FSS sensors, combined with an antenna-based reader circuit have been used for remote solid [360], liquid dielectric property characterization [361], pressure sensing [362], and biological applications [363]. They have also been used for wireless coating health monitoring using periodic array of resonators [364]. In all the works, the resonant frequency of the sensing unit (FSS) was monitored, which was dependent on the structural integrity of the coating layer. Additionally, the FSS-based sensors demonstrated high sensitivity to dielectric permittivity variations and were typically interrogated wirelessly from distances of at least one meter, making them well-suited for passive, remote sensing applications.

Waveguide-based wireless microwave sensors have also gained interest for their high sensitivity, and compatibility with external excitation over a smaller region in comparison to antennas. In wearable health monitoring, waveguide-integrated sensors have enabled real-time, wireless tracking of sweat secretion and composition, supporting continuous, non-invasive diagnostics [365]. Similarly, SIW designs have also been explored for gas sensing, demonstrating stable selective detection of volatile compounds through material-analyte interactions [366]. Additionally, coplanar waveguide sensors have demonstrated label-free, real-time biochemical detection, such as glucose monitoring, using planar fabrication on low-cost substrates [367].

VI. APPLICATIONS

The applications of planar microwave sensors are innumerable. This section highlights some representative applications grouped by strategic sectors, from the perspective of the authors.

A. BIOSENSING

Planar microwave sensors are widely developed for biological and medical applications. As expressed in Section III-C, this has been facilitated by the advent of micro and nanotechnologies of microwave circuits and their compatibility with microfluidic systems, opening new perspectives for the non-invasive and non-destructive analysis of ultra-small living organisms at a previously inaccessible scale. Large samples and equipment dominated this research domain until the article of Stuchly et al. in 1998, who pioneered the concept of integrating planar waveguides topped with a fluid container to dielectrically characterize liquids such as water and alcohols [368]. Since then, the development of microwave circuits for chemical and biological detections, as well as for healthcare applications has been growing steadily.

Interest ranges from *in vitro* molecular and cellular characterizations to organs and *in vivo* investigations. This is due to two key features brought by the microwave range. First,

water molecules, the major constituent of living organisms, play an important role in intracellular biological processes as well as in the global functioning of the organism or body. Water molecules present indeed a strong affinity with ions and molecules and are involved in biological exchanges, at the cellular level with intra and extracellular transfers, as well as in the internal circulation of bioliquids. Highly sensitive to the water molecules network and associated modifications, electromagnetic waves may be considered as an intrinsic marker of living organisms in the microwave range. Another important characteristic is directly related to the frequency band. Microwaves indeed penetrate the lipid membrane of cells, allowing for the sensing of intracellular mechanisms. Depending on the frequency and dielectric properties of the crossed biomaterials, electromagnetic waves also penetrate inside the body. Non-destructive and non-invasive analysis, and even imaging of internal organs, is made possible.

Accordingly, a wide variety of microwave sensor configurations and sizes have been established and tested, including planar ones. Their design is defined based on their end use. If the dielectric properties of the material under test are desired, broadband sensors based on microwave dielectric spectroscopy are then preferred, while resonant structures are usually chosen for ultra-sensitive and ultra-rapid detection, as required for the analysis of individual cells in suspension during flow cytometry, for instance. To better highlight these approaches and the selected topologies, examples are provided in this section for different types of biological elements.

Regarding molecular sensing, one of the main studied molecules is glucose, whose detection aims at the non-invasive diagnosis of diabetes. The literature is dominated by resonant sensors to reach the level of sensitivity encountered with diabetes [369], [370], [371]. As a first illustration, a detection threshold for glucose in aqueous solution is defined at 0.3 g/l at a resonant frequency of 7.5 GHz, using a microstrip quarter wavelength stub terminated by an interdigitated capacitor [370]. More recently, glucose detection ranging from 0.8 to 1.2 g/l has been demonstrated with a multi frequency sensor configuration based on three circular-shaped complementary split ring resonators, using a more complex and realistic liquid model with synthetic blood samples [371]. Given that a normal blood glucose level is considered between 0.7 and 1.1 g/l of fasting blood and diagnosed diabetes is above 1.26 g/l, these demonstrations with planar microwave sensors make this sensing technique remarkable. Another example of sensor is a microstrip transmission line terminated by a semi-lumped LC resonator used to detect the concentration of sepia melanin in water solutions ranging from 5 to 100 g/l [372]. Detection and quantification of such a biomolecule are achieved.

In addition, broadband investigations are also carried out to complete the dielectric library of biological materials and also contribute to a better understanding from a physical point of view of living organisms and their interactions at the

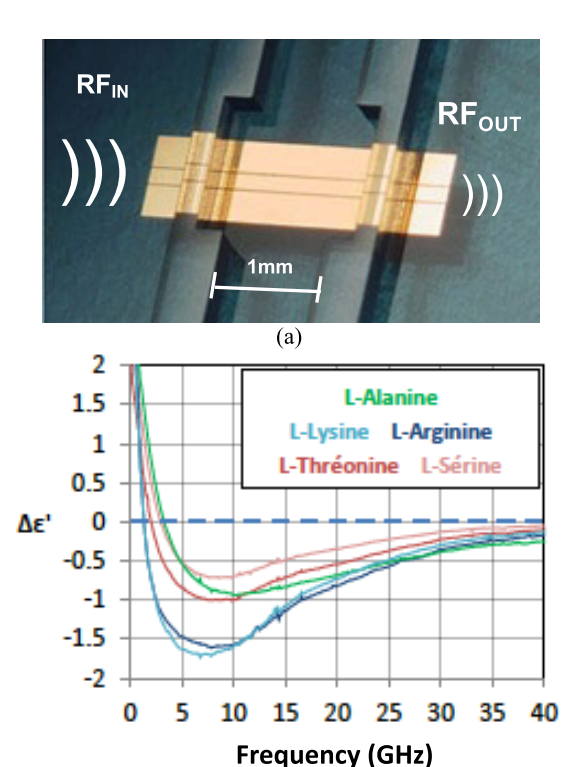


FIGURE 30. Broadband microwave dielectric spectroscopy: a) microfluidic microwave coplanar sensor; b) dielectric contrasts of five amino acids in aqueous solution at a concentration of 0.1M. Reprinted with permission from [374]; copyright 2018 IEEE.

microscopic scale. This dielectric spectroscopy is performed with microfluidic microwave coplanar waveguides for both molecular, cellular and tissue studies [162], [163], [169], [170], [171], [172], [373], [374], [375], [376], [377], [378], [379], [380], [381], [382], [383], [384]. Figure 30(a) illustrates the configuration of such a sensor. In this case, a liquid volume of only 1 μ l is needed to perform the analysis from 40 MHz to 40 GHz [162]. Examples of dielectric spectra measured for different biological materials are also indicated in Figure 30(b), which shows the dielectric response of five amino acids measured in aqueous solution at a concentration of 0.1 M [374]. Due to the large variation in permittivity dominated by the aqueous medium over the considered frequency range, a mathematical differential approach is applied. It consists of subtracting the impact of water when the sensor is only loaded with the host medium from the dielectric response of the molecules in aqueous solution. Obtaining distinct dielectric spectra shows the possible discrimination of these small molecules (of 100 Da approximately) due to their variation in composition and their affinity with the water molecule network.

Similar broadband sensors have also been applied to the characterization of other proteins such as tubulin and microtubules made of tubulin molecules [381], as well as for the detection of conformational modifications [376], [378]. The analysis of suspended DNA tweezer solutions exhibiting two conformational structures and the denaturation

of the large albumin molecule by urea used as a chaotropic agent have been demonstrated in [376] and [378] respectively. It highlights the ability of microwave sensing to detect molecular conformational variations. The detection of albumin denaturation has also been demonstrated with a narrowband differential configuration [10], which allows moving from expensive and cumbersome experiments with large vector network analyzer and probe station to low-cost equipment and SMA connected sensors, once the appropriate frequency range for detection has been identified with the broadband solution. Noteworthy, a narrowband interferometer operating near 10 GHz has been applied to analyze DNA strands with different structural compositions [385]. The chosen differential approach enables the measurement of nanoliter liquids with molecular concentrations down to tens of ng/ml.

As far as cellular investigations are concerned, several considerations have to be taken into account. Unlike most molecular research involving homogeneous liquid solutions, cells exhibit several features induced by their living nature. First, they have an intrinsic cycle, which lasts for a few tens of minutes for prokaryotic cells to hours or even days for eukaryotic cells. To keep them alive, cells must be kept in a medium, ideally a culture medium rich in ions and nutrients, to allow them to live normally without stress. This implies that this medium is gradually consumed by the cells, which can also release molecules. Finally, cells can exhibit very diverse individual responses, which should be taken into account depending on whether one is studying cells in suspension or at a single scale.

Due to these different considerations, various sensing strategies exist. Similar to the traditional optical flow cytometer, microwave sensors have been developed to analyze individual cells in flow in order to account for the heterogeneity of cell suspensions. Given the analysis speed required for this type of application, which involves thousands of cells to be probed, narrowband resonant sensors are preferred. A first microwave interferometric sensor operating at a frequency close to 5 GHz allowed the analysis of single yeast cells in deionized water and the identification of their pathological state, i.e. viable and non-viable [387]. The resonance peak shifts by approximately 50 MHz between the two states, while a quality factor of several thousand is required. A broadband microwave cytometer using notch frequencies also demonstrated the dielectric heterogeneity of single bacteria cells at 1.85 GHz in Yeast Peptone Dextrose (YPD) medium diluted 1:40 in de-ionized water, as illustrated in Figure 31 [386].

This heterogeneity is mainly dominated by the size and shape variabilities of the measured cells. Other resonant based sensors have also been developed in the MHz and GHz ranges to analyze single eukaryotic cells, which are larger than yeast or bacteria cells [388], [389], [390], [391], [392], [393]. Single-frequency [388], [389] and multi-frequency [390], [391] dielectrophoresis (DEP) flow cytometers have focused on the β -dispersion in the MHz



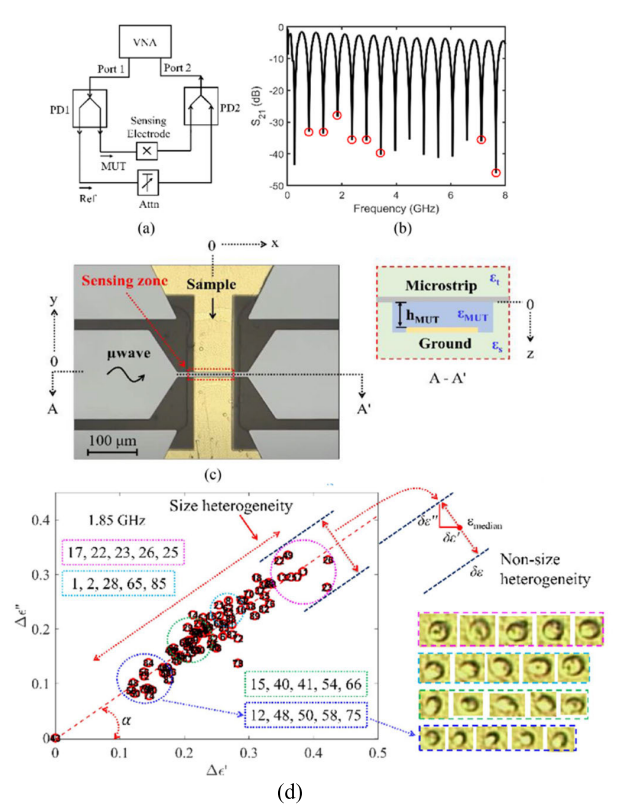


FIGURE 31. Microwave flow cytometer: a) Schematic of the test setup; b) measured example of the amplitude of S21 with notch frequencies; c) Picture of the sensing electrode and microfluidic channel, and its cross section; d) Permittivity variations of single C. tropicalis cells at 1.85 GHz. Reprinted with permission from [386]; copyright 2022 IEEE.

range, which is related to the cell membrane polarization. Cell viability and discrimination of mesenchymal stem cells during their differentiation in the osteoblastic pathway have been demonstrated with such sensors. Due to the frequency range, a depleted medium must be used to avoid ion screening. Other sensors also involved a resonant circuit design in the GHz frequencies, dealing with the γ -dispersion, which is dominated by water relaxation [392], [393]. The majority of cellular studies in the GHz range have focused on static measurements, i.e., the cell sample is stopped in the fluidic channel allowing broadband measurements [162], [373], [374], [375], [376], [377], [378], [379], [380], [381], [382], [383], [384]. Due to this configuration, a differential approach becomes mandatory to avoid any impact of the medium variability and to allow sufficient detection sensitivity compared to the dominant impact of water molecules on the dielectric response.

Figure 32 presents a broadband microwave sensor, which integrates a gold coplanar waveguide with a perpendicularly placed microfluidic channel [162]. A de-embedding technique first enables to extract the permittivity of the liquid under test, whilst a differential calculation using the measured permittivities of the culture medium and of the cell suspension is then applied to obtain the dielectric contrasts. Figure 32(b) illustrates the possible discrimination of cellular viability at the population level. Distinct dielectric spectra

are obtained for two cell suspensions exhibiting the same cell concentration, one containing viable cells and the other cells treated with saponin, a detergent that creates pores in the cell membrane and causes artificial cell death [384]. An important feature of this dielectric characterization is that the cells are maintained in their culture medium with the presence of ions. The broadband characterization is also rich in information, highlighting the frequency range offering the highest dielectric contrast, approximately 5 GHz in this case. Applied to the analysis of B-lymphoma cell subpopulations, it has also been shown that different dielectric responses may be obtained for three similar cell lines, OCI-LY7, OCI-LY10 and OCI-LY18 [cf. Figure 32(c)] [375]. To discriminate these cells, optical techniques are not sufficient, and cytogenetic analysis has to be employed. This result demonstrates that the microwave detection technique is not only sensitive to viability or size, but also to the internal molecular content. This has also been confirmed by a study dedicated to the monitoring of apoptosis, which highlighted the early detection of the biological phenomenon after only 2 hours of treatment, compared to 6 hours with the traditional biomarker technique [377]. It has also been shown that the microwave method is sensitive to mitochondrial depolarization.

Broadband microwave sensors suitable for single cell analysis have also been reported. They typically focus electromagnetic waves at the cell level with a narrow capacitive gap adapted to the size of the cells being measured [373], [379], [380], [383] or with a narrowed CPW [382]. The approach followed to trap individual cells may differ depending on the application. In [373], [382], and [383], a mechanical trap based on hydrodynamic flow in the channel is used, as illustrated in Figure 33(a). Cells may then be measured directly into their culture medium, which can be easily modified to monitor the impact of drugs in real time, for example. For tests over several days, time-lapse analyses are also possible [383]. Quantitative study of biological phenomena induced by chemical or electrical stress, as well as monitoring morphological or structural modifications are enabled. In [379] and [380], dielectrophoretic trapping is employed, which imposes a depleted host medium. It has been used to analyze the size of nucleus. To illustrate the sensitivity required to detect single eukaryotic cells, Figure 33(b) presents the measured capacitive contrasts of several THP-1 cells submitted to electrochemotherapy (ECT) treatment [171]. The obtained values are of the order of several tenths of a femtofarad. Each curve corresponds to an individual cell undergoing ECT treatment. The level of the capacitive contrast compared to the threshold indicated by the purple line allows to distinguish affected cells from unaffected ones.

Similar to the single cell microwave sensor architecture described in [375], a broadband device suitable for the analysis of spherical multicellular microtissues has been defined to complete the arsenal of microwave planar sensors for all biological model configurations [172]. Also addressing the analysis of cell clusters, resonant sensors based on split



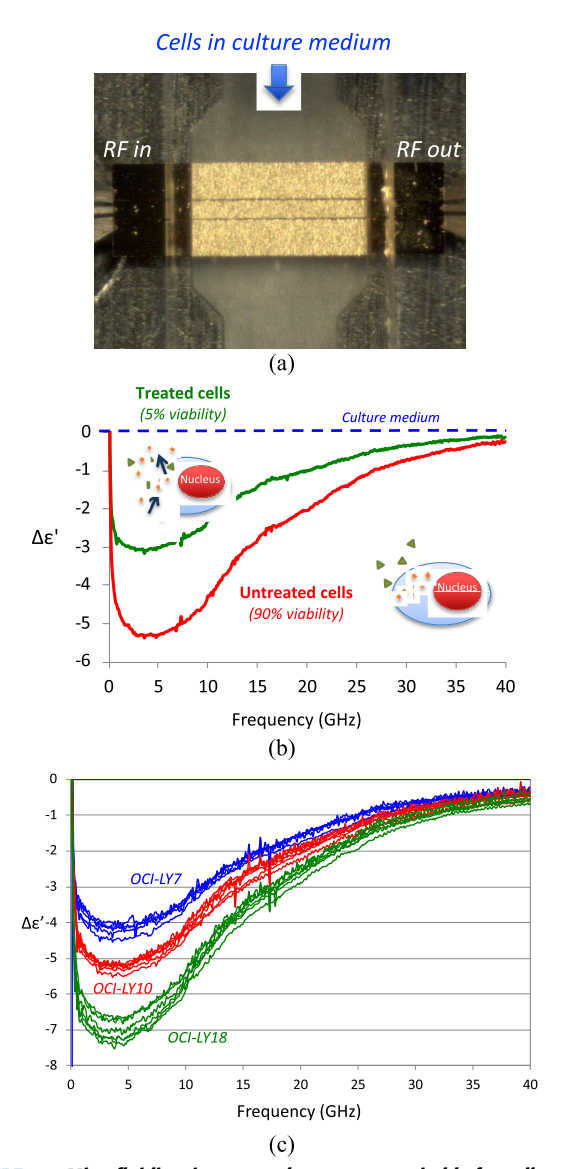


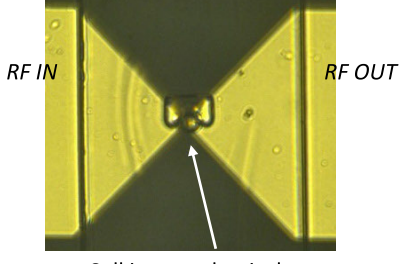
FIGURE 32. Microfluidic microwave planar sensor suitable for cell suspensions analysis: a) Picture of the sensor loaded with a cellular suspension; b) Measured mean permittivity contrasts of two DoHH2 cell suspensions in their culture medium (Roswell Park Memorial Institute medium - RPMI), viable cells and treated cells with saponin to induce cells poration; c) Measured permittivity contrasts of three different B-lymphoma cell lines in suspension maintained in their culture medium(RPMI), OCI-LY7, OCI-LY10 and OCI-LY18. Each cell lines have been measured 4 times independently.

ring resonators have been defined for monitoring bacterial proliferation and the impact of antibiotics [7], [8].

Numerous planar microwave sensors have been developed for biological and medical applications, with the aim of better understanding biological mechanisms and contributing to early diseases diagnosis and personalized medicine through rapid drug evaluation on patient cells. Future impacts on global healthcare are therefore expected.

B. SMART HEALTH

The electromagnetic waves oscillating at frequencies within the microwave region show interesting properties for several



Cell in a mechanical trap

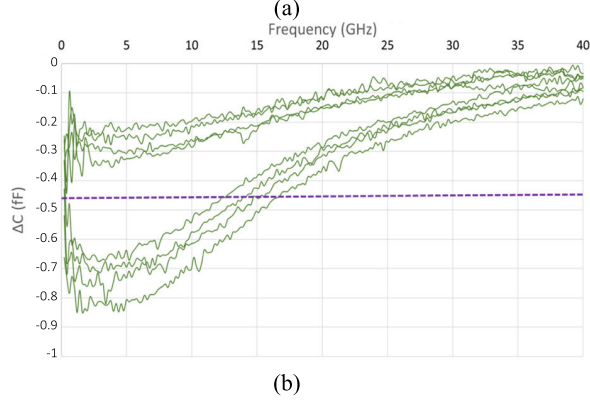


FIGURE 33. Microfluidic microwave planar sensor: a) Picture of the sensor loaded with a trapped individual cell; b). Measured capacitive contrasts of individual cells undergoing electrochemotherapy.

contexts, amid which the biomedical domain can be underscored. As reviewed here, microwave sensors are sensitive to variations of the complex permittivity in their vicinity. Since this complex permittivity indeed depends on the chemical composition of the materials, these sensors can perform as chemical composition sensors. When this circumstance is mingled with non-invasive measurement capabilities, the potential use of this technology for medical and smart health purposes seems enticing.

The dielectric properties of most biological tissues have been painstakingly inspected for a wide frequency range [394], [395], [396]. Particularly, in addition to the general benefits of ease of integration, cost-effectiveness and compactness, at microwave frequencies up to roughly 20 GHz there are some unique advantages such as reduced MUT size (in the range of the wavelength), significant penetration depths in living matter and, most importantly, the dielectric relaxation processes of water and most biological systems are covered, yielding to a plethora of application possibilities of these sensors for health monitoring [397].

Relying on these principles, several biomedical and smart health uses of microwave sensors have been investigated, such as the quintessential sensing of blood glucose level [284], [398], [399]. As thoroughly characterized, a change in the glucose content of any solution, such as water or blood, leads to variations of the complex permittivity of the solution [400], [401], [402], [403], [404], [405], [406]. Essentially, for a fixed temperature, an increment in the glucose concentration in a pure water—glucose solution yields an increment of the viscosity of the solution [407], associated



with an increment of its dielectric relaxation time [408] with the consequent variations in the complex permittivity of the solution [409]. Microwave sensors are able to track these permittivity variations for indirect extraction of the glucose level.

A remarkable amount of works has been published as a result of the thoroughgoing efforts devoted to research this concept [284]. A ground-breaking work made use of a spiral resonator for such a purpose, tracking the changes in the resonance frequency [410], further investigated in [411]. Another seminal work, although out of a planar configuration, proposed the use of a SRR for resonance frequency-based measurements while having a second spatially-separated SRR for reference [197], [412]. These and other related works, while lacking enough accuracy to meet medical standards, showed evidence enough to attract the interest of a certain part of the microwave community for developing glucose content sensors for diabetes purposes.

Pursuing this objective, several measurement principles and metrics have been investigated with a heterogeneity of approaches and techniques. Frequency-variation and frequency-splitting sensors based on the variations of the resonance frequency have been proposed, both with static sample holders [413], [414], [415], [416], [417], [418], [419], [420], [421], [422], [423] or microfluidic channels [424], [425], [426], [427]. Magnitude-variation sensors have also been studied with static sample holders [418], [428], [429], [430], [431], [432], [433], [434] or microfluidic channels [370], [435], [436], [437], [438]. With a reduced amount, phase-variation sensors have also been analyzed [439], [440], [441], [442], [443]. In order to unify criteria and ease the comparison of the results, even between sensors lying on different principles, a Relative Sensitivity to Glucose, RS(G), was proposed [284].

The application of glucose detection shows certain particularities. Specifically, water or blood are highly lossy liquids from the dielectric point of view [444], [445], which contrasts with the usual low-permittivity substrates available and makes it difficult for approaches based on perturbation theory, such as most of the resonant ones. Furthermore, in the case of glucose content variation, the change in the imaginary part of the permittivity is considerably higher than that on its real part and with inverse trend [402], [404], [406], thus making more noticeable the changes in the loss tangent, directly related to the unloaded quality factor (Q_u) of the resonator. All these circumstances bespeak a high convenience of frequency-splitting variation sensors based on the Q_u as sensing metric, the so-called Q_u -based sensors [2], [446], [447].

Under this approach, low-cost certified biocompatible implementations were made with good results for diabetes management [2], as shown by the Clarke error grid test (a usual test for glucose sensors in clinical setups [448]), as can be seen in Figure 34. These sensors have been assessed with blood solutions [449] and even in real clinical trials [450], [451]. As described in Sect. IV-A, the use of coupled

resonators can also act as a sensitivity booster for this sensing paradigm [277], [283]. The last results suggest that currently these sensors will have to face several challenges for practical applicability, such as temperature correction [436], or dry layers (or dry films) compensation [453], [454], in addition to selective sensing [3].

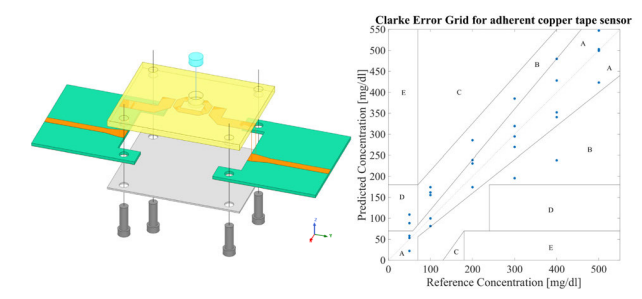


FIGURE 34. Picture (left) and results of the Clarke error grid test(right) for the Qu-based glucose sensor in [2] made with the surgical guide stereolithography resin FLSGAM01 from FormLabs (UE and USA certified biocompatible material). Reprinted with permission from [2]; copyright 2021 IEEE.

The overriding selectivity issue definitely poses a limit for real clinical use of these sensors, and efforts are nowadays being made to circumvent it. Thanks to coupled-resonator structures, multi-phenomena sensing was achieved with the simultaneous extraction of the concentrations of an ionic substance (NaCl) and a non-ionic one (sucrose) by defining ad hoc sensing metrics [280], [455]. This technique was also proved effective for temperature correction [292]. Modern machine learning techniques have also been used with optimistic results [456], [457], [458], and analytical simultaneous multi-parameter sensing is being researched [293]. Other current approaches include the measurement of glucose from saliva [201], surface plasmonic microwave glucose sensors [462].

Apart from glucose detection, similar techniques have been used for detecting other relevant compounds or analytes for general health monitoring or specific disease control. For example, blood lactate is a key indicator of muscular fatigue during physical exertion, and it is also used for fast diagnosis and prognosis of septic patients during medical emergencies. Thus, research on non-invasive microwave planar lactate sensors is active [292], [463], [464], [465]. Another interesting field is the detection of urea level [466], [467], [468], which is related to several symptoms and impairments, such as uremic neuropathy, urinary tract obstruction, renal failure, liver failure, cachexia, etc. [469], as well as treatments such as dialysis, in addition to edible milk and dairy products impurity assessment [470], [471], [472], [473], [474]. Following kindred principles, other applications of these sensors include, but are not limited to: detection of bovine serum albumin (BSA) concentration (used in many protein assays and in studies of the circulatory system) [3], [10], [475], [476], [477], characterization of electrolyte content in urine samples for screening hydration



and blood pH-related disorders [5] or detection or sweat or urine leakages [244].

Nowadays, the advances on sophisticated signal processing techniques have opened new research lines based on planar antenna sensors through the analysis of the transmitted and backscattered signals. In the smart health and biomedical realm, two main lines are thriving. On the one hand, medical microwave imaging (MWI) techniques show great interest for detection of several cancers [478], [479], [480] and other surgical applications [481], [482], [483], [484]. On the other hand, recent advances have been made for the non-invasive detection of vital signs, such as heart rate, respiration rate and even lung water level by means of microwave antenna sensors [485], [486], [487] (a breath rate monitoring system based on a stretchable planar sensor is reported in [127]).

In addition to the technical specifications, the devices devoted to health or medical realm, devoted to be used on humans, must comply with specific regulations. In general, the devices reported here operate with electromagnetic exposure durations of no more than one minute (much less in most of the cases), and the radiated waves at these frequencies are non-ionizing. Additionally, the radiating elements usually radiate at power levels near to 0 dBm (1 mW), which is 10 to 100 times lower than the typical output of a modern smartphone. This power level is also 100 times below the threshold needed to achieve the maximum permissible Specific Absorption Rate (SAR) under U. S. and European Union regulatory standards [480]. Given these factors, these sensors and systems can be considered safe for human exposure and fully compliant with SAR regulations.

C. SMART AGRICULTURE AND AGRIFOOD INDUSTRY

The advent of novel smart electronic processes of agricultural products and food products necessitate new smart and low-cost sensors for continuous monitoring of the product quality attributes [488]. Planar microwave sensors are ideal candidates for such applications because of their compatibility with low cost and flexible electronics, high-sensitivity and non-invasive detection together with their real-time response [489]. Furthermore, due to the wide microwave frequency spectrum and diversity of microwave-based measurement techniques (i.e. free space, waveguide, planar sensors), the microwave techniques offer high flexibility and adaptability to the requirements of the specific product [490]. Microwave-based dielectric sensors are of great importance in these applications as water is a fundamental constituent in agrifood products. With this background, a major category of microwave sensors has been developed for monitoring the moisture content in agricultural goods. In fact, the water content is a key indicative parameter in quality monitoring of food and agricultural products. On the other hand, it is well-known that the water content has a direct effect on the effective dielectric properties of the materials. Thus, measuring the dielectric properties is of high interest for quality monitoring in the agrifood industry [491], [492], [493].

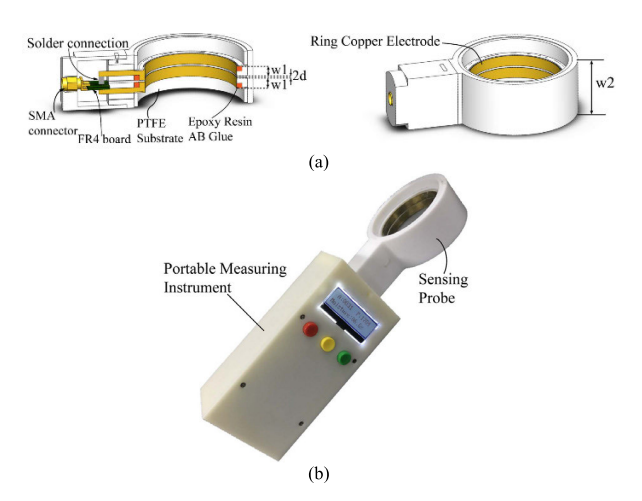


FIGURE 35. Handheld sensor for quality monitoring of corn ears in [493].

(a) Conceptual schematic of the sensor. (b) The fabricated handheld sensor prototype. Reprinted with permission from [493];copyright 2020 IEEE.

An example of the planar microwave sensor for product quality monitoring based on the moisture content is the handheld sensor designed in [493] using a dual ring probe shown in Figure 35. The sensor is designed using two ring electrodes printed on a Teflon⁶ (PTFE) substrate. When applied on a corn ear, the water content of the corn has a direct effect on the total capacitance in between the probe at microwave frequencies. Such an effect modulates the reflection phase and amplitude of the sensor. A dedicated readout circuit was designed to perform the measurement in a portable manner and the sensor offers dynamic range of 15.7%–31.5% moisture content in corn samples with maximum measurement error of 3.4%.

Planar microwave sensors have also been applied in process and quality monitoring of food and beverages. An example is the sensor in [494] that was designed for monitoring the fermentation process in alcoholic beverages. During the fermentation process the sugar and alcohol content vary in a dynamic fashion resulting in variation of the dielectric properties of the beverage. Such process can be monitored in real-time using a microwave dielectric sensor as proved in [494]. The sensor in [494] is designed using a combination of U-shaped and trapezoidal-shaped SRR coupled to a microstrip transmission line as shown in Figure 36. For fermentation monitoring, the sugar and ethanol content should be monitored simultaneously within the solution. This requires at least two resonance modes produced by the two resonators. The resonance frequency shifts of the two resonant modes are used for sugar and alcohol content detection in water enabling the fermentation process monitoring.

Another application of planar microwave sensors in smart agriculture is real-time monitoring of soil moisture. The soil moisture level is highly important for smart water management in advanced agriculture technologies [495]. The water content affects the dielectric properties of soil. Thus, planar microwave-based permittivity sensors can be



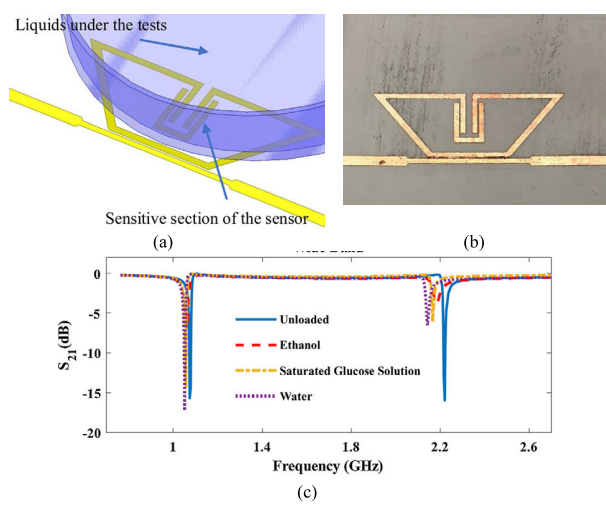


FIGURE 36. Microwave planar sensor developed in [494] for alcohol and sugar content measurement in beverages. (a) Layout of the sensor. (b) The fabricated sensor prototype. (c) Measured sensor response for different solutions. Reprinted with permission from [494]; copyright 2021 Elsevier.

adopted for monitoring the soil moisture content. Various types of sensors such as interdigital electrodes [496], and planar resonators (SRRs) coupled to transmission lines [497], [498], [499] are developed in the literature for moisture level monitoring of soil. The principle of operation in all these sensors is variation of the S-parameters signatures (i.e. resonance frequency, phase, and amplitude) due to the change of the dielectric properties of soil, which is a function of the water content.

D. AMBIENT MONITORING

Due to their real-time response, low-cost, and adoptability with mass electronic fabrication technologies, microwave sensors have found their way into ambient condition monitoring in various scenarios and applications. The microwave sensors can be deployed as passive or active tags in the IoT networks offering a cheap and efficient platform for monitoring various environmental factors such as temperature, humidity, UV radiation level, water and air pollution levels. In some of the applications such as ambient temperature sensors, the measurement is performed in a mediator-free manner using the microwave circuits and resonators since the temperature directly affects the resonance frequency of the resonators due to the size expansions as a result of the temperature variations [500], [501], [502], [503]. An example of this type of sensor is presented in [502], where a ring resonator coupled to strip lines were implemented for high temperature sensing. A schematic of the designed sensor together with a fabricated prototype are presented in Figure 37. Realization of the sensor in strip line technology helps in preserving the sensor against environmental disturbances such as dust, debris, humidity that might produce cross-sensitivity and measurement error. The experimental measurements shown around 25 MHz variation in the resonance frequency as a result of the temperature variation between $30^{\circ}\text{C} - 80^{\circ}\text{C}$.

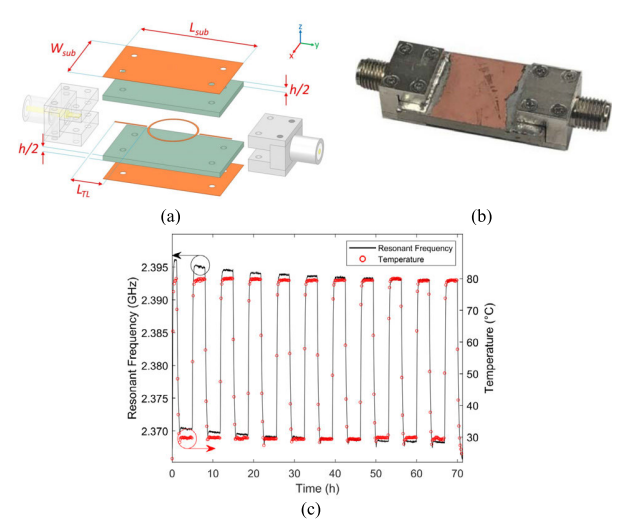


FIGURE 37. The strip line sensor in [502] for high temperature sensing. (a) Expanded schematic of the sensor. (b) The fabricated sensor prototype. (c) Measured resonance frequency variations due to the temperature change in continuous time cycles. Reprinted under CC-BY license from [502].

The measurements in another category of the environmental monitoring sensors is performed by integration of advanced functional materials such as carbon nanotubes, graphene, and functional polymers into the microwave planar sensors [174], [291], [504], [505], [506]. The functional materials help in improving the sensitivity and selectivity of the microwave sensors to a specific environmental factor. The changes in the environmental signatures (i.e. gas content, UV level, humidity) modify the dielectric and/or conductivity of the functional materials. Such variations can be detected through the resonance frequency changes or phase and amplitude variations in the scattering parameters of the microwave sensors. A clear example of such sensors are the microwave-based gas sensors that will be studied in detail in Section VI-H. Another example application is the UV level monitoring [193], [314]. The UV radiation level detection is of high importance for skin care purposes. The sensor in [314] is designed using a SRR coupled to microstrip feedlines as shown in Figure 38, where a positive feedback loop using a transistor is used to improve the resonance quality factor and thus the sensitivity. TiO2 nanotube is embedded within the capacitive gap of the SRR as a functional UV sensitive material. The measurement results show resonance frequency shift as well as peak amplitude variation as a result of varying the UV radiation level [Figure 38(c)].

E. STRUCTURAL HEALTH MONITORING AND CIVIL ENGINEERING

During the last decades, microwave technology has also proved useful for certain non-destructive testing (NDT) applications, chiefly leveraging the dispersive penetration features of electromagnetic fields [507]. NDT techniques are essential for many verification and monitoring contexts where an assessment of the quality or integrity of the product

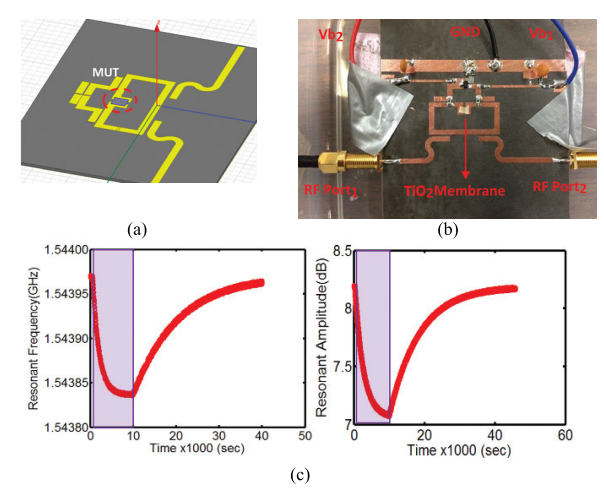


FIGURE 38. Microwave planar sensor in [314] for UV level detection.
(a) Layout of the sensor. (b) The fabricated sensor prototype. (c)Measured resonance frequency and amplitude variations during the illumination and relaxation time periods. Reprinted with permission from [314]; copyright 2018 RSC.

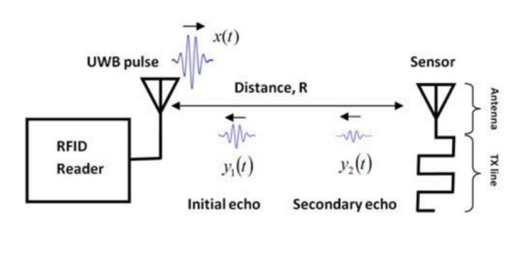
or sample is required, and they became particularly relevant for structural health monitoring (SHM). Identifying as soon as possible when the integrity of a civil structure is in jeopardy is of paramount importance for preventing it from imperiling the lives of people nearby. Microwave NDT instruments are able to retrieve pertinent data about the composition and current state of materials or structures, which are fundamental for evaluating or identifying potential damages in civil and urban infrastructures.

Aware of this, the microwave community is actively endeavoring to develop sensors for continuous SHM in civil and urban infrastructures. The inclusion of pervasive embedded sensors at critical points or locations in the structure can be useful for condition-based real-time monitoring of civil structures such as buildings, bridges, docks, dams, military structures or railway tracks, among others [508]. The structures deteriorate with time due to multiple factors such as aging of materials, overload, overuse, poor maintenance or external events (earthquakes, collisions...), thereby posing safety concerns [81].

SHM techniques can screen from the first deterioration symptoms by means of crack and strain sensing systems. However, the traditional techniques for such a purpose require lengthy communication cables (with protective pipelines) for data transmission, which entail high installation and maintenance costs [509]. Any valid wireless alternative will therefore save notable amounts of money while increasing flexibility and efficiency. It is in this context where microwave chipless RFID sensors are attracting an exponentially-growing attention [81]. These sensors can be easily attached to the structure and their information can be wirelessly obtained by means of an interrogating antenna [510].

Crack/defect detection epitomizes the application of NDT techniques [22]. The research on RFID crack detection sensors for SHM is therefore a remarkably active field [25].

The RFID tag is composed of a broadband antenna (usually a circular microstrip patch antenna, CMPA) and a meander transmission line terminated with an open or short circuit. The interrogating antenna, or RFID reader, sends a broadband RF pulse and measures the backscatter from the RFID tag sensor. When the pulse reaches the sensor, a portion is immediately reflected and another portion is harnessed by the RFID antenna, which then travels through the meander line, being finally reflected back at the open- or short-circuited termination. The interrogating antenna thereby receives two echoes (namely the initial reflection off the sensor and the secondary re-transmission of the harnessed energy). By means of the computation of the time difference of arrival (TDOA) between the echoes it can be identified whether the secondary signal travelled through the entire meander line (in the absence of cracks) or if the meander line is prematurely interrupted with a new open-circuited termination due to a crack or defect in the material it is attached to [511] and [512], as shown in Figure 39.



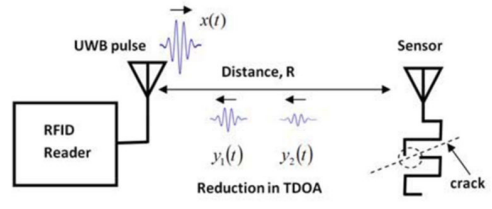


FIGURE 39. Working principle of RFID wireless crack detection. Operation in the absence (top) and presence (bottom) of crack. Reprinted with permission from [511]; copyright 2012 IEEE.

Following these principles, several approaches and designs have been proposed [75]. For example, multiresonance RFID sensor tags were proved effective for crack and corrosion detection in metallic structures by means of Principal Component Analysis algorithms [513]. These multiresonant arrays, with their characteristic spatial signatures, are of particular interest for pipeline integrity monitoring [514] and coating defect detection [24]. Frequency selective surface RFID tags were combined with feature fusion techniques (simple sum and confidence weighted averaging) with good results [515]. Proposals have been made in the modern context of the IoT, such as a 7-bit chipless RFID multiparameter sensor for temperature and crack sensing [80], or novel frequency selective surface strips effective for uninterrupted detection of cracks with 0.5 mm width resolution [81].

Similar to crack detection and equally crucial is strain sensing. Proposals relying on resistive strain gauges inside a Wheatstone bridge integrated into a resistance-to-frequency



converter have been made, wirelessly read by RFID communication channels [516], although requiring constant voltage supply, which entails battery-based maintenance. This drawback, accentuated by the requirements of IoT context, led in the recent years to the development of chipless RFID strain sensors [517]. Thanks to sophisticated aerosolized nanocomposites printing techniques, an IDC (Inter-Digital Capacitor) structure was printed into a stretchable RFID tag for effective sensing of normal and shear strain [518]. Other flexible implementations were researched for wide-range strain sensing through electric-LC resonators [519] and LC structures with a parallel-plate capacitance unit (likely to be cracked due to strain) [520] printed into RFID tags. The last advancements achieved passive RFID strain sensing for directional-independent structural deformation monitoring and crack detection by means of mutually coupled resonant rings [521], [522].

Last, but not least, the fundamental principles reviewed here as for material characterization through permittivity variations were also applied to SHM realm. In particular, monitoring of concrete mixture composition (with special emphasis on its water content) is essential for punctual control of the curing and dying phases and also for humidity content sensing, related to aging and corrosion of concrete [523], which can be achieved by usual planar resonating sensors [524]. For long-term concrete testing in SHM, chipless RFID solutions have been shown [525], for example based on meander delay lines, the introduced delay depending on the effective permittivity, it depending in turn on the concrete mixture composition [526]. In a different approach, the sensing tag was made of a depolarizing dipole resonator loaded with printed capacitors, the capacitance of which depends on the effective permittivity [74]. These principles have also been applied for steel pipeline health monitoring [23]. A recent developed sensor based on a slot resonator has been proposed to detect the onset of corrosion in urban metallic infrastructures, such as streetlights and traffic lamps [527]. Such sensor is sensitive to changes in the permittivity caused by oxidation and by other chemical processes on the corroded samples.

F. AUTOMOTIVE AND SPACE INDUSTRY

Planar microwave resonators hold significant potential for use in industrial settings and platforms due to their high sensitivity, mechanical flexibility, and the ability to integrate electronics on the same substrate [1]. Their planar geometry supports fabrication of compact sensors on both rigid and flexible substrates, making them ideal for miniaturized sensing systems. Their compatibility with CMOS technology further enables integration with signal processing and wireless communication circuits [528]. The localized sensing feature of planar microwave sensors makes them a good candidate in ice and snow sensing applications.

For location-based sensing, Shah et al. [529] developed a network of three planar complementary split ring resonator (CSRR) sensors, utilizing radar-inspired time-domain reflectometry (TDR) techniques. These epoxy-coated sensors exhibited a sensitivity of 60 MHz in response to a 0.1 ml frozen droplet and about 35 MHz for a 1 mm thick layer of dry snow. The system can effectively differentiate between identical microwave sensors within a cascaded sensor configuration. Subsequently, Shah et al. [27] introduced a dual-frequency sensor for in-flight ice detection on critical aircraft surfaces using microwave splitring resonator (SRR) sensors. This sensor effectively detected the onset of icing, tracked the growth of ice accretion, and identified the point of ice shedding.

On the other hand, the outer surfaces of structures such as aircraft and automobiles are susceptible to erosive wear, which causes irreversible surface degradation and poses significant safety risks. To address this, Balasubramanian et al. [345] developed a real-time planar microwave sensor integrated with a smart, embedded monitoring circuit for detecting erosive wear in coatings. Balasubramanian and Zarifi [364] later introduced a novel passive and battery-free array of SRR sensors integrated with cloud-based augmented reality for the inspection of coating damage. This integration allows for real-time visualization of damage assessments, offering a low-cost and efficient solution for monitoring areas that are typically difficult to access or evaluate.

While planar microwave resonators are well-suited for embedded sensing applications, remote detection remains essential in situations where sensor placement is impractical. To address such need, Niknahad et al. [530] introduced a microwave waveguide sensor capable of detecting thin ice layers on metallic surfaces without the need for embedded components. This sensor, based on a WR-62 waveguide with an engineered slit by machining aluminum serving as an impedance-matching element, was designed to operate at a resonant frequency of 15.6 GHz. The developed sensor demonstrated high sensitivity not only to the presence of ice but also to variations in ice thickness and salt content. Experimental results revealed that the sensor could detect as little as $100~\mu L$ of ice with a frequency shift of 87 MHz.

G. MOTION CONTROL

Motion control is a transverse discipline, necessary in scenarios as diverse as civil engineering, industrial engineering, heavy industry, automotive/space industry, robotics, etc. The idea behind motion control is to gather information of certain motion variables in a mechanical system (typically displacements—linear, angular, or combined— and velocities) to take corrective actions, or other actions, from the retrieved information. Thus, motion sensors are key components in any motion control system.

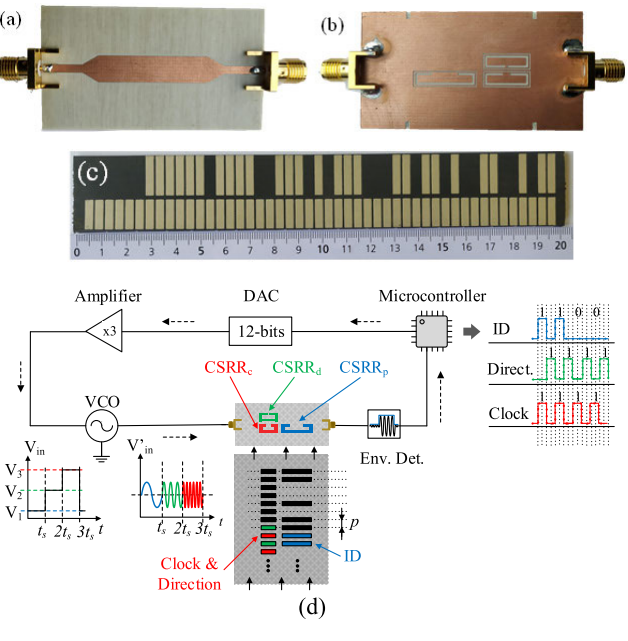
Motion sensors can be classified according to many criteria, but concerning motion sensors based on microwave technology, the interest in this review paper, an important categorization differentiates between short-range and medium/long-range sensors. By short-range motion sensors, we refer to sensors able to measure displacements in the cm and sub-cm range, whereas medium/long-range motion



sensors are those devoted to measuring displacements in the scale of various cm and beyond. This distinction is made according to the typical dimensions of planar microwave resonators operating at microwave frequencies, few cm or below. Namely, for the measurement of short-range displacements (linear or angular), as defined, sensor topologies based on a transmission line structure and a movable resonator coupled to it have been considered [140], [141], [142], [143], [144], [145], [146], [147], [148]. The motion of the movable resonator in proximity to the line perturbs the transmission or reflection coefficient, generating an output variable related to its relative motion. Sensors of this kind have been applied to the measurement of linear and angular displacements and velocities [140], [141], [142], [143], [144], [145], [146], [147], [148].

When medium/long range measurements are needed, one solution is to implement an electromagnetic encoder system, a device where the static part is a harmonic-fed transmission line, and the movable part is a chain, or various chains, of metallic or dielectric inclusions [29], [30], [31], [149], [150], [151], [152]. Such chain/s is/are linear in the so-called linear encoders, and circular (located in the periphery of a dielectric disc) in rotary encoders. When the chain moves on top of the line at short vertical distance, pulses in either the magnitude or phase of the transmission coefficient at the operating frequency are generated, and the relative position and velocity between the encoder and the static part (sometime called reader) can be inferred.

To illustrate the potential of electromagnetic encoders in industrial engineering, Figure 40 reports a sensor system where the encoder is implemented in a rubber elevator belt (emulating e.g., a conveyor belt) [31]. The inclusions are rectangular patches, and two parallel chains are visible in the encoder. One chain is periodic, whereas the other one contains only some of the patches present in the positions of the patches of the other chain. That is, this second chain is equipped with a certain ID code (with the logic state determined by the presence or absence of patch), which is used to determine the absolute position of the encoder (for that purpose, the ID code of the whole encoder must follow the so-called De Bruijn sequence, where any subset of adjacent N-bits does not repeat, see further details in [31]). When the patches cross the complementary split ring resonators (CSRRs) of the reader line, pulses are generated in the envelope function of the harmonic signals that feed the line (a harmonic signal per each CSRR). One of the three signals at the output port is periodic and is used as clock signal and to determine the encoder velocity (from the time lapse between adjacent pulses in the envelope function). A second signal provides the ID code, from which the encoder position can be inferred (by reading each bit plus the previous N-1 bits). Finally, the third signal is redundant, but with a lead or lag as compared to the clock signal and is used to determine the motion direction of the encoder. In the sketch of Figure 40(d), it is shown that the three harmonic signals are generated by means of a VCO managed by a microcontroller,



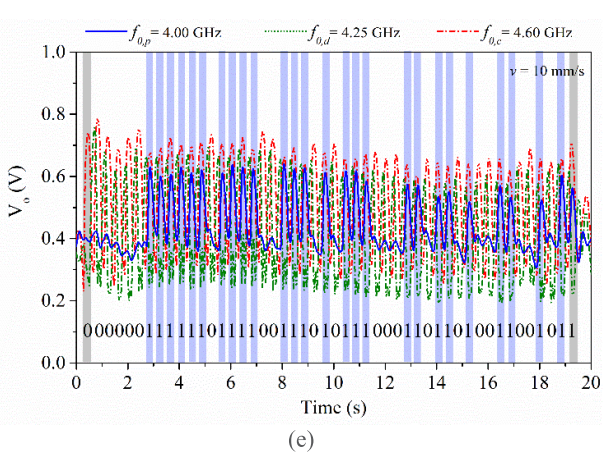


FIGURE 40. Electromagnetic encoder system based on a reader line loaded with three CSRRs, and encoder implemented on a rubber elevator belt by means of two chains of metallic patches. (a) Photograph of the top view of the reader line; (b) photograph of the bottom view of the reader line; (c) photograph of the encoder; (d) sketch of the complete system, managed by means of a microcontroller to feed the line with the three harmonic signals at different instants of time; (e) envelope functions for the three harmonic signals of the encoder. Substrate characteristics and dimensions of the reader and encoder are given in [31]. In(e), $f_{\rm op}$, $f_{\rm od}$, and $f_{\rm oc}$ are the carrier frequencies of the position signal, direction signal, and clock signal, respectively. The pulses in the envelope function of the position signal correlate with the ID code of the encoder. In the reported result, the encoder was displaced at a constant velocity of 10 mm/s. Reprinted with permission from [31]; copyright 2023 IEEE.

which separates also the three envelope functions that result at the output port of the reader line [Figure 40(e)].

Electromagnetic encoders cannot compete against optical encoders [531], [532], [533], [534], [535], [536] in terms of resolution, dictated by the period of the chain. However, such optical encoders are more prone to the effects of pollution and dirtiness, encountered in many industrial environments. There are also magnetic encoders and Hall-effect sensors [537], [538], [539], [540], [541], [542],



TABLE 2. Summary of representative examples for different sensor types and applications.

Ref.	Sensor type	Frequency of operation	Sensitivity	Proposed application	Remarks
[56]	Frequency variation	1.91 GHz	0.90 %	Volume fraction detection in water- methanol mixtures	Microstrip transmission line loaded with an SIR; low sample volume required
[221]	Frequency variation	2.45 GHz	0.68 %	Volume fraction detection in water–isopropanol mixtures	A circular SIW resonator housing in its center a transversal glass pipe covered with a metallic sheath
[66]	Frequency variation	2.63 GHz	19.95 MHz/vol%	Volume fraction detection in water-ethanol and water-NaCl mixtures	A microfluidic channel embedded into the substrate, with a SRR and an active feedback loop
[2]	Frequency variation $(Q_u$ -based)	4.62 GHz	2.73 %/vol%	Glucose concentration detection in aqueous solutions	3-D printed Q_u -based SRR with a certified biocompatible material for biomedical applications
[97]	Frequency splitting	3.00 GHz	2.70 MHz/μL	Detection of deionized water absorption; quantification of deionized water drops	Microstrip transmission line loaded with two SIRs; embroidered in fabric with conductive yarn
[27]	Frequency splitting	2.13 GHz	30.00 MHz/melt%	In-flight ice detection on aircraft surfaces	Microstrip line loaded with two SRRs
[108]	Phase variation	2.00 GHz	528.70°	Dielectric constant characterization in solid samples	Two cascaded microstrip section lines alternating high and low impedance
[130]	Phase variation	2.64 GHz	2291°/mm	Detection of submillimeter proximity changes with a solid sample	JFET-driven losses-assisted sensor made of a microstrip transmission line terminated with an SIR
[155]	Magnitude variation	2.12 GHz	0.28 dB/vol%	Dielectric constant characterization in solid and liquid samples, volume fraction detection in liquid samples	Microstrip transmission line loaded with a shunt connection to a SIR and a grounded inductive strip
[556]	Magnitude variation	4.94 GHz	0.045 dB/ppm	Gas sensing: ammonia detection in air	A SRR made of PEDOT:PSS with 8% (v/v) dimethyl sulfoxide
[207]	Magnitude and phase variation	6.00 GHz	-0.26 dB/vol% -0.04°/vol%	Complex permittivity characterization for liquid samples, including wide permittivity ranges	3-D printed structure with the liquid sandwiched between two coupled strip lines
[160]	Differential mode	1.05 GHz	10.08 dB·L/g	Detection of NaCl concentration in diluted water solutions	Microstrip defected ground structure made with two dumbbell slots
[375]	Microwave spectroscopy	Up to 40.00 GHz	_	Discrimination between three different B lymphoma cell lines	Coplanar waveguide with integrated microfluidic sensor, as shown in [162]
[293]	Multi- parameter sensing	Up to 3.00 GHz	_	Simultaneous analytical determination of dielectric constant, loss tangent and thickness of solid samples	Three mutually-coupled SRRs in two PCBs with the solid sample sandwiched between the PCBs

[543], [544], [545], [546], [547], [548], [549], but such motion sensors typically utilize inductive coils or magnets. By contrast electromagnetic encoders are merely based on a reader line fed by a harmonic signal (or a set of harmonic signals) and the encoder (made of a dielectric substrate with metallic inclusions etched or printed on it). It is worth noting that electromagnetic encoders can also be used as near-field chipless-RFID tags, see [550] and references therein. In such an application, tag reading by proximity and proper alignment is a due, but the number of bits is only limited by the size of the tag, a competitive advantage as compared to far-field backscattered or retransmission chipless-RFID tags, as discussed in [550].

To end this subsection, it should be mentioned that there are also microwave proximity sensors able to measure vertical distances, between the reader and the movable part, at the micrometer scale [130], [132], [133]. It is

worth to highlight a recent work [132], consisting of a capacitive proximity sensor, that uses microwave technology for sensing, particularly the phase of the reflection coefficient at a fixed frequency, in a CPW transmission line terminated with a coupled (vertically movable) SIR. That sensor exhibits a maximum sensitivity of 3722°/mm, and it can detect separations as small as 10 μ m. Proximity sensors based on the vertical motion of a dielectric slab, based on the change in the effective dielectric constant "seen" by the sensor [130], [133], do not exhibit, in general such excellent sensitivities. The reason is that a vertical motion of an element constituting a broadside capacitance, like the one of the SIR coupled to the CPW line, generates a dramatic variation in the capacitance of the resonant element, much higher than the capacitance variation generated by motion of a dielectric slab on top of a resonator. Nevertheless, remarkable sensitivities and resolutions have also been achieved with such proximity



(actually permittivity) sensors based on the vertical motion of a dielectric slab (especially with the sensor in [130], which exhibits a maximum sensitivity of 2291°/mm, as indicated before).

H. GAS SENSING

Planar microwave resonator structures exhibit notable sensitivity and selectivity when detecting liquids and solid materials. However, their inherent limitation in accurately monitoring gas concentrations in the surrounding environment highlights the need for integrating gas-sensitive interface layers [177], [551], [552], [553]. By incorporating gas-sensitive materials into microwave structures, target gas molecules are attracted to the sensitive layer, where they are absorbed or adsorbed onto the material interface [176], [554]. This interaction between the sensitive material and the target gas perturbs the electromagnetic field in the vicinity, resulting in measurable changes in the dielectric properties of the material-coated planar microwave structures [356].

The gas detection mechanism in polymer-integrated planar microwave structures primarily arises from changes in electrical conductivity, swelling of the polymer layer, or both. For instance, exposing DMSO-doped PEDOT:PSS polymer to ammonia gas leads to reduced electrical conductivity through two key processes: (1) Electron-donating ammonia interacts with the p-doped PEDOT:PSS backbone, immobilizing charge carriers and lowering their mobility and density, a common phenomenon in conductive polymers like polyaniline and polypyrrole. (2) Ammonia absorption increases the spacing between PEDOT layers, introducing potential barriers that further hinder conductivity. Unlike frequency shifts, these conductivity changes directly influence the magnitude of scattering parameters of microwave devices [555], [556].

In swelling-based detection, the absorption of a compatible solvent gas by a polymer like PDMS induces swelling, resulting in a volumetric expansion of the PDMS structure. This change in volume is reliably detected using planar microwave structures, which monitor correlated alterations in permittivity and electromagnetic loss. Several factors influence PDMS swelling, including the compatibility and solubility parameters of PDMS and the target gas, gas volume, and environmental temperature. Variations in gas concentration and type within the PDMS directly affect the polymer's effective permittivity, leading to change in the response of the planar microwave sensor, enabling precise gas detection [176], [557]. Polymer-based sensing can be effectively integrated with microwave design techniques, such as low-cost and robust differential microwave resonators, to make it suitable for VOC monitoring. By utilizing differential planar resonators combined with a Wilkinson power divider and a thin PDMS layer, this approach enables precise and accurate gas detection while being less prone to the impact of environmental parameters such as temperature and humidity, enhancing the system's reliability and practicality for various monitoring applications [558].

Recent studies in material integrated microwave planar structures emphasize the significant impact of porosity on polymer-gas interactions and their detection. Porous polydimethylsiloxane (PDMS) structures, due to their increased surface area and interconnected voids, exhibit enhanced gas absorption compared to solid PDMS. This results in more pronounced shifts in the resonant frequency of the split ring resonator (SRR), reflecting greater sensitivity to gas concentration. Additionally, porosity facilitates faster diffusion and interaction of gases, improving both response time and measurement accuracy. These findings underscore the potential of leveraging porosity to optimize microwave resonator-based sensors for studying gas-polymer interactions and for developing advanced applications in environmental monitoring and material characterization [557].

VII. CONCLUSION

In conclusion, this paper has reviewed the recent advances and applications of planar microwave sensors from the perspective and experience of the authors. As a summary, Table 2 compares some representative examples of the different sensor types and applications reviewed here. The work has discussed the main working principles, with emphasis on their advantages and limitations, it has presented the main materials and technologies for sensing (e.g., functional films, liquid metals, organic materials, microfluidics, SIW, 3-D printing, textile-based technology, etc.), and it has presented several strategies for sensor performance optimization, including sensitivity, resolution, and selectivity (in the latter case with special emphasis on artificial intelligencebased approaches). A section has also been dedicated to wireless and antenna-assisted sensors, due to exponentially growing interest for such sensors within the framework of the IoT. Finally, the last section has been focused on highlighting some applications of planar microwave sensors, including biosensors, sensors for smart healthcare, sensors for smart agriculture and agrifood industry, sensors for ambient monitoring, sensors for structural health monitoring, sensors for the automotive and space industry, sensors for motion control applications and gas sensors.

REFERENCES

- F. Martín, P. Vélez, J. Muñoz-Enano, and L. Su, *Planar Microwave Sensors*. Hoboken, NJ, USA: Wiley, 2022.
- [2] C. G. Juan, B. Potelon, C. Quendo, H. García-Martínez, E. Ávila-Navarro, E. Bronchalo, and J. M. Sabater-Navarro, "Study of Q_u-based resonant microwave sensors and design of 3-D-printed devices dedicated to glucose monitoring," *IEEE Trans. Instrum. Meas.*, vol. 70, pp. 1–16, 2021.
- [3] C. G. Juan, E. Bronchalo, B. Potelon, C. Quendo, V. F. Muñoz, J. M. Ferrández-Vicente, and J. M. Sabater-Navarro, "On the selectivity of planar microwave glucose sensors with multicomponent solutions," *Electronics*, vol. 12, no. 1, p. 191, Dec. 2022.
- [4] P. Vélez, J. Muñoz-Enano, K. Grenier, J. Mata-Contreras, D. Dubuc, and F. Martín, "Split ring resonator-based microwave fluidic sensors for electrolyte concentration measurements," *IEEE Sensors J.*, vol. 19, no. 7, pp. 2562–2569, Apr. 2019.



- [5] J. Muñoz-Enano, P. Vélez, M. Gil, E. Jose-Cunilleras, A. Bassols, and F. Martín, "Characterization of electrolyte content in urine samples through a differential microfluidic sensor based on dumbbell-shaped defected ground structures," *Int. J. Microw. Wireless Technol.*, vol. 12, no. 9, pp. 817–824, Nov. 2020.
- [6] R. Narang, S. Mohammadi, M. M. Ashani, H. Sadabadi, H. Hejazi, M. H. Zarifi, and A. Sanati-Nezhad, "Sensitive, real-time and nonintrusive detection of concentration and growth of pathogenic bacteria using microfluidic-microwave ring resonator biosensor," Sci. Rep., vol. 8, no. 1, Oct. 2018, Art. no. 15807.
- [7] S. Mohammadi, A. V. Nadaraja, K. Luckasavitch, M. C. Jain, D. J. Roberts, and M. H. Zarifi, "A label-free, non-intrusive, and rapid monitoring of bacterial growth on solid medium using microwave biosensor," *IEEE Trans. Biomed. Circuits Syst.*, vol. 14, no. 1, pp. 2–11, Feb. 2020.
- [8] M. C. Jain, A. V. Nadaraja, R. Narang, and M. H. Zarifi, "Rapid and real-time monitoring of bacterial growth against antibiotics in solid growth medium using a contactless planar microwave resonator sensor," *Sci. Rep.*, vol. 11, no. 1, Jul. 2021, Art. no. 14775.
- [9] M. C. Jain, A. V. Nadaraja, S. Mohammadi, B. M. Vizcaino, and M. H. Zarifi, "Passive microwave biosensor for real-time monitoring of subsurface bacterial growth," *IEEE Trans. Biomed. Circuits Syst.*, vol. 15, no. 1, pp. 122–132, Feb. 2021.
- [10] J. Muñoz-Enano, O. Peytral-Rieu, P. Vélez, D. Dubuc, K. Grenier, and F. Martín, "Characterization of the denaturation of bovine serum albumin (BSA) protein by means of a differential-mode microwave microfluidic sensor based on slot resonators," *IEEE Sensors J.*, vol. 22, no. 14, pp. 14075–14083, Jul. 2022.
- [11] I. Piekarz, J. Sorocki, S. Gorska, K. Wincza, and S. Gruszczynski, "Microwave biosensors for label-free bacteria detection," in *IEEE MTT-S Int. Microw. Symp. Dig.*, Leuven, Belgium, Sep. 2023, pp. 109–111.
- [12] N. Celik, R. Gagarin, H.-S. Youn, and M. F. Iskander, "A noninvasive microwave sensor and signal processing technique for continuous monitoring of vital signs," *IEEE Antennas Wireless Propag. Lett.*, vol. 10, pp. 286–289, 2011.
- [13] M. Elgeziry, F. Costa, A. Tognetti, and S. Genovesi, "Wearable textile-based sensor tag for breath rate measurement," *IEEE Sensors J.*, vol. 22, no. 23, pp. 22610–22619, Dec. 2022.
- [14] S. V. S. T. Jonnalagadda, D. P. Mishra, and S. K. Behera, "Chipless RF identification sensors for vital signs monitoring: A comprehensive review," *IEEE Microw. Mag.*, vol. 24, no. 11, pp. 53–70, Nov. 2023.
- [15] D. Girbau, Á. Ramos, A. Lazaro, S. Rima, and R. Villarino, "Passive wireless temperature sensor based on time-coded UWB chipless RFID tags," *IEEE Trans. Microw. Theory Techn.*, vol. 60, no. 11, pp. 3623–3632, Nov. 2012.
- [16] W. M. Abdulkawi and A.-F.-A. Sheta, "Chipless RFID sensors based on multistate coupled line resonators," *Sens. Actuators A, Phys.*, vol. 309, Jul. 2020, Art. no. 112025.
- [17] J. Yeo, J.-I. Lee, and Y. Kwon, "Humidity-sensing chipless RFID tag with enhanced sensitivity using an interdigital capacitor structure," *Sensors*, vol. 21, no. 19, p. 6550, Sep. 2021.
- [18] E. Md. Amin, Md. S. Bhuiyan, N. C. Karmakar, and B. Winther-Jensen, "Development of a low cost printable chipless RFID humidity sensor," *IEEE Sensors J.*, vol. 14, no. 1, pp. 140–149, Jan. 2014.
- [19] C. Occhiuzzi, A. Rida, G. Marrocco, and M. Tentzeris, "RFID passive gas sensor integrating carbon nanotubes," *IEEE Trans. Microw. Theory Techn.*, vol. 59, no. 10, pp. 2674–2684, Oct. 2011.
- [20] R. A. Potyrailo and C. Surman, "A passive radio-frequency identification (RFID) gas sensor with self-correction against fluctuations of ambient temperature," Sens. Actuators B, Chem., vol. 185, pp. 587–593, Aug. 2013.
- [21] A. A. Kutty, T. Björninen, L. Sydänheimo, and L. Ukkonen, "A novel carbon nanotube loaded passive UHF RFID sensor tag with built-in reference for wireless gas sensing," in *IEEE MTT-S Int. Microw. Symp. Dig.*, San Francisco, CA, USA, May 2016, pp. 1–4.
- [22] A. Ali, M. E. Badawe, and O. M. Ramahi, "Microwave imaging of subsurface flaws in coated metallic structures using complementary split-ring resonators," *IEEE Sensors J.*, vol. 16, no. 18, pp. 6890–6898, Sep. 2016.
- [23] Z. Abbasi, H. Niazi, M. Abdolrazzaghi, W. Chen, and M. Daneshmand, "Monitoring pH level using high-resolution microwave sensor for mitigation of stress corrosion cracking in steel pipelines," *IEEE Sensors J.*, vol. 20, no. 13, pp. 7033–7043, Jul. 2020.

- [24] S. Deif and M. Daneshmand, "Long array of microwave sensors for real-time coating defect detection," *IEEE Trans. Microw. Theory Techn.*, vol. 68, no. 7, pp. 2856–2866, Jul. 2020.
- [25] T. S. Yee, N. H. M. M. Shrifan, A. J. A. Al-Gburi, N. A. M. Isa, and M. F. Akbar, "Prospect of using machine learning-based microwave nondestructive testing technique for corrosion under insulation: A review," *IEEE Access*, vol. 10, pp. 88191–88210, 2022.
- [26] O. Niksan, K. Colegrave, and M. H. Zarifi, "Battery-free, artificial neural network-assisted microwave resonator array for ice detection," *IEEE Trans. Microw. Theory Techn.*, vol. 71, no. 2, pp. 698–709, Feb. 2023.
- [27] A. Shah, O. Niksan, F. Niknahad, M. C. Jain, D. Fuleki, F. Rasinarzabadi, and M. H. Zarifi, "Unlocking conformal microwave split ring resonant sensors for in-flight ice sensing," *IEEE Trans. Aerosp. Electron. Syst.*, vol. 60, no. 1, pp. 525–536, Feb. 2024.
- [28] A. Shah, O. Niksan, M. C. Jain, K. Colegrave, M. Wagih, and M. H. Zarifi, "Microwaves see thin ice: A review of ice and snow sensing using microwave techniques," *IEEE Microw. Mag.*, vol. 24, no. 10, pp. 24–39, Oct. 2023.
- [29] A. Karami-Horestani, F. Paredes, and F. Martín, "High data density absolute electromagnetic encoders based on hybrid time/frequency domain encoding," *IEEE Sensors J.*, vol. 22, no. 24, pp. 23866–23876, Dec. 2022.
- [30] A. Karami-Horestani, F. Paredes, and F. Martín, "Hybrid time/phase domain synchronous electromagnetic encoders for near-field chipless-RFID and motion control applications," *IEEE Trans. Microw. Theory Techn.*, vol. 71, no. 12, pp. 5457–5469, Dec. 2023.
- [31] F. Paredes, A. Moya, M. Berenguel-Alonso, D. Gonzalez, P. Bruguera, C. Delgado-Simao, and F. Martín, "Motion control system for industrial scenarios based on electromagnetic encoders," *IEEE Trans. Instrum. Meas.*, vol. 72, 2023, Art. no. 2003612.
- [32] N. K. Tiwari, S. P. Singh, and M. J. Akhtar, "Novel improved sensitivity planar microwave probe for adulteration detection in edible oils," *IEEE Microw. Wireless Compon. Lett.*, vol. 29, no. 2, pp. 164–166, Feb. 2019.
- [33] M. Erdoğan, E. Ünal, F. Ö. Alkurt, Y. I. Abdulkarim, L. Deng, and M. Karaaslan, "Determination of frying sunflower oil usage time for local potato samples by using microwave transmission line based sensors," *Measurement*, vol. 163, Oct. 2020, Art. no. 108040.
- [34] M. R. Islam, M. T. Islam, A. Hoque, M. S. Soliman, B. Bais, N. M. Sahar, and S. H. A. Almalki, "Tri circle split ring resonator shaped metamaterial with mathematical modeling for oil concentration sensing," *IEEE Access*, vol. 9, pp. 161087–161102, 2021.
- [35] J. Muñoz-Enano, P. Vélez, P. Casacuberta, L. Su, and F. Martín, "Characterization of edible oils subjected to industrial frying processes through high sensitivity microwave sensors," in *Proc. 53rd Eur. Microw. Conf. (EuMC)*, Berlin, Germany, Sep. 2023, pp. 737–740.
- [36] M. Shaji and M. J. Akhtar, "Microwave coplanar sensor system for detecting contamination in food products," in *IEEE MTT-S Int. Microw.* Symp. Dig., New Delhi, India, Dec. 2013, pp. 1–4.
- [37] R. Raju, G. E. Bridges, and S. Bhadra, "Wireless passive sensors for food quality monitoring: Improving the safety of food products," *IEEE Antennas Propag. Mag.*, vol. 62, no. 5, pp. 76–89, Oct. 2020.
- [38] L. A. P. Silva, F. D. A. B. Filho, and H. D. de Andrade, "Soil moisture monitoring system based on metamaterial-inspired microwave sensor for precision agriculture applications," *IEEE Sensors J.*, vol. 23, no. 19, pp. 23713–23720, Oct. 2023.
- [39] A. Ebrahimi, W. Withayachumnankul, S. Al-Sarawi, and D. Abbott, "High-sensitivity metamaterial-inspired sensor for microfluidic dielectric characterization," *IEEE Sensors J.*, vol. 14, no. 5, pp. 1345–1351, May 2014.
- [40] M. Puentes, C. Weiß, M. Schüßler, and R. Jakoby, "Sensor array based on split ring resonators for analysis of organic tissues," in *IEEE MTT-S Int. Microw. Symp. Dig.*, Baltimore, MD, USA, Jun. 2011, pp. 1–4.
- [41] M. Schueler, C. Mandel, M. Puentes, and R. Jakoby, "Metamaterial inspired microwave sensors," *IEEE Microw. Mag.*, vol. 13, no. 2, pp. 57–68, Mar. 2012.
- [42] M. S. Boybay and O. M. Ramahi, "Material characterization using complementary split-ring resonators," *IEEE Trans. Instrum. Meas.*, vol. 61, no. 11, pp. 3039–3046, Nov. 2012.
- [43] C.-S. Lee and C.-L. Yang, "Complementary split-ring resonators for measuring dielectric constants and loss tangents," *IEEE Microw. Wireless Compon. Lett.*, vol. 24, no. 8, pp. 563–565, Aug. 2014.



- [44] C.-L. Yang, C.-S. Lee, K.-W. Chen, and K.-Z. Chen, "Noncontact measurement of complex permittivity and thickness by using planar resonators," *IEEE Trans. Microw. Theory Techn.*, vol. 64, no. 1, pp. 247–257, Jan. 2016.
- [45] L. Su, J. Mata-Contreras, P. Vélez, and F. Martín, "Estimation of the complex permittivity of liquids by means of complementary split ring resonator (CSRR) loaded transmission lines," in *IEEE MTT-S Int. Microw. Symp. Dig.*, Pavia, Italy, Sep. 2017, pp. 1–3.
- [46] L. Su, J. Mata-Contreras, P. Vélez, A. Fernández-Prieto, and F. Martín, "Analytical method to estimate the complex permittivity of oil samples," *Sensors*, vol. 18, no. 4, p. 984, Mar. 2018.
- [47] M. Abdolrazzaghi, M. H. Zarifi, W. Pedrycz, and M. Daneshmand, "Robust ultra-high resolution microwave planar sensor using fuzzy neural network approach," *IEEE Sensors J.*, vol. 17, no. 2, pp. 323–332, Jan. 2017.
- [48] M. Abdolrazzaghi, M. H. Zarifi, and M. Daneshmand, "Sensitivity enhancement of split ring resonator based liquid sensors," in *Proc. IEEE SENSORS*, Orlando, FL, USA, Oct. 2016, pp. 1–3.
- [49] M. H. Zarifi and M. Daneshmand, "Monitoring solid particle deposition in lossy medium using planar resonator sensor," *IEEE Sensors J.*, vol. 17, no. 23, pp. 7981–7989, Dec. 2017.
- [50] M. H. Zarifi, S. Deif, M. Abdolrazzaghi, B. Chen, D. Ramsawak, M. Amyotte, N. Vahabisani, Z. Hashisho, W. Chen, and M. Daneshmand, "A microwave ring resonator sensor for early detection of breaches in pipeline coatings," *IEEE Trans. Ind. Electron.*, vol. 65, no. 2, pp. 1626–1635, Feb. 2018.
- [51] M. Abdolrazzaghi, M. Daneshmand, and A. K. Iyer, "Strongly enhanced sensitivity in planar microwave sensors based on metamaterial coupling," *IEEE Trans. Microw. Theory Techn.*, vol. 66, no. 4, pp. 1843–1855, Apr. 2018.
- [52] J. Muñoz-Enano, P. Vélez, C. Herrojo, M. Gil, and F. Martín, "On the sensitivity of microwave sensors based on slot resonators and frequency variation," in *Proc. Int. Conf. Electromagn. Adv. Appl. (ICEAA)*, Granada, Spain, Sep. 2019, pp. 112–115.
- [53] H. Lobato-Morales, J. H. Choi, H. Lee, and J. L. Medina-Monroy, "Compact dielectric-permittivity sensors of liquid samples based on substrate-integrated-waveguide with negative-order-resonance," *IEEE Sensors J.*, vol. 19, no. 19, pp. 8694–8699, Oct. 2019.
- [54] A. K. Jha, N. Delmonte, A. Lamecki, M. Mrozowski, and M. Bozzi, "Design of microwave-based angular displacement sensor," *IEEE Microw. Wireless Compon. Lett.*, vol. 29, no. 4, pp. 306–308, Apr. 2019.
- [55] M. Saadat-Safa, V. Nayyeri, M. Khanjarian, M. Soleimani, and O. M. Ramahi, "A CSRR-based sensor for full characterization of magneto-dielectric materials," *IEEE Trans. Microw. Theory Techn.*, vol. 67, no. 2, pp. 806–814, Feb. 2019.
- [56] A. Ebrahimi, J. Scott, and K. Ghorbani, "Ultrahigh-sensitivity microwave sensor for microfluidic complex permittivity measurement," *IEEE Trans. Microw. Theory Techn.*, vol. 67, no. 10, pp. 4269–4277, Oct. 2019.
- [57] M. Saadat-Safa, V. Nayyeri, A. Ghadimi, M. Soleimani, and O. M. Ramahi, "A pixelated microwave near-field sensor for precise characterization of dielectric materials," *Sci. Rep.*, vol. 9, no. 1, Sep. 2019, Art. no. 13310.
- [58] M. Abdolrazzaghi and M. Daneshmand, "Exploiting sensitivity enhancement in micro-wave planar sensors using intermodulation products with phase noise analysis," *IEEE Trans. Circuits Syst. I, Reg. Papers*, vol. 67, no. 12, pp. 4382–4395, Dec. 2020.
- [59] A. Ebrahimi, J. Scott, and K. Ghorbani, "Microwave reflective biosensor for glucose level detection in aqueous solutions," *Sens. Actuators A*, *Phys.*, vol. 301, Jan. 2020, Art. no. 111662.
- [60] A. Ebrahimi, J. Scott, and K. Ghorbani, "Dual-mode resonator for simultaneous permittivity and thickness measurement of dielectrics," *IEEE Sensors J.*, vol. 20, no. 1, pp. 185–192, Jan. 2020.
- [61] H. Abdelwahab, A. Ebrahimi, F. J. Tovar-Lopez, G. Beziuk, and K. Ghorbani, "Extremely sensitive microwave microfluidic dielectric sensor using a transmission line loaded with shunt LC resonators," *Sensors*, vol. 21, no. 20, p. 6811, Oct. 2021.
- [62] J. Muñoz-Enano, J. Martel, P. Vélez, F. Medina, L. Su, and F. Martín, "Parametric analysis of the edge capacitance of uniform slots and application to frequency-variation permittivity sensors," *Appl. Sci.*, vol. 11, no. 15, p. 7000, Jul. 2021.

- [63] N. Kazemi, M. Abdolrazzaghi, and P. Musilek, "Comparative analysis of machine learning techniques for temperature compensation in microwave sensors," *IEEE Trans. Microw. Theory Techn.*, vol. 69, no. 9, pp. 4223–4236, Sep. 2021.
- [64] Z. Mehrjoo, A. Ebrahimi, and K. Ghorbani, "Microwave resonance-based reflective mode displacement sensor with wide dynamic range," *IEEE Trans. Instrum. Meas.*, vol. 71, pp. 1–9, 2022.
- [65] J. Muñoz-Enano, P. Vélez, M. Gil, and F. Martín, "Frequency-variation sensors for permittivity measurements based on dumbbell-shaped defect ground structures (DB-DGS): Analytical method and sensitivity analysis," *IEEE Sensors J.*, vol. 22, no. 10, pp. 9378–9386, May 2022.
- [66] S. Mohammadi, K. K. Adhikari, M. C. Jain, and M. H. Zarifi, "High-resolution, sensitivity-enhanced active resonator sensor using substrate-embedded channel for characterizing low-concentration liquid mixtures," *IEEE Trans. Microw. Theory Techn.*, vol. 70, no. 1, pp. 576–586, Jan. 2022.
- [67] M. Moradpour and M. H. Zarifi, "High-resolution PEDOT:PSS-based planar microwave resonator sensor," *IEEE Sensors J.*, vol. 23, no. 18, pp. 21216–21225, Sep. 2023.
- [68] M. A. Rafi, F. Niknahad, B. D. Wiltshire, A. Salim, and M. H. Zarifi, "Dynamically tunable planar microwave resonator sensor using liquid metal alloy," *IEEE Trans. Microw. Theory Techn.*, vol. 72, no. 7, pp. 4103–4113, Jul. 2024.
- [69] Y. Feng, L. Xie, Q. Chen, and L.-R. Zheng, "Low-cost printed chipless RFID humidity sensor tag for intelligent packaging," *IEEE Sensors J.*, vol. 15, no. 6, pp. 3201–3208, Jun. 2015.
- [70] M. M. Forouzandeh and N. Karmakar, "Towards the improvement of frequency-domain chipless RFID readers," in *Proc. IEEE Wireless Power Transf. Conf. (WPTC)*, Montreal, QC, Canada, Jun. 2018, pp. 1–4.
- [71] N. Javed, A. Habib, Y. Amin, J. Loo, A. Akram, and H. Tenhunen, "Directly printable moisture sensor tag for intelligent packaging," *IEEE Sensors J.*, vol. 16, no. 16, pp. 6147–6148, Aug. 2016.
- [72] M. Borgese, F. A. Dicandia, F. Costa, S. Genovesi, and G. Manara, "An inkjet printed chipless RFID sensor for wireless humidity monitoring," *IEEE Sensors J.*, vol. 17, no. 15, pp. 4699–4707, Aug. 2017.
- [73] H. E. Matbouly, K. Zannas, Y. Duroc, and S. Tedjini, "Chipless wireless temperature sensor based on C-like scatterer for standard RFID reader," in Proc. XXXIInd Gen. Assem. Scientific Symp. Int. Union Radio Sci. (URSI GASS), Montreal, QC, Canada, Aug. 2017, pp. 1–3.
- [74] A. Lázaro, R. Villarino, F. Costa, S. Genovesi, A. Gentile, L. Buoncristiani, and D. Girbau, "Chipless dielectric constant sensor for structural health testing," *IEEE Sensors J.*, vol. 18, no. 13, pp. 5576–5585, Jul. 2018.
- [75] A. M. J. Marindra and G. Y. Tian, "Chipless RFID sensor tag for metal crack detection and characterization," *IEEE Trans. Microw. Theory Techn.*, vol. 66, no. 5, pp. 2452–2462, May 2018.
- [76] J. A. Satti, A. Habib, H. Anam, S. Zeb, Y. Amin, J. Loo, and H. Tenhunen, "Miniaturized humidity and temperature sensing RFID enabled tags," *Int. J. RF Microw. Comput.-Aided Eng.*, vol. 28, no. 1, Jan. 2018, Art. no. e21151.
- [77] N. Javed, A. Habib, T. Noor, Y. Amin, and H. Tenhunen, "RFID enabled chipless humidity sensor," *Nucleus*, vol. 56, no. 1, pp. 27–30, Jun. 2019.
- [78] W. M. Abdulkawi and A.-F.-A. Sheta, "Two-bit chipless RFID for temperature and humidity sensing," in *Proc. IEEE Asia Pacific Microw. Conf. (APMC)*, Dec. 2019, pp. 1443–1445.
- [79] D. P. Mishra, T. K. Das, and S. K. Behera, "Design of a 3-bit chipless RFID tag using circular split-ring resonators for retail and healthcare applications," in *Proc. Nat. Conf. Commun. (NCC)*, Kharagpur, India, Feb. 2020, pp. 1–4.
- [80] N. Javed, M. A. Azam, and Y. Amin, "Chipless RFID multisensor for temperature sensing and crack monitoring in an IoT environment," *IEEE Sensors Lett.*, vol. 5, no. 6, pp. 1–4, Jun. 2021.
- [81] S. Dey, R. Bhattacharyya, S. E. Sarma, and N. C. Karmakar, "A novel 'smart skin' sensor for chipless RFID-based structural health monitoring applications," *IEEE Internet Things J.*, vol. 8, no. 5, pp. 3955–3971, Mar. 2021.
- [82] H. Jiang, J. Sanders, J. Yao, and H. Huang, "Patch antenna based temperature sensor," *Proc. SPIE*, vol. 9063, pp. 398–406, Apr. 2014.
- [83] H. Huang, F. Farahanipad, and A. K. Singh, "A stacked dual-frequency microstrip patch antenna for simultaneous shear and pressure displacement sensing," *IEEE Sensors J.*, vol. 17, no. 24, pp. 8314–8323, Dec. 2017.



- [84] F. M. Tchafa and H. Huang, "Microstrip patch antenna for simultaneous temperature sensing and superstrate characterization," *Smart Mater. Struct.*, vol. 28, no. 10, Oct. 2019, Art. no. 105009.
- [85] G. Muntoni, M. B. Lodi, A. Fedeli, A. Melis, C. Macciò, M. Pastorino, A. Randazzo, G. Mazzarella, and A. Fanti, "Preliminary design and test of a microwave inline moisture sensor for the carasau bread industry," *IEEE Open J. Antennas Propag.*, vol. 5, pp. 1166–1180, 2024.
- [86] A. Aquino, C. G. Juan, B. Potelon, and C. Quendo, "Dielectric permittivity sensor based on planar open-loop resonator," *IEEE Sensors Lett.*, vol. 5, no. 3, pp. 1–4, Mar. 2021.
- [87] A. K. Horestani, J. Naqui, Z. Shaterian, D. Abbott, C. Fumeaux, and F. Martín, "Two-dimensional alignment and displacement sensor based on movable broadside-coupled split ring resonators," *Sens. Actuators A, Phys.*, vol. 210, pp. 18–24, Apr. 2014.
- [88] L. Su, J. Naqui, J. Mata-Contreras, and F. Martín, "Modeling metamaterial transmission lines loaded with pairs of coupled split-ring resonators," *IEEE Antennas Wireless Propag. Lett.*, vol. 14, pp. 68–71, 2015.
- [89] L. Su, J. Naqui, J. Mata-Contreras, and F. Martín, "Modeling and applications of metamaterial transmission lines loaded with pairs of coupled complementary split-ring resonators (CSRRs)," *IEEE Antennas Wireless Propag. Lett.*, vol. 15, pp. 154–157, 2016.
- [90] J. Naqui, C. Damm, A. Wiens, R. Jakoby, L. Su, J. Mata-Contreras, and F. Martín, "Transmission lines loaded with pairs of stepped impedance resonators: Modeling and application to differential permittivity measurements," *IEEE Trans. Microw. Theory Techn.*, vol. 64, no. 11, pp. 3864–3877, Nov. 2016.
- [91] L. Su, J. Mata-Contreras, P. Velez, and F. Martin, "Splitter/combiner microstrip sections loaded with pairs of complementary split ring resonators (CSRRs): Modeling and optimization for differential sensing applications," *IEEE Trans. Microw. Theory Techn.*, vol. 64, no. 12, pp. 4362–4370, Dec. 2016.
- [92] M. H. Zarifi, S. Farsinezhad, B. D. Wiltshire, M. Abdorrazaghi, N. Mahdi, P. Kar, M. Daneshmand, and K. Shankar, "Effect of phosphonate monolayer adsorbate on the microwave photoresponse of TiO₂ nanotube membranes mounted on a planar double ring resonator," *Nanotechnology*, vol. 27, no. 37, Sep. 2016, Art. no. 375201.
- [93] P. Vélez, L. Su, K. Grenier, J. Mata-Contreras, D. Dubuc, and F. Martín, "Microwave microfluidic sensor based on a microstrip splitter/combiner configuration and split ring resonators (SRRs) for dielectric characterization of liquids," *IEEE Sensors J.*, vol. 17, no. 20, pp. 6589–6598, Oct. 2017.
- [94] A. Ebrahimi, J. Scott, and K. Ghorbani, "Differential sensors using microstrip lines loaded with two split-ring resonators," *IEEE Sensors J.*, vol. 18, no. 14, pp. 5786–5793, Jul. 2018.
- [95] A. Ebrahimi, J. Scott, and K. Ghorbani, "Transmission lines terminated with LC resonators for differential permittivity sensing," *IEEE Microw. Wireless Compon. Lett.*, vol. 28, no. 12, pp. 1149–1151, Dec. 2018.
- [96] A. Ebrahimi, G. Beziuk, J. Scott, and K. Ghorbani, "Microwave differential frequency splitting sensor using magnetic-LC resonators," *Sensors*, vol. 20, no. 4, p. 1066, Feb. 2020.
- [97] P. Vélez, F. Martín, R. Fernández-García, and I. Gil, "Embroidered textile frequency-splitting sensor based on stepped-impedance resonators," *IEEE Sensors J.*, vol. 22, no. 9, pp. 8596–8603, May 2022.
- [98] C. Damm, M. Schüßler, M. Puentes, H. Maune, M. Maasch, and R. Jakoby, "Artificial transmission lines for high sensitive microwave sensors," in *Proc. IEEE Sensors*, Christchurch, New Zealand, Oct. 2009, pp. 755–758.
- [99] F. Ferrández-Pastor, J. García-Chamizo, and M. Nieto-Hidalgo, "Electromagnetic differential measuring method: Application in microstrip sensors developing," *Sensors*, vol. 17, no. 7, p. 1650, Jul. 2017.
- [100] J. Muñoz-Enano, P. Vélez, M. G. Barba, and F. Martín, "An analytical method to implement high-sensitivity transmission line differential sensors for dielectric constant measurements," *IEEE Sensors J.*, vol. 20, no. 1, pp. 178–184, Jan. 2020.
- [101] M. Gil, P. Vélez, F. Aznar-Ballesta, J. Muñoz-Enano, and F. Martín, "Differential sensor based on electroinductive wave transmission lines for dielectric constant measurements and defect detection," *IEEE Trans. Antennas Propag.*, vol. 68, no. 3, pp. 1876–1886, Mar. 2020.
- [102] J. Muñoz-Enano, P. Vélez, M. G. Barba, J. Mata-Contreras, and F. Martín, "Differential-mode to common-mode conversion detector based on ratrace hybrid couplers: Analysis and application to differential sensors and comparators," *IEEE Trans. Microw. Theory Techn.*, vol. 68, no. 4, pp. 1312–1325, Apr. 2020.

- [103] J. Coromina, J. Muñoz-Enano, P. Vélez, A. Ebrahimi, J. Scott, K. Ghorbani, and F. Martín, "Capacitively-loaded slow-wave transmission lines for sensitivity improvement in phase-variation permittivity sensors," in *Proc. 50th Eur. Microw. Conf. (EuMC)*, Utrecht, Netherlands, Jan. 2021, pp. 491–494.
- [104] A. Ebrahimi, J. Coromina, J. Muñoz-Enano, P. Vélez, J. Scott, K. Ghorbani, and F. Martín, "Highly sensitive phase-variation dielectric constant sensor based on a capacitively-loaded slow-wave transmission line," *IEEE Trans. Circuits Syst. I, Reg. Papers*, vol. 68, no. 7, pp. 2787–2799, Jul. 2021.
- [105] L. Su, J. Muñoz-Enano, P. Vélez, P. Casacuberta, M. Gil, and F. Martín, "Phase-variation microwave sensor for permittivity measurements based on a high-impedance half-wavelength transmission line," *IEEE Sensors J.*, vol. 21, no. 9, pp. 10647–10656, May 2021.
- [106] A. Ebrahimi, J. Muñoz-Enano, P. Vélez, J. Scott, K. Ghorbani, and F. Martín, "Phase variation microfluidic permittivity sensor using a dispersive transmission line," in *Proc. IEEE Sensors*, Dallas, TX, USA, Oct. 2022, pp. 1–4.
- [107] A. K. Jha, A. Lamecki, M. Mrozowski, and M. Bozzi, "A highly sensitive planar microwave sensor for detecting direction and angle of rotation," *IEEE Trans. Microw. Theory Techn.*, vol. 68, no. 4, pp. 1598–1609, Apr. 2020.
- [108] J. Muñoz-Enano, P. Vélez, L. Su, M. Gil, P. Casacuberta, and F. Martín, "On the sensitivity of reflective-mode phase-variation sensors based on open-ended stepped-impedance transmission lines: Theoretical analysis and experimental validation," *IEEE Trans. Microw. Theory Techn.*, vol. 69, no. 1, pp. 308–324, Jan. 2021.
- [109] L. Su, J. Muñoz-Enano, P. Velez, P. C. Orta, M. Gil, and F. Martin, "Highly sensitive phase variation sensors based on step-impedance coplanar waveguide (CPW) transmission lines," *IEEE Sensors J.*, vol. 21, no. 3, pp. 2864–2872, Feb. 2021.
- [110] P. Casacuberta, J. Muñoz-Enano, P. Vélez, L. Su, M. Gil, and F. Martín, "Highly sensitive reflective-mode defect detectors and dielectric constant sensors based on open-ended stepped-impedance transmission lines," *Sensors*, vol. 20, no. 21, p. 6236, Oct. 2020.
- [111] L. Su, J. Muñoz-Enano, P. Vélez, M. Gil-Barba, P. Casacuberta, and F. Martin, "Highly sensitive reflective-mode phase-variation permittivity sensor based on a coplanar waveguide terminated with an open complementary split ring resonator (OCSRR)," *IEEE Access*, vol. 9, pp. 27928–27944, 2021.
- [112] P. Casacuberta, P. Vélez, J. Muñoz-Enano, L. Su, M. G. Barba, A. Ebrahimi, and F. Martín, "Circuit analysis of a coplanar waveguide (CPW) terminated with a step-impedance resonator (SIR) for highly sensitive one-port permittivity sensing," *IEEE Access*, vol. 10, pp. 62597–62612, 2022.
- [113] Z. Mehrjoo, A. Ebrahimi, and K. Ghorbani, "Phase variation reflective-mode displacement sensor using a CPW loaded with dumbbell-shaped resonator," in *Proc. IEEE Asia–Pacific Microw. Conf. (APMC)*, Nov. 2021, pp. 467–469.
- [114] A. K. Horestani, Z. Shaterian, and F. Martín, "Rotation sensor based on the cross-polarized excitation of split ring resonators (SRRs)," *IEEE Sensors J.*, vol. 20, no. 17, pp. 9706–9714, Sep. 2020.
- [115] J. Muñoz-Enano, P. Vélez, L. Su, M. Gil-Barba, and F. Martín, "A reflective-mode phase-variation displacement sensor," *IEEE Access*, vol. 8, pp. 189565–189575, 2020.
- [116] P. Casacuberta, P. Vélez, J. Muñoz-Enano, L. Su, and F. Martín, "Highly sensitive reflective-mode phase-variation permittivity sensors using coupled line sections," *IEEE Trans. Microw. Theory Techn.*, vol. 71, no. 7, pp. 2970–2984, Jul. 2023.
- [117] P. Casacuberta, P. Vélez, J. Muñoz-Enano, L. Su, M. Gil, and F. Martín, "Reflective-mode phase-variation permittivity sensors based on coupled resonators," in *Proc. IEEE Sensors*, Oct. 2022, pp. 1–12.
- [118] M. Elgeziry, F. Paredes, P. Vélez, F. Costa, S. Genovesi, and F. Martín, "A method to retrieve the output variables in reflective-mode phase-variation sensors," in *Proc. 52nd Eur. Microw. Conf. (EuMC)*, Milan, Italy, Sep. 2022, pp. 516–519.
- [119] P. Vélez, F. Paredes, P. Casacuberta, M. Elgeziry, L. Su, J. Muñoz-Enano, F. Costa, S. Genovesi, and F. Martín, "Portable reflective-mode phase-variation microwave sensor based on a rat-race coupler pair and gain/phase detector for dielectric characterization," *IEEE Sensors J.*, vol. 23, no. 6, pp. 5745–5756, Mar. 2023.



- [120] L. Su, P. Casacuberta, P. Vélez, J. Muñoz-Enano, M. Gil, and F. Martín, "Reflective-mode submersible microwave sensor," in *Proc. IEEE Sensors*, Dallas, TX, USA, Oct. 2022, pp. 1–4.
- [121] P. Vélez, X. Canalias, J. Muñoz-Enano, P. Casacuberta, L. Su, and F. Martín, "Effects of losses on the sensitivity of reflective-mode phasevariation liquid sensors," *IEEE Trans. Microw. Theory Techn.*, vol. 72, no. 2, pp. 903–918, Feb. 2024.
- [122] P. Casacuberta, P. Vélez, J. Muñoz-Enano, L. Su, and F. Martín, "Losses assisted sensitivity enhancement in reflective-mode phase-variation permittivity sensors based on weakly coupled distributed resonators," *IEEE Sensors Lett.*, vol. 7, no. 8, pp. 1–4, Aug. 2023.
- [123] P. Casacuberta, P. Vélez, J. Muñoz-Enano, L. Su, and F. Martín, "Highly sensitive coplanar waveguide (CPW) reflective-mode phasevariation permittivity sensors based on weakly coupled step-impedance resonators (SIRs)," *IEEE Trans. Microw. Theory Techn.*, vol. 72, no. 3, pp. 1739–1753, Mar. 2024.
- [124] L. Su, P. Vélez, P. Casacuberta, J. Muñoz-Enano, M. Gil-Barba, and F. Martín, "Reflective-mode phase-variation submersible sensor for liquid characterization," *IEEE Trans. Instrum. Meas.*, vol. 72, pp. 1–12, 2023.
- [125] Z. Mehrjoo, A. Ebrahimi, and K. Ghorbani, "Analytical design of phase variation-based dielectric constant sensors," in *Proc. 53rd Eur. Microw. Conf. (EuMC)*, Berlin, Germany, Sep. 2023, pp. 729–732.
- [126] J. Muñoz-Enano, P. Vélez, P. Casacuberta, L. Su, and F. Martín, "Reflective-mode phase-variation permittivity sensor based on a stepimpedance microstrip line terminated with a slot resonator for solid and liquid characterization," *IEEE Trans. Microw. Theory Techn.*, vol. 72, no. 4, pp. 2519–2533, Apr. 2024.
- [127] A. Karami-Horestani, F. Paredes, and F. Martín, "Phase-variation microwave displacement sensor with good linearity and application to breath rate monitoring," *IEEE Sensors J.*, vol. 23, no. 19, pp. 22486–22495, Oct. 2023.
- [128] Z. Mehrjoo, A. Ebrahimi, G. Beziuk, F. Martín, and K. Ghorbani, "Microwave rotation sensor based on reflection phase in transmission lines terminated with lumped resonators," *IEEE Sensors J.*, vol. 23, no. 7, pp. 6571–6580, Apr. 2023.
- [129] M. Elgeziry, F. Costa, P. Vélez, F. Paredes, F. Martín, and S. Genovesi, "Toward a low-cost portable reader for reflective-mode microwave sensors," *IEEE Trans. Instrum. Meas.*, vol. 73, pp. 1–9, 2023.
- [130] P. Casacuberta, P. Vélez, L. Su, X. Canalias, and F. Martín, "Highly sensitive lossy tunable permittivity sensor," *IEEE Microw. Wireless Technol. Lett.*, vol. 34, no. 6, pp. 687–690, Jun. 2024.
- [131] P. Casacuberta, P. Vélez, J. Muñoz-Enano, L. Su, and F. Martín, "Highly sensitive microwave sensors for monitoring the corrosion in urban and industrial scenarios," in *IEEE MTT-S Int. Microw. Symp. Dig.*, San Diego, CA, USA, Jun. 2023, pp. 1–2.
- [132] A. Karami-Horestani, F. Paredes, P. Casacuberta, A. Ebrahimi, P. Vélez, K. A. Saura, K. Ghorbani, and F. Martín, "Reflective-mode phase-variation sensors based on a movable step impedance resonator (SIR) and application to micrometer-scale motion sensing," *IEEE Trans. Microw. Theory Techn.*, vol. 73, no. 1, pp. 592–605, Jan. 2025.
- [133] X. Canalias, P. Vélez, P. Casacuberta, L. Su, and F. Martín, "Transmission-mode phase-variation planar microwave sensor based on a step-impedance shunt stub for high sensitivity defect detection, dielectric constant, and proximity measurements," *IEEE Trans. Microw. Theory Techn.*, vol. 73, no. 2, pp. 1017–1028, Feb. 2025.
- [134] P. Casacuberta, P. Vélez, L. Su, X. Canalias, and F. Martín, "Sensitive microfluidic sensor with weakly coupled dumbbell defect-ground-structure resonators for volume fraction determination in liquid mixtures," *IEEE Microw. Wireless Technol. Lett.*, vol. 34, no. 12, pp. 1411–1414, Dec. 2024.
- [135] P. Casacuberta, A. Ebrahimi, P. Vélez, L. Su, X. Canalias, K. Ghorbani, and F. Martín, "Sensitivity optimization in single-frequency planar microwave sensors for solid and liquid characterization and microfluidics," *IEEE Trans. Microw. Theory Techn.*, vol. 73, no. 3, pp. 1581–1609, Mar. 2025.
- [136] X. Canalias, P. Casacuberta, P. Vélez, L. Su, and F. Martín, "Highly sensitive transmission-mode phase-variation permittivity sensor based on resonance and antiresonance," *IEEE Trans. Microw. Theory Techn.*, vol. 73, no. 3, pp. 1619–1631, Mar. 2025.
- [137] P. Casacuberta, P. Vélez, L. Su, X. Canalias, and F. Martín, "Engineering with loss to enhance sensitivity in microwave sensors," *IEEE Microw. Mag.*, vol. 26, no. 5, pp. 52–66, May 2025.

- [138] N. Kurniawati, P. Vélez, P. Casacuberta, L. Su, X. Canalias, and F. Martín, "Highly sensitive phase-variation microwave sensor operating in transmission based on an open split ring resonator (OSRR)," *IEEE Sensors J.*, vol. 24, no. 24, pp. 40749–40763, Dec. 2024.
- [139] J. Borrès-Sarsa, P. Casacuberta, P. Vélez, L. Su, X. Canalias, and F. Martín, "Microstrip configurations of reflective-mode phase-variation permittivity sensors based on weakly coupled step impedance resonators (SIR): An analysis to the light of circuit duality," *IEEE Access*, vol. 13, pp. 85838–85856, 2025, doi: 10.1109/ACCESS.2025.3569452.
- [140] J. Naqui, M. Durán-Sindreu, and F. Martín, "Novel sensors based on the symmetry properties of split ring resonators (SRRs)," *Sensors*, vol. 11, no. 8, pp. 7545–7553, Jul. 2011.
- [141] J. Naqui, M. Durán-Sindreu, and F. Martín, "Alignment and position sensors based on split ring resonators," *Sensors*, vol. 12, no. 9, pp. 11790–11797, Aug. 2012.
- [142] A. K. Horestani, C. Fumeaux, S. F. Al-Sarawi, and D. Abbott, "Displacement sensor based on diamond-shaped tapered split ring resonator," *IEEE Sensors J.*, vol. 13, no. 4, pp. 1153–1160, Apr. 2013.
- [143] A. K. Horestani, J. Naqui, D. Abbott, C. Fumeaux, and F. Martín, "Two-dimensional displacement and alignment sensor based on reflection coefficients of open microstrip lines loaded with split ring resonators," *Electron. Lett.*, vol. 50, no. 8, pp. 620–622, Apr. 2014.
- [144] A. K. Horestani, D. Abbott, and C. Fumeaux, "Rotation sensor based on horn-shaped split ring resonator," *IEEE Sensors J.*, vol. 13, no. 8, pp. 3014–3015, Aug. 2013.
- [145] J. Naqui, M. Durán-Sindreu, and F. Martín, "Transmission lines loaded with bisymmetric resonators and applications," in *IEEE MTT-S Int. Microw. Symp. Dig.*, Seattle, WA, USA, Jun. 2013, pp. 1–3.
- [146] J. Naqui and F. Martiín, "Transmission lines loaded with bisymmetric resonators and their application to angular displacement and velocity sensors," *IEEE Trans. Microw. Theory Techn.*, vol. 61, no. 12, pp. 4700–4713, Dec. 2013.
- [147] J. Naqui and F. Martín, "Angular displacement and velocity sensors based on electric-LC (ELC) loaded microstrip lines," *IEEE Sensors J.*, vol. 14, no. 4, pp. 939–940, Apr. 2014.
- [148] J. Naqui, J. Coromina, A. Karami-Horestani, C. Fumeaux, and F. Martín, "Angular displacement and velocity sensors based on coplanar waveguides (CPWs) loaded with S-shaped split ring resonators (S-SRR)," Sensors, vol. 15, no. 5, pp. 9628–9650, Apr. 2015.
- [149] J. Mata-Contreras, C. Herrojo, and F. Martín, "Application of split ring resonator (SRR) loaded transmission lines to the design of angular displacement and velocity sensors for space applications," *IEEE Trans. Microw. Theory Techn.*, vol. 65, no. 11, pp. 4450–4460, Nov. 2017.
- [150] J. Mata-Contreras, C. Herrojo, and F. Martín, "Detecting the rotation direction in contactless angular velocity sensors implemented with rotors loaded with multiple chains of resonators," *IEEE Sensors J.*, vol. 18, no. 17, pp. 7055–7065, Sep. 2018.
- [151] C. Herrojo, F. Paredes, and F. Martín, "Double-stub loaded microstrip line reader for very high data density microwave encoders," *IEEE Trans. Microw. Theory Techn.*, vol. 67, no. 9, pp. 3527–3536, Sep. 2019.
- [152] F. Paredes, C. Herrojo, A. Moya, M. B. Alonso, D. Gonzalez, P. Bruguera, C. D. Simao, and F. Martín, "Electromagnetic encoders screen-printed on rubber belts for absolute measurement of position and velocity," *Sensors*, vol. 22, no. 5, p. 2044, Mar. 2022.
- [153] J. Naqui, Symmetry Properties in Transmission Lines Loaded With Electrically Small Resonators: Circuit Modelling and Applications. Heidelberg, Germany: Springer, 2016.
- [154] P. Vélez, J. Muñoz-Enano, A. Ebrahimi, C. Herrojo, F. Paredes, J. Scott, K. Ghorbani, and F. Martín, "Single-frequency amplitude-modulation sensor for dielectric characterization of solids and microfluidics," *IEEE Sensors J.*, vol. 21, no. 10, pp. 12189–12201, May 2021.
- [155] A. Ebrahimi, G. Beziuk, and K. Ghorbani, "Amplitude variation microwave sensors for high-sensitivity detection of solid and microfluidic dielectrics," *IEEE Trans. Microw. Theory Techn.*, vol. 72, no. 11, pp. 6460–6472, Nov. 2024.
- [156] Z. R. Omam, V. Nayyeri, S.-H. Javid-Hosseini, and O. M. Ramahi, "Simple and high-sensitivity dielectric constant measurement using a high-directivity microstrip coupled-line directional coupler," *IEEE Trans. Microw. Theory Techn.*, vol. 70, no. 8, pp. 3933–3942, Aug. 2022.
- [157] A. Ebrahimi and K. Ghorbani, "High-sensitivity detection of solid and liquid dielectrics using a branch line coupler sensor," *IEEE Trans. Microw. Theory Techn.*, vol. 71, no. 12, pp. 5233–5245, Dec. 2023.



- [158] F. Martin and F. Medina, "Balanced microwave transmission lines, circuits, and sensors," *IEEE J. Microw.*, vol. 3, no. 1, pp. 398–440, Jan. 2023.
- [159] P. Vélez, K. Grenier, J. Mata-Contreras, D. Dubuc, and F. Martín, "Highly-sensitive microwave sensors based on open complementary split ring resonators (OCSRRs) for dielectric characterization and solute concentration measurement in liquids," *IEEE Access*, vol. 6, pp. 48324–48338, 2018.
- [160] P. Vélez, J. Muñoz-Enano, M. Gil, J. Mata-Contreras, and F. Martín, "Differential microfluidic sensors based on dumbbell-shaped defect ground structures in microstrip technology: Analysis, optimization, and applications," Sensors, vol. 19, no. 14, p. 3189, Jul. 2019.
- [161] A. Ebrahimi, F. J. Tovar-Lopez, J. Scott, and K. Ghorbani, "Differential microwave sensor for characterization of glycerol-water solutions," Sens. Actuators B, Chem., vol. 321, Oct. 2020, Art. no. 128561.
- [162] K. Grenier, D. Dubuc, P.-E. Poleni, M. Kumemura, H. Toshiyoshi, T. Fujii, and H. Fujita, "Integrated broadband microwave and microfluidic sensor dedicated to bioengineering," *IEEE Trans. Microw. Theory Techn.*, vol. 57, no. 12, pp. 3246–3253, Dec. 2009.
- [163] K. Grenier, D. Dubuc, T. Chen, F. Artis, T. Chretiennot, M. Poupot, and J.-J. Fournié, "Recent advances in microwave-based dielectric spectroscopy at the cellular level for cancer investigations," *IEEE Trans. Microw. Theory Techn.*, vol. 61, no. 5, pp. 2023–2030, May 2013.
- [164] J. Sorocki, K. Wincza, S. Gruszczynski, and I. Piekarz, "Direct broadband dielectric spectroscopy of liquid chemicals using microwave-fluidic twowire transmission line sensor," *IEEE Trans. Microw. Theory Techn.*, vol. 69, no. 5, pp. 2569–2578, May 2021.
- [165] E. L. Chuma, Y. Iano, G. Fontgalland, L. L. B. Roger, and H. Loschi, "PCB-integrated non-destructive microwave sensor for liquid dielectric spectroscopy based on planar metamaterial resonator," *Sens. Actuators A, Phys.*, vol. 312, Sep. 2020, Art. no. 112112.
- [166] N. Hosseini, M. Baghelani, and M. Daneshmand, "Discrete microwave spectroscopy using planar resonator," in *Proc. IEEE Can. Conf. Electr. Comput. Eng. (CCECE)*, Edmonton, AB, Canada, May 2019, pp. 1–4.
- [167] W. Zhu, M. Baghelani, and A. K. Iyer, "Dielectric spectrum extraction of liquids using noncontact microwave split ring resonator," *IEEE Trans. Microw. Theory Techn.*, vol. 72, no. 10, pp. 5859–5871, Oct. 2024.
- [168] F. Kremer and A. Schönhals, Broadband Dielectric Spectroscopy. Berlin, Germany: Springer, 2003.
- [169] J. C. Booth, N. D. Orloff, J. Mateu, M. Janezic, M. Rinehart, and J. A. Beall, "Quantitative permittivity measurements of nanoliter liquid volumes in microfluidic channels to 40 GHz," *IEEE Trans. Instrum. Meas.*, vol. 59, no. 12, pp. 3279–3288, Dec. 2010.
- [170] S. Liu, N. D. Orloff, C. A. E. Little, W. Zhao, J. C. Booth, D. F. Williams, I. Ocket, D. M. M.-P. Schreurs, and B. Nauwelaers, "Hybrid characterization of nanolitre dielectric fluids in a single microfluidic channel up to 110 GHz," *IEEE Trans. Microw. Theory Techn.*, vol. 65, no. 12, pp. 5063–5073, Dec. 2017.
- [171] A. Tamra, A. Zedek, M.-P. Rols, D. Dubuc, and K. Grenier, "Single cell microwave biosensor for monitoring cellular response to electrochemotherapy," *IEEE Trans. Biomed. Eng.*, vol. 69, no. 11, pp. 3407–3414, Nov. 2022.
- [172] O. Peytral-Rieu, D. Dubuc, and K. Grenier, "Microwave-based sensor for the noninvasive and real-time analysis of 3-D biological microtissues: Microfluidic improvement and sensitivity study," *IEEE Trans. Microw. Theory Techn.*, vol. 71, no. 11, pp. 4996–5003, Nov. 2023.
- [173] N. R. Tanguy, B. Wiltshire, M. Arjmand, M. H. Zarifi, and N. Yan, "Highly sensitive and contactless ammonia detection based on nanocomposites of phosphate-functionalized reduced graphene oxide/polyaniline immobilized on microstrip resonators," ACS Appl. Mater. Interfaces, vol. 12, no. 8, pp. 9746–9754, Feb. 2020.
- [174] M. A. Ali, M. Ming-Cheng Cheng, J. Ching-Ming Chen, and C. M. Wu, "Microwave gas sensor based on graphene-loaded substrate integrated waveguide cavity resonator," in *IEEE MTT-S Int. Microw. Symp. Dig.*, San Francisco, CA, USA, May 2016, pp. 1–4.
- [175] W. Kudpun, N. Duangrit, N. Chudpooti, P. Lorwongtragool, S. Seewattanapon, and P. Akkaraekthalin, "A microwave gas sensor using interdigital resonator coated with conducting polymer for agricultural applications," in *Proc. IEEE Conf. Antenna Meas. Appl.* (CAMA), Kuta, Bali, Indonesia, Oct. 2019, pp. 225–227.

- [176] A. Sohrabi, P. M. Shaibani, M. H. Zarifi, M. Daneshmand, and T. Thundat, "A novel technique for rapid vapor detection using swelling polymer covered microstrip ring resonator," in *IEEE MTT-S Int. Microw. Symp. Dig.*, Tampa, FL, USA, Jun. 2014, pp. 1–4.
- [177] Y. Wu, G. R. Pecorella, G. Verderame, D. Annicchiarico, T. Galhena, S. Hodge, H. J. Joyce, P. Livreri, and A. Lombardo, "Microwave gas sensor based on graphene aerogels," *IEEE Sensors J.*, vol. 23, no. 17, pp. 19282–19289, Sep. 2023.
- [178] N. R. Tanguy, M. Moradpour, M. C. Jain, N. Yan, and M. H. Zarifi, "Exploring the potential of cellulose nanofibrils for humidity sensing using an organic microwave resonator," in *Proc. IEEE Sensors*, Sydney, NSW, Australia, Oct. 2021, pp. 1–4.
- [179] N. R. Tanguy, M. Moradpour, M. C. Jain, N. Yan, and M. H. Zarifi, "Transient and recyclable organic microwave resonator using nanocellulose for 5G and Internet of Things applications," *Chem. Eng. J.*, vol. 466, Jun. 2023, Art. no. 143061.
- [180] M. Panahi-Sarmad, S. Samsami, A. Ghaffarkhah, S. A. Hashemi, S. Ghasemi, M. Amini, S. Wuttke, O. Rojas, K. C. Tam, F. Jiang, M. Arjmand, F. Ahmadijokani, and M. Kamkar, "MOF-based electromagnetic shields multiscale design: Nanoscale chemistry, microscale assembly, and macroscale manufacturing," Adv. Funct. Mater., vol. 34, no. 43, Oct. 2024, Art. no. 2304473.
- [181] O. Niksan, L. Bi, Y. Gogotsi, and M. H. Zarifi, "MXene-based kirigami designs: Showcasing reconfigurable frequency selectivity in microwave regime," *Nature Commun.*, vol. 15, no. 1, p. 7793, Sep. 2024.
- [182] O. Niksan, L. Bi, K. K. Kazemi, R. Rakhmanov, Y. Gogotsi, and M. H. Zarifi, "MXene guides microwaves through 3D polymeric structures," *Mater. Today*, vol. 73, pp. 47–55, Mar. 2024.
- [183] M. Saeed, R. S. U. Haq, S. Ahmed, F. Siddiqui, and J. Yi, "Recent advances in carbon nanotubes, graphene and carbon fibers-based microwave absorbers," *J. Alloys Compounds*, vol. 970, Jan. 2024, Art. no. 172625.
- [184] J.-Y. Zong and M.-S. Cao, "Graphene-like MXene-based microwave absorbers and shields: Latest progress and perspectives," *Mater. Today Phys.*, vol. 43, Apr. 2024, Art. no. 101400.
- [185] K. K. Kazemi, E. Hosseini, S. Hu, R. Narang, S. Li, M. Arjmand, and M. H. Zarifi, "MXene membrane in planar microwave resonant structures for 5G applications," *Appl. Mater. Today*, vol. 26, Mar. 2022, Art. no. 101294.
- [186] O. Niksan, B. C. Wyatt, K. K. Kazemi, B. Anasori, and M. H. Zarifi, "MXene free standing films: Unlocking the impact of flake sizes in microwave resonant structures in humid environments," *Small*, vol. 19, no. 37, Sep. 2023, Art. no. 2300848.
- [187] K. K. Kazemi, S. Hu, O. Niksan, K. K. Adhikari, N. R. Tanguy, S. Li, M. Arjmand, and M. H. Zarifi, "Low-profile planar antenna sensor based on Ti₃C₂T_x MXene membrane for VOC and humidity monitoring," *Adv. Mater. Interfaces*, vol. 9, no. 13, May 2022, Art. no. 2102411.
- [188] S. Noothongkaew, O. Thumthan, and K.-S. An, "Minimal layer graphene/TiO₂ nanotube membranes used for enhancement of UV photodetectors," *Mater. Lett.*, vol. 218, pp. 274–279, May 2018.
- [189] B. D. Wiltshire, M. A. Rafi, and M. H. Zarifi, "Microwave resonator array with liquid metal selection for narrow band material sensing," Sci. Rep., vol. 11, no. 1, Apr. 2021, Art. no. 8598.
- [190] M. H. Zarifi, A. Mohammadpour, S. Farsinezhad, B. D. Wiltshire, M. Nosrati, A. M. Askar, M. Daneshmand, and K. Shankar, "Timeresolved microwave photoconductivity (TRMC) using planar microwave resonators: Application to the study of long-lived charge pairs in photoexcited titania nanotube arrays," *J. Phys. Chem. C*, vol. 119, no. 25, pp. 14358–14365, Jun. 2015.
- [191] M. H. Zarifi, S. Farsinezhad, M. Abdolrazzaghi, M. Daneshmand, and K. Shankar, "Selective microwave sensors exploiting the interaction of analytes with trap states in TiO₂ nanotube arrays," *Nanoscale*, vol. 8, no. 14, pp. 7466–7473, Mar. 2016.
- [192] M. H. Zarifi, B. D. Wiltshire, N. Mahdi, K. Shankar, and M. Daneshmand, "Distinguishing between deep trapping transients of electrons and holes in TiO₂ nanotube arrays using planar microwave resonator sensor," ACS Appl. Mater. Interfaces, vol. 10, no. 35, pp. 29857–29865, Sep. 2018.
- [193] B. D. Wiltshire and M. H. Zarifi, "TiO₂ nanotube-integrated microwave planar resonator sensor for ultraviolet transmission-based liquid characterization," Sens. Actuators B, Chem., vol. 341, Aug. 2021, Art. no. 130014.



- [194] M. Alijani, B. D. Wiltshire, H. Sopha, Z. Sarpanah, J. Mistrik, L. Hromadko, M. H. Zarifi, and J. M. Macak, "Investigating the thickness-effect of free-standing high aspect-ratio TiO₂ nanotube layers on microwave-photoresponse using planar microwave resonators," *Appl. Mater. Today*, vol. 32, Jun. 2023, Art. no. 101832.
- [195] M. A. Rafi, B. D. Wiltshire, and M. H. Zarifi, "Wideband tunable modified split ring resonator structure using liquid metal and 3-D printing," *IEEE Microw. Wireless Compon. Lett.*, vol. 30, no. 5, pp. 469–472, May 2020.
- [196] T. Chretiennot, D. Dubuc, and K. Grenier, "A microwave and microfluidic planar resonator for efficient and accurate complex permittivity characterization of aqueous solutions," *IEEE Trans. Microw. Theory Techn.*, vol. 61, no. 2, pp. 972–978, Feb. 2013.
- [197] H. Choi, J. Naylon, S. Luzio, J. Beutler, J. Birchall, C. Martin, and A. Porch, "Design and in vitro interference test of microwave noninvasive blood glucose monitoring sensor," *IEEE Trans. Microw. Theory Techn.*, vol. 63, no. 10, pp. 3016–3025, Oct. 2015.
- [198] A. A. Abduljabar, N. Clark, J. Lees, and A. Porch, "Dual mode microwave microfluidic sensor for temperature variant liquid characterization," *IEEE Trans. Microw. Theory Techn.*, vol. 65, no. 7, pp. 2572–2582, Jul. 2017.
- [199] M. A. Masoumabad, N. Delmonte, L. Silvestri, L. Perregrini, and M. Bozzi, "Integrated liquid–liquid percentage determination microwave sensor exploiting single-frequency transmission amplitude measurement technique," *Microw. Opt. Technol. Lett.*, vol. 66, no. 7, Jun. 2024, Art. no. e34237.
- [200] J. Zhu, Y. Yang, M. Li, D. Mcgloin, S. Liao, J. Nulman, M. Yamada, and F. Iacopi, "Additively manufactured millimeter-wave dual-band singlepolarization shared aperture Fresnel zone plate metalens antenna," *IEEE Trans. Antennas Propag.*, vol. 69, no. 10, pp. 6261–6272, Oct. 2021.
- [201] I. Piekarz, K. Skarzynski, B. Piekarz, K. Wincza, S. Gruszczynski, M. Sloma, and J. Sorocki, "Additively manufactured microwave sensor for glucose level detection in saliva," *Sci. Rep.*, vol. 14, no. 1, Nov. 2024, Art. no. 28235.
- [202] A. Karami-Horestani, S. Rodini, S. Genovesi, F. Paredes, F. Costa, and F. Martín, "Microwave capacitive pressure sensor based on an additively manufactured elastic layer," *IEEE Sensors J.*, vol. 25, no. 2, pp. 2618–2628, Jan. 2025.
- [203] W. Su, B. S. Cook, and M. M. Tentzeris, "Additively manufactured microfluidics-based 'peel-and-replace' RF sensors for wearable applications," *IEEE Trans. Microw. Theory Techn.*, vol. 64, no. 6, pp. 1928–1936, Jun. 2016.
- [204] Y. Kim, Y. Cui, M. M. Tentzeris, and S. Lim, "Additively manufactured electromagnetic based planar pressure sensor using substrate integrated waveguide technology," *Additive Manuf.*, vol. 34, Aug. 2020, Art. no. 101225.
- [205] H. Peng, X. Yang, S. Long, Y. Xie, T. Zhang, F. Gao, and Y. Meng, "Design and fabrication of 3-D printed RF temperature sensor based on microwave coaxial resonator," *IEEE Trans. Microw. Theory Techn.*, vol. 72, no. 1, pp. 212–222, Jan. 2024.
- [206] G. M. Rocco, M. Bozzi, D. Schreurs, L. Perregrini, S. Marconi, G. Alaimo, and F. Auricchio, "3-D printed microfluidic sensor in SIW technology for liquids' characterization," *IEEE Trans. Microw. Theory Techn.*, vol. 68, no. 3, pp. 1175–1184, Mar. 2020.
- [207] J. Sorocki, I. Piekarz, K. Wincza, S. Gruszczynski, and J. Papapolymerou, "Broadband microwave microfluidic coupled-line sensor with 3-Dprinted channel for industrial applications," *IEEE Trans. Microw. Theory Techn.*, vol. 68, no. 7, pp. 2808–2822, Jul. 2020.
- [208] X.-P. Chen and K. Wu, "Substrate integrated waveguide filter: Basic design rules and fundamental structure features," *IEEE Microw. Mag.*, vol. 15, no. 5, pp. 108–116, Jul. 2014.
- [209] K. Wu, M. Bozzi, and N. J. G. Fonseca, "Substrate integrated transmission lines: Review and applications," *IEEE J. Microw.*, vol. 1, no. 1, pp. 345–363, Jan. 2021.
- [210] M. Bozzi, A. Georgiadis, and K. Wu, "Review of substrate-integrated waveguide circuits and antennas," *IET Microw., Antennas Propag.*, vol. 5, no. 8, pp. 909–920, Jun. 2011.
- [211] N. S. Khair, N. A. T. Yusof, Y. A. Wahab, B. S. Bari, N. I. Ayob, and M. Zolkapli, "Substrate-integrated waveguide (SIW) microwave sensor theory and model in characterising dielectric material: A review," *Sensors Int.*, vol. 4, Jul. 2023, Art. no. 100244.

- [212] P. K. Varshney and M. J. Akhtar, "Permittivity estimation of dielectric substrate materials via enhanced SIW sensor," *IEEE Sensors J.*, vol. 21, no. 10, pp. 12104–12112, May 2021.
- [213] N. K. Tiwari, A. K. Jha, S. P. Singh, Z. Akhter, P. K. Varshney, and M. J. Akhtar, "Generalized multimode SIW cavity-based sensor for retrieval of complex permittivity of materials," *IEEE Trans. Microw. Theory Techn.*, vol. 66, no. 6, pp. 3063–3072, Jun. 2018.
- [214] P. Mohammadi, H. Teimouri, A. Mohammadi, S. Demir, and A. Kara, "Dual band, miniaturized permittivity measurement sensor with negative-order SIW resonator," *IEEE Sensors J.*, vol. 21, no. 20, pp. 22695–22702, Oct. 2021.
- [215] H. Hao, D. Wang, and Z. Wang, "Design of substrate-integrated waveguide loading multiple complementary open resonant rings (CSRRs) for dielectric constant measurement," *Sensors*, vol. 20, no. 3, p. 857, Feb. 2020.
- [216] E. Silavwe, N. Somjit, and I. D. Robertson, "A microfluidic-integrated SIW lab-on-substrate sensor for microliter liquid characterization," *IEEE Sensors J.*, vol. 16, no. 21, pp. 7628–7635, Nov. 2016.
- [217] C. Liu and F. Tong, "An SIW resonator sensor for liquid permittivity measurements at C band," *IEEE Microw. Wireless Compon. Lett.*, vol. 25, no. 11, pp. 751–753, Nov. 2015.
- [218] A. Soltan, R. A. Sadeghzadeh, and S. Mohammad-Ali-Nezhad, "Microwave sensor for liquid classification and permittivity estimation of dielectric materials," *Sens. Actuators A, Phys.*, vol. 336, Apr. 2022, Art. no. 113397.
- [219] L. Zhang, S. Su, F. Xu, T. Ren, and J. Xiong, "High sensitivity SIW-CSRR temperature sensor based on microwave scattering," *IEEE Sensors J.*, vol. 23, no. 13, pp. 13900–13908, Jul. 2023.
- [220] H. Kou, Q. Tan, Y. Wang, G. Zhang, S. Shujing, and J. Xiong, "A microwave SIW sensor loaded with CSRR for wireless pressure detection in high-temperature environments," *J. Phys. D, Appl. Phys.*, vol. 53, no. 8, Feb. 2020, Art. no. 085101.
- [221] E. Massoni, G. Siciliano, M. Bozzi, and L. Perregrini, "Enhanced cavity sensor in SIW technology for material characterization," *IEEE Microw. Wireless Compon. Lett.*, vol. 28, no. 10, pp. 948–950, Oct. 2018.
- [222] A. K. Jha and M. J. Akhtar, "SIW cavity based RF sensor for dielectric characterization of liquids," in *Proc. IEEE Conf. Antenna Meas. Appl.* (CAMA), Nov. 2014, pp. 1–11.
- [223] H. Lobato-Morales, A. Corona-Chávez, J. L. Olvera-Cervantes, R. A. Chávez-Pérez, and J. L. Medina-Monroy, "Wireless sensing of complex dielectric permittivity of liquids based on the RFID," *IEEE Trans. Microw. Theory Techn.*, vol. 62, no. 9, pp. 2160–2167, Sep. 2014.
- [224] A. A. M. Bahar, Z. Zakaria, M. K. M. Arshad, A. A. M. Isa, Y. Dasril, and R. A. Alahnomi, "A novel differential capacitive humidity sensor on SIW re-entrant cavity microwave resonators with PEDOT:PSS film," Sci. Rep., vol. 9, no. 1, Apr. 2019, Art. no. 5467.
- [225] M. Memon and S. Lim, "Microfluidic high-Q circular substrate-integrated waveguide (SIW) cavity for radio frequency (RF) chemical liquid sensing," Sensors, vol. 18, no. 1, p. 143, Jan. 2018.
- [226] Z. Wei, J. Huang, J. Li, G. Xu, Z. Ju, X. Liu, and X. Ni, "A high-sensitivity microfluidic sensor based on a substrate integrated waveguide re-entrant cavity for complex permittivity measurement of liquids," *Sensors*, vol. 18, no. 11, p. 4005, Nov. 2018.
- [227] Y. Chen, J. Huang, Y. Xiang, L. Fu, W. Gu, and Y. Wu, "A modified SIW re-entrant microfluidic microwave sensor for characterizing complex permittivity of liquids," *IEEE Sensors J.*, vol. 21, no. 13, pp. 14838–14846, Jul. 2021.
- [228] H. Yue, Q. Zhao, S. Zhu, and J. Huang, "A miniaturized active dual SIW re-entrant resonators for high-resolution and ultra-low-limitconcentration detection to glucose solutions," *IEEE Trans. Microw. Theory Techn.*, vol. 71, no. 4, pp. 1587–1599, Apr. 2023.
- [229] Z. Wei, J. Huang, J. Li, J. Li, X. Liu, and X. Ni, "A compact double-folded substrate integrated waveguide re-entrant cavity for highly sensitive humidity sensing," *Sensors*, vol. 19, no. 15, p. 3308, Jul. 2019.
- [230] C. Jia, J. Huang, L. Fu, Y. Xiang, Y. Chen, H. Yue, Q. Zhao, W. Gu, Y. Wu, and J. Zhang, "A novel differential capacitive humidity sensor on SIW re-entrant cavity microwave resonators with PEDOT:PSS film," *IEEE Sensors J.*, vol. 22, no. 7, pp. 6576–6585, Apr. 2022.
- [231] B. D. Gates, "Flexible electronics," *Science*, vol. 323, no. 5921, pp. 1566–1567, Mar. 2009.



- [232] H. Zhang, Y. Lan, S. Qiu, S. Min, H. Jang, J. Park, S. Gong, and Z. Ma, "Flexible and stretchable microwave electronics: Past, present, and future perspective," *Adv. Mater. Technol.*, vol. 6, no. 1, Jan. 2021, Art. no. 2000759.
- [233] A. E. Ostfeld, I. Deckman, A. M. Gaikwad, C. M. Lochner, and A. C. Arias, "Screen printed passive components for flexible power electronics," Sci. Rep., vol. 5, no. 1, Oct. 2015, Art. no. 15959.
- [234] M. Ali, D. Prakash, T. Zillger, P. K. Singh, and A. C. Hübler, "Printed piezoelectric energy harvesting device," *Adv. Energy Mater.*, vol. 4, no. 2, Jan. 2014, Art. no. 1300427.
- [235] R. Fernandez-Garcia and I. Gil, "Textile Yagi antenna at 1.8 GHz," in Proc. Prog. Electromagn. Res. Symp.-Spring (PIERS), Russia, 2017, pp. 652–654.
- [236] L. Su, X. Huang, W. Guo, and H. Wu, "A flexible microwave sensor based on complementary spiral resonator for material dielectric characterization," *IEEE Sensors J.*, vol. 20, no. 4, pp. 1893–1903, Feb. 2020.
- [237] T. Yilmaz, R. Foster, and Y. Hao, "Detecting vital signs with wearable wireless sensors," Sensors, vol. 10, no. 12, pp. 10837–10862, Dec. 2010.
- [238] J. M. Vicente, E. Avila-Navarro, C. G. Juan, N. García, and J. M. Sabater-Navarro, "Design of a wearable bio-patch for monitoring patient's temperature," in *Proc. 38th Annu. Int. Conf. IEEE Eng. Med. Biol. Soc. (EMBC)*, Orlando, FL, USA, Aug. 2016, pp. 4792–4795.
- [239] H. Xiaomu, S. Yan, and G. A. E. Vandenbosch, "Wearable button antenna for dual-band WLAN applications with combined on and offbody radiation patterns," *IEEE Trans. Antennas Propag.*, vol. 65, no. 3, pp. 1384–1387, Mar. 2017.
- [240] A. Hajiaghajani, A. H. Afandizadeh Zargari, M. Dautta, A. Jimenez, F. Kurdahi, and P. Tseng, "Textile-integrated metamaterials for near-field multibody area networks," *Nature Electron.*, vol. 4, no. 11, pp. 808–817, Nov. 2021.
- [241] Z. He, X. Lin, X. Yang, and C. Li, "A flexible microwave ablation antenna for lung cancer treatment," *IEEE Antennas Wireless Propag. Lett.*, vol. 22, pp. 3147–3151, 2023.
- [242] B. B. Ngoune, H. Hallil, S. Bila, D. Baillargeat, B. Bondu, E. Cloutet, and C. Dejous, "Humidity and temperature dual flexible microwave sensor," in *Proc. 29th IEEE Int. Conf. Electron., Circuits Syst. (ICECS)*, Glasgow, United Kingdom, Oct. 2022, pp. 1–4.
- [243] B. B. Ngoune, H. Hallil, B. Lebental, G. Perrin, S. Shinde, E. Cloutet, J. George, S. Bila, D. Baillargeat, and C. Dejous, "Selective outdoor humidity monitoring using epoxybutane polyethyleneimine in a flexible microwave sensor," *Chemosensors*, vol. 11, no. 1, p. 16, Dec. 2022.
- [244] L. Su, P. Vélez, P. Casacuberta, J. Muñoz-Enano, and F. Martín, "Microwave humidity sensor for early detection of sweat and urine leakage," *Electronics*, vol. 12, no. 10, p. 2276, May 2023.
- [245] I. Royo, R. Fernández-García, and I. Gil, "Microwave resonators for wearable sensors design: A systematic review," *Sensors*, vol. 23, no. 22, p. 9103, Nov. 2023.
- [246] V. Mecnika, M. Hoerr, I. Krievins, S. Jockenhoevel, and T. Gries, "Technical embroidery for smart textiles: Review," *Mater. Sci. Textile Clothing Technol.*, vol. 9, pp. 56–63, Mar. 2015.
- [247] T. C. Baum, R. W. Ziolkowski, K. Ghorbani, and K. J. Nicholson, "Embroidered active microwave composite preimpregnated electronics—Pregtronics," *IEEE Trans. Microw. Theory Techn.*, vol. 64, no. 10, pp. 3175–3186, Oct. 2016.
- [248] O. Tangsirinaruenart and G. Stylios, "A novel textile stitch-based strain sensor for wearable end users," *Materials*, vol. 12, no. 9, p. 1469, May 2019.
- [249] A. Ehrmann, F. Heimlich, A. Brücken, M. Weber, and R. Haug, "Suitability of knitted fabrics as elongation sensors subject to structure, stitch dimension and elongation direction," *Textile Res. J.*, vol. 84, no. 18, pp. 2006–2012, Nov. 2014.
- [250] O. Atalay and W. Kennon, "Knitted strain sensors: Impact of design parameters on sensing properties," *Sensors*, vol. 14, no. 3, pp. 4712–4730, Mar. 2014.
- [251] G. Gioverto, C. Compton, and L. Dunne, "Machine-stitched E-textile stretch sensors," Sens. Transducers, vol. 202, no. 7, pp. 25–37, Jul. 2016.
- [252] T. Grethe, S. Borczyk, K. Plenkmann, M. Normann, M. Rabe, and A. Schwarz-Pfeiffer, "Textile humidity sensors," in *Proc. Symp. Design*, *Test, Integr. Packag. MEMS MOEMS (DTIP)*, Rome, Italy, May 2018, pp. 1–3.

- [253] A. Shah and P. Patel, "Suspended embroidered triangular e-textile broadband antenna loaded with shorting pins," AEU - Int. J. Electron. Commun., vol. 130, Feb. 2021, Art. no. 153573.
- [254] B. Moradi, R. Fernández-García, and I. Gil, "Meander microwave bandpass filter on a flexible textile substrate," *Electronics*, vol. 8, no. 1, p. 11, Dec. 2018.
- [255] B. Moradi, M. Martínez, R. Fernández-García, and I. Gil, "Study of double ring resonator embroidered wearable antennas for microwave applications," in *Proc. 13th Eur. Conf. Antennas Propag. (EuCAP)*, Krakow, Poland, Mar. 2019, pp. 1–5.
- [256] C. Luo, R. Fernández-García, and I. Gil, "Embroidered textile capacitive sensor for sucrose solutions measurement," in *Proc. IEEE Int. Conf.* Flexible Printable Sensors Syst. (FLEPS), Manchester, U.K., Aug. 2020, pp. 1–4.
- [257] D. Elsheikh and A. R. Eldamak, "Microwave textile sensors for breast cancer detection," in *Proc. 38th Nat. Radio Sci. Conf. (NRSC)*, vol. 1, Mansoura, Egypt, Jul. 2021, pp. 288–294.
- [258] S. Zahertar, E. Laurin, L. E. Dodd, and H. Torun, "Embroidered rectangular split-ring resonators for the characterization of dielectric materials," *IEEE Sensors J.*, vol. 20, no. 5, pp. 2434–2439, Mar. 2020.
- [259] H. R. Nejad, M. P. Punjiya, and S. Sonkusale, "Washable thread based strain sensor for smart textile," in *Proc. 19th Int. Conf. Solid-State Sensors, Actuat. Microsyst. (TRANSDUCERS)*, Kaohsiung, Taiwan, Jun. 2017, pp. 1183–1186.
- [260] M. Martínez-Estrada, I. Gil, and R. Fernández-García, "An alternative method to develop embroidery textile strain sensors," *Textiles*, vol. 1, no. 3, pp. 504–512, Nov. 2021.
- [261] E. Ismar, X. Tao, F. Rault, F. Dassonville, and C. Cochrane, "Towards embroidered circuit board from conductive yarns for E-textiles," *IEEE Access*, vol. 8, pp. 155329–155336, 2020.
- [262] R. Lin, H.-J. Kim, S. Achavananthadith, Z. Xiong, J. K. W. Lee, Y. L. Kong, and J. S. Ho, "Digitally-embroidered liquid metal electronic textiles for wearable wireless systems," *Nature Commun.*, vol. 13, no. 1, Apr. 2022, Art. no. 2190.
- [263] I. Cunha, R. Barras, P. Grey, D. Gaspar, E. Fortunato, R. Martins, and L. Pereira, "Reusable cellulose-based hydrogel sticker film applied as gate dielectric in paper electrolyte-gated transistors," Adv. Funct. Mater., vol. 27, no. 16, Apr. 2017, Art. no. 1606755.
- [264] Y. Zheng, Z. He, Y. Gao, and J. Liu, "Direct desktop printed-circuits-on-paper flexible electronics," Sci. Rep., vol. 3, no. 1, May 2013, Art. no. 1786.
- [265] S. Khan, L. Lorenzelli, and R. S. Dahiya, "Technologies for printing sensors and electronics over large flexible substrates: A review," *IEEE Sensors J.*, vol. 15, no. 6, pp. 3164–3185, Jun. 2015.
- [266] G. Sico, M. Montanino, A. De Girolamo Del Mauro, A. Imparato, G. Nobile, and C. Minarini, "Effects of the ink concentration on multi-layer gravure-printed PEDOT:PSS," *Organic Electron.*, vol. 28, pp. 257–262, Jan. 2016.
- [267] L. Nayak, S. Mohanty, S. K. Nayak, and A. Ramadoss, "A review on inkjet printing of nanoparticle inks for flexible electronics," *J. Mater. Chem. C*, vol. 7, no. 29, pp. 8771–8795, Jul. 2019.
- [268] H. Sirringhaus, T. Kawase, R. H. Friend, T. Shimoda, M. Inbasekaran, W. Wu, and E. P. Woo, "High-resolution inkjet printing of all-polymer transistor circuits," *Science*, vol. 290, no. 5499, pp. 2123–2126, Dec. 2000.
- [269] L. Roselli, EuMA High Frequency Technologies Series. Cambridge, U.K.: Cambridge Univ. Press, Sep. 2014.
- [270] L. Yang, D. Staiculescu, R. Zhang, C. P. Wong, and M. M. Tentzeris, "A novel 'green' fully-integrated ultrasensitive RFID-enabled gas sensor utilizing inkjet-printed antennas and carbon nanotubes," in *Proc. IEEE Antennas Propag. Soc. Int. Symp.*, North Charleston, SC, USA, Jun. 2009, pp. 1–4.
- [271] N. Javed, M. A. Azam, I. Qazi, Y. Amin, and H. Tenhunen, "A novel multi-parameter chipless RFID sensor for green networks," AEU-Int. J. Electron. Commun., vol. 128, Jan. 2021, Art. no. 153512.
- [272] M. Moras, C. Martínez-Domingo, R. Escudé, C. Herrojo, F. Paredes, L. Terés, F. Martín, and E. Ramon, "Programmable organic chipless RFID tags inkjet printed on paper substrates," *Appl. Sci.*, vol. 11, no. 17, p. 7832, Aug. 2021.
- [273] H. Ling, S. Liu, Z. Zheng, and F. Yan, "Organic flexible electronics," Small Methods, vol. 2, no. 10, Oct. 2018, Art. no. 1800070.
- [274] F. Martín and E. Bronchalo, Coupled Structures for Microwave Sensing, vol. 1150. Cham, Switzerland: Springer, Apr. 2024.



- [275] M. Abdolrazzaghi, V. Nayyeri, and F. Martin, "Techniques to improve the performance of planar microwave sensors: A review and recent developments," *Sensors*, vol. 22, no. 18, p. 6946, Sep. 2022.
- [276] J.-S. Hong, Microstrip Filters for RF/Microwave Applications, 2nd ed., Hoboken, NJ, USA: Wiley, 2011.
- [277] C. G. Juan, B. Potelon, C. Quendo, E. Bronchalo, and J. M. Sabater-Navarro, "Highly-sensitive glucose concentration sensor exploiting inter-resonators couplings," in *Proc. 49th Eur. Microw Conf. (EuMC)*, Oct. 2019, pp. 662–665.
- [278] M. H. Zarifi and M. Daneshmand, "Wide dynamic range microwave planar coupled ring resonator for sensing applications," *Appl. Phys. Lett.*, vol. 108, no. 23. Jun. 2016. Art. no. 232906.
- [279] L.-V. Herrera-Sepulveda, J.-L. Olvera-Cervantes, A. Corona-Chavez, and T. Kaur, "Sensor and methodology for determining dielectric constant using electrically coupled resonators," *IEEE Microw. Wireless Compon. Lett.*, vol. 29, no. 9, pp. 626–628, Sep. 2019.
- [280] O. S. Bakam Nguenouho, A. Chevalier, B. Potelon, J. Benedicto, and C. Quendo, "Dielectric characterization and modelling of aqueous solutions involving sodium chloride and sucrose and application to the design of a bi-parameter RF-sensor," Sci. Rep., vol. 12, no. 1, May 2022, Art. no. 7209.
- [281] E. Bronchalo, "Coupled planar microwave resonators and transmission-line structures," in *Coupled Structures for Microwave Sensing*, vol. 1150, F. Martín and E. Bronchalo, Eds., Cham, Switzerland: Springer, Apr. 2024, pp. 95–145.
- [282] G. L. Matthaei, Y. L. Young, and E. M. T. Jones, Microwave Filters, Impedance-Matching Networks, and Coupling Structures. New York, NY, USA: McGraw-Hill, 1964.
- [283] B. Potelon, E. Bronchalo, C. G. Juan, C. Quendo, and A. Chevalier, "Solute concentration sensing in aqueous solutions with coupled microstrip resonators," in *Coupled Structures for Microwave Sensing*, vol. 1150. Cham, Switzerland: Springer, Apr. 2024, pp. 375–425.
- [284] C. G. Juan, B. Potelon, C. Quendo, and E. Bronchalo, "Microwave planar resonant solutions for glucose concentration sensing: A systematic review," *Appl. Sci.*, vol. 11, no. 15, p. 7018, Jul. 2021.
- [285] L.-V. Herrera-Sepulveda, J.-L. Olvera-Cervantes, A. Corona-Chavez, and T. Kaur, "New methodology to determine the loss tangent of dielectric planar samples by using electrically coupled resonators," *J. Electromagn. Waves Appl.*, vol. 34, no. 18, pp. 2410–2418, Dec. 2020.
- [286] L. V. H. Sepulveda, J. L. O. Cervantes, and C. E. Saavedra, "Multifrequency coupled-resonator sensor for dielectric characterization of liquids," *IEEE Trans. Instrum. Meas.*, vol. 70, pp. 1–7, 2021.
- [287] H.-N. Morales-Lovera, J.-L. Olvera-Cervantes, A. Corona-Chavez, and T. K. Kataria, "Dielectric characterization of anisotropic 3D-printed biodegradable substrates based on polylactic acid [application notes]," *IEEE Microw. Mag.*, vol. 22, no. 9, pp. 18–100, Sep. 2021.
- [288] H.-N. Morales-Lovera, J.-L. Olvera-Cervantes, A. Corona-Chavez, and T. K. Kataria, "Dielectric anisotropy sensor using coupled resonators," *IEEE Trans. Microw. Theory Techn.*, vol. 68, no. 4, pp. 1610–1616, Apr. 2020.
- [289] H.-N. Morales-Lovera, J.-L. Olvera-Cervantes, A.-E. Perez-Ramos, A. Corona-Chavez, and C. E. Saavedra, "Microstrip sensor and methodology for the determination of complex anisotropic permittivity using perturbation techniques," Sci. Rep., vol. 12, no. 1, Feb. 2022, Art. no. 2205.
- [290] M. H. Zarifi, "Sensitivity and selectivity enhancement in coupling ring resonator sensors using splitting resonant frequencies," in *IEEE MTT-S Int. Microw. Symp. Dig.*, Philadelphia, PA, USA, Jun. 2018, pp. 36–39.
- [291] Z. Abbasi, P. Shariaty, M. Nosrati, Z. Hashisho, and M. Daneshmand, "Dual-band microwave circuits for selective binary gas sensing system," *IEEE Trans. Microw. Theory Techn.*, vol. 67, no. 10, pp. 4206–4219, Oct. 2019.
- [292] O. S. B. Nguenouho, A. Chevalier, B. Potelon, C. Quendo, J. Benedicto, and B. Simon, "Electromagnetic characterization of aqueous sodium lactate solutions and its application for enhanced concentration monitoring," *IEEE Trans. Instrum. Meas.*, vol. 72, pp. 1–8, 2023.
- [293] C. G. Juan, B. Potelon, A. Aquino, H. García-Martínez, and C. Quendo, "Multi-parameter simultaneous extraction with a novel microwave sensor based on coupled resonators," *Sci. Rep.*, vol. 14, no. 1, Oct. 2024, Art. no. 23076.

- [294] P. Casacuberta, P. Vélez, J. Muñoz-Enano, L. Su, and F. Martín, "Reflective-mode permittivity sensors based on distributed and semilumped coupled resonators," in *Coupled Structures for Microwave Sensing*, vol. 1150, F. Martín and E. Bronchalo, Eds., Cham, Switzerland: Springer, Apr. 2024, pp. 243–281.
- [295] A. M. Albishi, M. K. E. Badawe, V. Nayyeri, and O. M. Ramahi, "Enhancing the sensitivity of dielectric sensors with multiple coupled complementary split-ring resonators," *IEEE Trans. Microw. Theory Techn.*, vol. 68, no. 10, pp. 4340–4347, Oct. 2020.
- [296] Z. Xu, Y. Wang, and S. Fang, "Dielectric characterization of liquid mixtures using EIT-like transmission window," *IEEE Sensors J.*, vol. 21, no. 16, pp. 17859–17867, Aug. 2021.
- [297] Z. Xu, Y. Wang, J. Chang, and T. J. Cui, "Multiple spoof plasmonically induced transparency for sensing applications," *Phys. Rev. Appl.*, vol. 18, no. 2, Aug. 2022, Art. no. 024035.
- [298] I. Piekarz, J. Sorocki, K. Wincza, and S. Gruszczynski, "Coupled-line sensor with Marchand balun as RF system for dielectric sample detection," *IEEE Sensors J.*, vol. 16, no. 1, pp. 88–96, Jan. 2016.
- [299] I. Piekarz, J. Sorocki, K. Wincza, and S. Gruszczynski, "Microwave sensors for dielectric sample measurement based on coupled-line section," *IEEE Trans. Microw. Theory Techn.*, vol. 65, no. 5, pp. 1615–1631, May 2017.
- [300] L.-C. Fan, W.-S. Zhao, D.-W. Wang, Q. Liu, S. Chen, and G. Wang, "An ultrahigh sensitivity microwave sensor for microfluidic applications," *IEEE Microw. Wireless Compon. Lett.*, vol. 30, no. 12, pp. 1201–1204, Dec. 2020.
- [301] W.-J. Wu, W.-S. Zhao, D.-W. Wang, B. Yuan, and G. Wang, "Ultrahigh-sensitivity microwave microfluidic sensors based on modified complementary electric-LC and split-ring resonator structures," *IEEE Sensors J.*, vol. 21, no. 17, pp. 18756–18763, Sep. 2021.
- [302] A. Ebrahimi, W. Withayachumnankul, S. F. Al-Sarawi, and D. Abbott, "Dual-mode behavior of the complementary electric-LC resonators loaded on transmission line: Analysis and applications," *J. Appl. Phys.*, vol. 116, no. 8, Aug. 2014, Art. no. 083705.
- [303] U. Ali, A. Jabbar, X. Yi, M. A. Naveed, M. Q. Mehmood, M. Zubair, and Y. Massoud, "A novel fractal Hilbert curve-based low-cost and highly sensitive microwave sensor for dielectric characterization of liquid materials," *IEEE Sensors J.*, vol. 23, no. 20, pp. 23950–23957, Oct. 2023.
- [304] K. K. Adhikari and N.-Y. Kim, "Ultrahigh-sensitivity mediator-free biosensor based on a microfabricated microwave resonator for the detection of micromolar glucose concentrations," *IEEE Trans. Microw. Theory Techn.*, vol. 64, no. 1, pp. 319–327, Jan. 2016.
- [305] N.-Y. Kim, K. K. Adhikari, R. Dhakal, Z. Chuluunbaatar, C. Wang, and E.-S. Kim, "Rapid, sensitive and reusable detection of glucose by a robust radiofrequency integrated passive device biosensor chip," *Sci. Rep.*, vol. 5, no. 1, Jan. 2015, Art. no. 7807.
- [306] N. Y. Kim, R. Dhakal, K. K. Adhikari, E. S. Kim, and C. Wang, "A reusable robust radio frequency biosensor using microwave resonator by integrated passive device technology for quantitative detection of glucose level," *Biosensors Bioelectron.*, vol. 67, pp. 687–693, May 2015.
- [307] A. A. Abduljabar, D. J. Rowe, A. Porch, and D. A. Barrow, "Novel microwave microfluidic sensor using a microstrip split-ring resonator," *IEEE Trans. Microw. Theory Techn.*, vol. 62, no. 3, pp. 679–688, Mar. 2014.
- [308] M. Wagih and J. Shi, "Scalable all-printed microwave microfluidic sensor for multi-liquid characterization based on a stub-loaded microstrip line," *TechRxiv*, Aug. 2021, doi: 10.36227/techrxiv.15067551.v1.
- [309] Y. Liang, M. Ma, F. Zhang, F. Liu, T. Lu, Z. Liu, and Y. Li, "Wireless microfluidic sensor for metal ion detection in water," ACS Omega, vol. 6, no. 13, pp. 9302–9309, Apr. 2021.
- [310] M. Abdolrazzaghi and M. Daneshmand, "Compelling impact of intermodulation products of regenerative active resonators on sensitivity," in *IEEE MTT-S Int. Microw. Symp. Dig.*, Honololu, HI, USA, Jun. 2017, pp. 1018–1021.
- [311] M. H. Zarifi, T. Thundat, and M. Daneshmand, "High resolution microwave microstrip resonator for sensing applications," Sens. Actuators A, Phys., vol. 233, pp. 224–230, Sep. 2015.
- [312] M. H. Zarifi, S. Farsinezhad, K. Shankar, and M. Daneshmand, "Liquid sensing using active feedback assisted planar microwave resonator," *IEEE Microw. Wireless Compon. Lett.*, vol. 25, no. 9, pp. 621–623, Sep. 2015.



- [313] M. Abdolrazzaghi, M. H. Zarifi, C. F. A. Floquet, and M. Daneshmand, "Contactless asphaltene detection using an active planar microwave resonator sensor," *Energy Fuels*, vol. 31, no. 8, pp. 8784–8791, Aug. 2017.
- [314] M. H. Zarifi, B. Wiltshire, N. Mahdi, P. Kar, K. Shankar, and M. Daneshmand, "Ultraviolet sensing using a TiO₂ nanotube integrated high resolution planar microwave resonator device," *Nanoscale*, vol. 10, no. 10, pp. 4882–4889, Mar. 2018.
- [315] M. H. Zarifi and M. Daneshmand, "Non-contact liquid sensing using high resolution microwave microstrip resonator," in *IEEE MTT-S Int. Microw.* Symp. Dig., Phoenix, AZ, USA, May 2015, pp. 1–4.
- [316] M. H. Zarifi, M. Fayaz, J. Goldthorp, M. Abdolrazzaghi, Z. Hashisho, and M. Daneshmand, "Microbead-assisted high resolution microwave planar ring resonator for organic-vapor sensing," *Appl. Phys. Lett.*, vol. 106, no. 6, Feb. 2015, Art. no. 062903.
- [317] M. H. Zarifi, A. Gholidoust, M. Abdolrazzaghi, P. Shariaty, Z. Hashisho, and M. Daneshmand, "Sensitivity enhancement in planar microwave active-resonator using metal organic framework for CO₂ detection," Sens. Actuators B, Chem., vol. 255, pp. 1561–1568, Feb. 2018.
- [318] J. Liang, H. Yang, Y. Fu, X. Zhou, R. Zhao, and J. Jin, "A high q factor sensor to measure the complex permittivity and effective permittivity based on a band stop frequency-selective surface," *Measurement*, vol. 237, Sep. 2024, Art. no. 115279.
- [319] M. R. Islam, M. T. Islam, A. Hoque, B. Bais, H. Alsaif, M. S. Islam, and M. S. Soliman, "Quad-band split ring resonator-based sensor for microwave sensing application," *Sci. Rep.*, vol. 15, no. 1, Feb. 2025, Art. no. 6888.
- [320] A. Buragohain, G. S. Das, Y. Beria, A. J. A. Al-Gburi, P. P. Kalita, and T. Doloi, "Highly sensitive differential hexagonal split ring resonator sensor for material characterization," *Sens. Actuators A, Phys.*, vol. 363, Dec. 2023, Art. no. 114704.
- [321] X. Han, P. Peng, C. Fu, L. Qiao, Z. Ma, K. Liu, and S. Zhang, "Highly integrated improved hexagonal CSRR-based fluid sensor for complex dielectric parameter detection," *IEEE Sensors J.*, vol. 24, no. 13, pp. 20559–20570. Jul. 2024.
- [322] W.-J. Wu, H. Xie, W.-S. Zhao, and W. Wang, "A microwave sensor system based on M-SRRs for assessing the complex permittivity of liquid samples," *IEEE Sensors J.*, vol. 24, no. 24, pp. 40827–40838, Dec. 2024.
- [323] J. Lei Yong, P. Li, X. L. He, M. S. Tong, L. T. Guo, and Y. J. Zhang, "Multifrequency microwave liquid identification sensor based on interdigital split ring resonators," *IEEE Trans. Instrum. Meas.*, vol. 74, pp. 1–10, 2025.
- [324] J. Hu, W.-J. Wu, W.-S. Zhao, and W. Wang, "Novel high-sensitivity differential microwave sensor for permittivity determination of ethanol water solutions," *IEEE Sensors J.*, vol. 25, no. 9, pp. 15043–15054, May 2025.
- [325] N. Hosseini, M. Baghelani, and M. Daneshmand, "Selective volume fraction sensing using resonant- based microwave sensor and its harmonics," *IEEE Trans. Microw. Theory Techn.*, vol. 68, no. 9, pp. 3958–3968, Sep. 2020.
- [326] M. Mertens, R. Trouillon, T. Markovic, K. Wu, and D. Schreurs, "Principal component regression for broadband microwave-microfluidic chemometrics on small sample counts," *IEEE J. Electromagn.*, RF Microw. Med. Biol., vol. 9, no. 2, pp. 1–9, Jun. 2025, doi: 10.1109/JERM.2025.3537462.
- [327] C. Gocen and M. Palandoken, "Machine learning assisted novel microwave sensor design for dielectric parameter characterization of water-ethanol mixture," *IEEE Sensors J.*, vol. 22, no. 3, pp. 2119–2127, Feb. 2022.
- [328] X. Zhang, C. Ruan, T. U. Haq, and K. Chen, "High-sensitivity microwave sensor for liquid characterization using a complementary circular spiral resonator," *Sensors*, vol. 19, no. 4, p. 787, Feb. 2019.
- [329] J.-H. Pan, W.-J. Wu, Q. Q. Liu, W.-S. Zhao, D.-W. Wang, X. Hu, Y. Hu, J. Wang, J. Liu, and L. Sun, "Deep reinforcement learning based optimization of microwave microfluidic sensor," *IEEE Microw. Wireless Technol. Lett.*, vol. 34, no. 11, pp. 1309–1312, Nov. 2024.
- [330] X. Han, K. Liu, P. Peng, and S. Zhang, "Novel high-sensitivity differential microwave sensor for permittivity determination of ethanol water solutions," *IEEE Trans. Instrum. Meas.*, vol. 74, pp. 1–11, 2025.
- [331] M. Palandoken and C. Gocen, "RFID-enabled ML-assisted microwave liquid sensor design for complex dielectric characterization of watermethanol mixture," Sens. Actuators A, Phys., vol. 382, Feb. 2025, Art. no. 116142.

- [332] M. Baghelani, N. Hosseini, and M. Daneshmand, "Artificial intelligence assisted noncontact microwave sensor for multivariable biofuel analysis," *IEEE Trans. Ind. Electron.*, vol. 68, no. 11, pp. 11492–11500, Nov. 2021.
- [333] N. Kazemi and P. Musilek, "Enhancing microwave sensor performance with ultrahigh Q features using CycleGAN," *IEEE Trans. Microw. Theory Techn.*, vol. 70, no. 12, pp. 5369–5382, Dec. 2022.
- [334] Z. Wang, X. Xiao, C. Yang, and T. Kikkawa, "Combined approach to estimate blood glucose level in noninvasive monitoring: Ultra-wide band microwave and cascaded general regression neural network," *IEEE Trans. Ind. Informat.*, vol. 18, no. 8, pp. 5105–5114, Aug. 2022.
- [335] S. Srisai, P. Kongkeaw, and S. Harnsoongnoen, "Noncontact and noninvasive detection of glucose concentration using a single-port microwave sensor coupled with artificial neural networks," *IEEE Trans. Instrum. Meas.*, vol. 74, pp. 1–10, 2025.
- [336] P. Jeyakumar, S. Vishwa, and B. Yuvaprabha, "Non-invasive glucose monitoring using PCA-enhanced quadring resonator sensor," *Appl. Phys. A, Solids Surf.*, vol. 131, no. 5, Apr. 2025, Art. no. 350.
- [337] M. Martinic, M. Mertens, D. Schreurs, B. Nauwelaers, G. A. E. Vandenbosch, and T. Markovic, "Highly sensitive impedancematched microwave dielectric sensor for glucose concentration measurements," *IEEE Sensors J.*, vol. 25, no. 5, pp. 7962–7972, Mar. 2025.
- [338] N. Kazemi and P. Musilek, "Resolution enhancement of microwave sensors using super-resolution generative adversarial network," *Expert Syst. Appl.*, vol. 213, Mar. 2023, Art. no. 119252.
- [339] Z. Wang, X. Xiao, Y. Pang, W. Su, and T. Kikkawa, "Noninvasive, intelligent blood glucose monitoring on fingertip using dual-band fusion and LSTM-R network," *IEEE Sensors J.*, vol. 24, no. 3, pp. 3465–3476, Feb. 2024.
- [340] S. Harnsoongnoen, S. Srisai, P. Kongkeaw, and B. Buranrat, "Detection and classification of glucose solution concentration and blood sugar levels at the fingertip using a novel planar microwave sensor and deep learning techniques," Sens. Actuators B, Chem., vol. 430, May 2025, Art. no. 137322.
- [341] A. Khasnobish, A. Mazumder, V. K. Bharadwaj, T. Chakravarty, and M. J. Akhtar, "Novel microwave-based noncontact oedema severity monitoring with machine learning," *IEEE Sensors Lett.*, vol. 8, no. 12, Dec. 2024, Art. no. 6015104.
- [342] N. Khalid, M. Zubair, M. Q. Mehmood, and Y. Massoud, "Emerging paradigms in microwave imaging technology for biomedical applications: Unleashing the power of artificial intelligence," *npj Imag.*, vol. 2, no. 1, Jun. 2024, Art. no. 13.
- [343] P. Kongkeaw, S. Srisai, and S. Harnsoongnoen, "Detection and quantification of water contamination in fuel oil using substrate integrated waveguide resonator-based microwave sensors coupled with multilayer perceptron neural networks," Sens. Actuators A, Phys., vol. 384, Apr. 2025, Art. no. 116280.
- [344] I. B. Syed, B. Sundaram, S. Ayothiraman, and S. Yuvaraj, "Planar microwave sensor suitable for artificial-intelligence (AI) based detection of volatile organic compounds," AEU-Int. J. Electron. Commun., vol. 185, Oct. 2024, Art. no. 155444.
- [345] V. Balasubramanian, O. Niksan, M. C. Jain, K. Golovin, and M. H. Zarifi, "Non-destructive erosive wear monitoring of multi-layer coatings using AI-enabled differential split ring resonator based system," *Nature Commun.*, vol. 14, no. 1, Aug. 2023, Art. no. 4916.
- [346] N. Kazemi, N. Gholizadeh, and P. Musilek, "Selective microwave zerothorder resonator sensor aided by machine learning," *Sensors*, vol. 22, no. 14, p. 5362, Jul. 2022.
- [347] M. Abdolrazzaghi, N. Kazemi, V. Nayyeri, and F. Martin, "AI-assisted ultra-high-sensitivity/resolution active-coupled CSRR-based sensor with embedded selectivity," *Sensors*, vol. 23, no. 13, p. 6236, Jul. 2023.
- [348] M. Abdolrazzaghi, S. Hashemy, and A. Abdolali, "Fast-forward solver for inhomogeneous media using machine learning methods: Artificial neural network, support vector machine and fuzzy logic," *Neural Comput. Appl.*, vol. 29, no. 12, pp. 1583–1591, Jun. 2018.
- [349] H.-Y. Gan, W.-S. Zhao, Q. Liu, D.-W. Wang, L. Dong, G. Wang, and W.-Y. Yin, "Differential microwave microfluidic sensor based on microstrip complementary split-ring resonator (MCSRR) structure," *IEEE Sensors J.*, vol. 20, no. 11, pp. 5876–5884, Jun. 2020.
- [350] N. Kazemi, M. Abdolrazzaghi, P. Musilek, and M. Daneshmand, "A temperature-compensated high-resolution microwave sensor using artificial neural network," *IEEE Microw. Wireless Compon. Lett.*, vol. 30, no. 9, pp. 919–922, Sep. 2020.



- [351] J. Rivera, M. Carrillo, M. Chacón, G. Herrera, and G. Bojorquez, "Self-calibration and optimal response in intelligent sensors design based on artificial neural networks," *Sensors*, vol. 7, no. 8, pp. 1509–1529, Aug. 2007.
- [352] D. Kilani, O. Niksan, and M. H. Zarifi, "Intelligent ice detection based on artificial neural network using microwave sensor," in *Proc. URSI Int. Symp. Electromagn. Theory (EMTS)*, Vancouver, BC, Canada, May 2023, pp. 188–191.
- [353] V. Balasubramanian, O. Niksan, M. C. Jain, K. Golovin, and M. H. Zarifi, "Augmented reality-enhanced microwave-based wireless monitoring system for smart coating applications," *IEEE Trans. Microw. Theory Techn.*, vol. 72, no. 12, pp. 6881–6889, Dec. 2024.
- [354] A. Darwish, M. Ricci, J. A. T. Vasquez, C. Migliaccio, and F. Vipiana, "Near-field microwave sensing technology enhanced with machine learning for the non-destructive evaluation of packaged food and beverage products," Sci. Rep., vol. 14, no. 1, Jun. 2024, Art. no. 13413.
- [355] N. Khalid, R. Mirzavand, and A. K. Iyer, "A survey on battery-less RFID-based wireless sensors," *Micromachines*, vol. 12, no. 7, p. 819, Jul. 2021.
- [356] H. Mirzaei, O. Niksan, M. Arjmand, and M. H. Zarifi, "Exploring microwave reconfigurable intelligent surface for wireless VOC detection: A comparative study of porous and solid PDMS interfaces," Adv. Mater. Technol., vol. 9, no. 18, Sep. 2024, Art. no. 2400348.
- [357] M. H. Zarifi, S. Deif, and M. Daneshmand, "Wireless passive RFID sensor for pipeline integrity monitoring," *Sens. Actuators A, Phys.*, vol. 261, pp. 24–29, Jul. 2017.
- [358] S. N. R. Kantareddy, I. Mathews, R. Bhattacharyya, I. M. Peters, T. Buonassisi, and S. E. Sarma, "Long range battery-less PV-powered RFID tag sensors," *IEEE Internet Things J.*, vol. 6, no. 4, pp. 6989–6996, Aug. 2019.
- [359] X. Yi, T. Wu, Y. Wang, R. T. Leon, M. M. Tentzeris, and G. Lantz, "Passive wireless smart-skin sensor using RFID-based folded patch antennas," *Int. J. Smart Nano Mater.*, vol. 2, no. 1, pp. 22–38, Feb. 2011.
- [360] A. Maleki Gargari, M. H. Zarifi, and L. Markley, "Passive matched mushroom structure for a high sensitivity low profile antenna-based material detection system," *IEEE Sensors J.*, vol. 19, no. 15, pp. 6154–6162, Aug. 2019.
- [361] M. L. Neyestanak, H. Moghadas, S. Mirabbasi, and P. Servati, "Compact fractal-shaped frequency selective surface for distant liquid sensing with multiple sensitive spots," *IEEE Sensors J.*, vol. 25, no. 9, pp. 15031–15042, May 2025.
- [362] S. Rodini, S. Genovesi, G. Manara, and F. Costa, "Wireless mm-wave chipless pressure sensor," *IEEE Trans. Microw. Theory Techn.*, vol. 72, no. 7, pp. 4163–4173, Jul. 2024.
- [363] U. Kose and M. Kartal, "Non-invasive microwave glucose sensor by using a hybrid sensor composed of a frequency selective surface and microstrip patch antenna," in *Proc. Photon. Electromagn. Res. Symp.* (PIERS), Prague, Czech Republic, Jul. 2023, pp. 1361–1367.
- [364] V. Balasubramanian and M. H. Zarifi, "Augmented reality-assisted battery-less microwave-based sensors for smart health monitoring of coatings," in *IEEE MTT-S Int. Microw. Symp. Dig.*, Washington, DC, USA, Jun. 2024, pp. 277–280.
- [365] V. Balasubramanian, F. Niknahad, and M. H. Zarifi, "Wireless real time sweat secretion monitoring using waveguide-based wearable sensor," in *IEEE MTT-S Int. Microw. Symp. Dig.*, Montreal, QC, Canada, Jun. 2024, pp. 81–83.
- [366] A. Kumar, C. Wang, F.-Y. Meng, C.-P. Jiang, G.-F. Yan, M. Zhao, C.-Q. Jing, and L. Wang, "Ultrafast detection and discrimination of methanol gas using a polyindole-embedded substrate integrated waveguide microwave sensor," ACS Sensors, vol. 5, no. 12, pp. 3939–3948, Dec. 2020.
- [367] M. Sameer and P. Agarwal, "Coplanar waveguide microwave sensor for label-free real-time glucose detection," *Radioengineering*, vol. 27, no. 2, pp. 491–495, Jun. 2019.
- [368] S. S. Stuchly and C. E. Bassey, "Microwave coplanar sensors for dielectric measurements," *Meas. Sci. Technol.*, vol. 9, no. 8, pp. 1324–1329, Aug. 1998.
- [369] L. Li and D. Uttamchandani, "A microwave dielectric biosensor based on suspended distributed MEMS transmission lines," *IEEE Sensors J.*, vol. 9, no. 12, pp. 1825–1830, Dec. 2009.
- [370] T. Chretiennot, D. Dubuc, and K. Grenier, "Microwave-based microfluidic sensor for non-destructive and quantitative glucose monitoring in aqueous solution," Sensors, vol. 16, no. 10, p. 1733, Oct. 2016.

- [371] A. E. Omer, G. Shaker, S. Safavi-Naeini, G. Alquie, F. Deshours, H. Kokabi, and R. M. Shubair, "Non-invasive real-time monitoring of glucose level using novel microwave biosensor based on triplepole CSRR," *IEEE Trans. Biomed. Circuits Syst.*, vol. 14, no. 6, pp. 1407–1420, Dec. 2020.
- [372] A. Ebrahimi, Z. Vilagosh, E. P. Ivanova, and K. Ghorbani, "Sepia melanin detection in water solutions using a microwave fluidic biosensor," in *Proc. IEEE Asia Pacific Microw. Conf. (APMC)*, Bali, Indonesia, Nov. 2024, pp. 196–198.
- [373] T. Chen, F. Artis, D. Dubuc, J-J. Fournié, M. Poupot, and K. Grenier, "Microwave biosensor dedicated to the dielectric spectroscopy of a single alive biological cell in its culture medium," in *IEEE MTT-S Int. Microw.* Symp. Dig., Seattle, WA, USA, Jun. 2013, pp. 1–4.
- [374] K. Grenier, A. Tamra, A. Zedek, G. Poiroux, F. Artis, T. Chen, W. Chen, M. Poupot, J.-J. Fournié, and D. Dubuc, "Low volume and label-free molecules characterization and cell monitoring with microwave dielectric spectroscopy," in *Proc. IEEE Int. Microw. Biomed. Conf. (IMBioC)*, Philadelphia, PA, USA, Jun. 2018, pp. 82–84.
- [375] K. Grenier, F. Artis, M. Poupot, and D. Dubuc, "Label-free discrimination of human lymphoma cell sub-populations with microwave dielectric spectroscopy," in *IEEE MTT-S Int. Microw. Symp. Dig. (IMS)*, Jun. 2018, pp. 907–910.
- [376] A. C. Stelson, M. Liu, C. A. E. Little, C. J. Long, N. D. Orloff, N. Stephanopoulos, and J. C. Booth, "Label-free detection of conformational changes in switchable DNA nanostructures with microwave microfluidics," *Nature Commun.*, vol. 10, no. 1, Mar. 2019, Art. no. 1174.
- [377] G. Poiroux, D. Dubuc, M. Hosseini, F. Artis, A. Tamra, M. Tosolini, F. Pont, C. Bosc, E. Saland, F. Lopez, J. Fournié, J. Sarry, K. Grenier, and M. Poupot, "Label-free detection of mitochondrial activity with microwave dielectric spectroscopy," *Int. J. Biotechnol. Bioeng.*, vol. 6, no. 5, pp. 1–14, Nov. 2020.
- [378] K. Grenier, G. Pratviel, H. Mazur, and D. Dubuc, "Detection of a macromolecule denaturation with microwave dielectric spectroscopy based on hydration modifications," in *IEEE MTT-S Int. Microw. Symp. Dig.*, Toulouse, France, Dec. 2020, pp. 1–4.
- [379] X. Du, C. Ladegard, X. Ma, X. Cheng, and J. C. M. Hwang, "Broadband electrical sensing of nucleus size in a live cell from 900 Hz to 40 GHz," in *IEEE MTT-S Int. Microw. Symp. Dig.*, Toulouse, France, Dec. 2020, pp. 1–4.
- [380] C. A. Ferguson, J. C. M. Hwang, Y. Zhang, and X. Cheng, "Single-cell classification based on population nucleus size combining microwave impedance spectroscopy and machine learning," *Sensors*, vol. 23, no. 2, p. 1001, Jan. 2023.
- [381] O. Krivosudský, D. Havelka, D. E. Chafai, and M. Cifra, "Microfluidic on-chip microwave sensing of the self-assembly state of tubulin," *Sens. Actuators B, Chem.*, vol. 328, Feb. 2021, Art. no. 129068.
- [382] W. Sun, J. Wang, Q. Wang, J. Chen, and L. Sun, "A broadband biosensor with high sensitivity up to 110 GHz for single cell," *IEEE Sensors J.*, vol. 24, no. 20, pp. 32425–32433, Oct. 2024.
- [383] A. Tamra, D. Dubuc, M.-P. Rols, and K. Grenier, "Microwave monitoring of single cell monocytes subjected to electroporation," *IEEE Trans. Microw. Theory Techn.*, vol. 65, no. 9, pp. 3512–3518, Sep. 2017.
- [384] F. Artis, T. Chen, T. Chretiennot, J.-J. Fournie, M. Poupot, D. Dubuc, and K. Grenier, "Microwaving biological cells: Intracellular analysis with microwave dielectric spectroscopy," *IEEE Microw. Mag.*, vol. 16, no. 4, pp. 87–96, May 2015.
- [385] Y. Cui, J. Li, W. Cao, and P. Wang, "Highly sensitive RF detection and analysis of DNA solutions," in *IEEE MTT-S Int. Microw. Symp. Dig.*, Tampa, FL, USA, Jun. 2014, pp. 1–4.
- [386] N. Dahal, J. A. Osterberg, B. Braun, T. P. Caldwell, R. Divan, S. W. Harcum, and P. Wang, "Spectroscopic analysis of candida species, viability, and antifungal drug effects with a microwave flow cytometer," *IEEE J. Electromagn.*, RF Microw. Med. Biol., vol. 6, no. 4, pp. 566–573, Dec. 2022.
- [387] Y. Yang, H. Zhang, J. Zhu, G. Wang, T.-R. Tzeng, X. Xuan, K. Huang, and P. Wang, "Distinguishing the viability of a single yeast cell with an ultrasensitive radio frequency sensor," *Lab Chip*, vol. 10, no. 5, pp. 553–555, Mar. 2010.
- [388] F. Hjeij, C. Dalmay, B. Bessette, G. Begaud, A. Bessaudou, P. Blondy, M. O. Jauberteau, F. Lalloue, C. B. Kaynak, M. Kaynak, W. Gamal, C. Palego, and A. Pothier, "Biological cell discrimination based on their high frequency dielectropheretic signatures at UHF frequencies," in *IEEE MTT-S Int. Microw. Symp. Dig.*, Honololu, HI, USA, Jun. 2017, pp. 533–536.



- [389] N. Blasco, A. Abélanet, E. Champion, A. Magnaudeix, A. Pothier, and C. Dalmay, "Ultra-high frequency dielectrophoresis to characterize mesenchymal stem cells differentiation: Application to bioceramics synthesis," in *Proc. 54th Eur. Microw. Conf. (EuMC)*, Paris, France, Sep. 2024, pp. 313–316.
- [390] S. Afshar, E. Salimi, K. Braasch, M. Butler, D. J. Thomson, and G. E. Bridges, "Multi-frequency DEP cytometer employing a microwave sensor for dielectric analysis of single cells," *IEEE Trans. Microw. Theory Techn.*, vol. 64, no. 3, pp. 991–998, Mar. 2016.
- [391] S. Afshar, A. Fazelkhah, K. Braasch, E. Salimi, M. Butler, D. J. Thomson, and G. E. Bridges, "Full beta-dispersion region dielectric spectra and dielectric models of viable and non-viable CHO cells," *IEEE J. Electromagn.*, RF Microw. Med. Biol., vol. 5, no. 1, pp. 70–77, Mar. 2021.
- [392] N. Meyne, G. Fuge, A.-P. Zeng, and A. F. Jacob, "Resonant microwave sensors for picoliter liquid characterization and nondestructive detection of single biological cells," *IEEE J. Electromagn.*, RF Microw. Med. Biol., vol. 1, no. 2, pp. 98–104, Dec. 2017.
- [393] A. Secme, U. Tefek, B. Sari, H. S. Pisheh, H. D. Uslu, Ö. A. Çaliskan, B. Kucukoglu, R. T. Erdogan, H. Alhmoud, O. Sahin, and M. S. Hanay, "High-resolution dielectric characterization of single cells and microparticles using integrated microfluidic microwave sensors," *IEEE Sensors J.*, vol. 23, no. 7, pp. 6517–6529, Apr. 2023.
- [394] S. Gabriel, R. W. Lau, and C. Gabriel, "The dielectric properties of biological tissues: II. Measurements in the frequency range 10 hz to 20 GHz," *Phys. Med. Biol.*, vol. 41, no. 11, pp. 2251–2269, Nov. 1996.
- [395] S. Gabriel, R. W. Lau, and C. Gabriel, "The dielectric properties of biological tissues: III. parametric models for the dielectric spectrum of tissues," *Phys. Med. Biol.*, vol. 41, no. 11, pp. 2271–2293, Nov. 1996.
- [396] C. Baumgartner, P. A. Hasgall, F. Di Gennaro, E. Neufeld, B. Lloyd, M. C. Gosselin, D. Payne, A. Klingenböck, and N. Kuster, "IT'IS database for thermal and electromagnetic parameters of biological tissues," Version 4.2, IT'IS Foundation, Apr. 2024, doi: 10.13099/VIP21000-04-2.
- [397] V. Raicu and Y. Feldman, Dielectric Relaxation in Biological Systems: Physical Principles, Methods and Applications. Oxford, U.K.: Oxford University Press, Jul. 2015.
- [398] C. G. Juan, Designing Microwave Sensors for Glucose Concentration Detection in Aqueous and Biological Solutions. Cham, Switzerland: Springer, Jun. 2021.
- [399] C. G. J. Poveda, E. Bronchalo, G. Torregrosa-Penalva, Á. G. Martínez, and J. M. Sabater-Navarro, "Microwave microstrip resonator for developing a non-invasive glucose sensor," *Int. J. Comput. Assist. Radiol. Surg.*, vol. 10, no. S1, pp. S172–S173, Jun. 2015.
- [400] K. Fuchs and U. Kaatze, "Molecular dynamics of carbohydrate aqueous solutions. Dielectric relaxation as a function of glucose and fructose concentration," *J. Phys. Chem. B*, vol. 105, no. 10, pp. 2036–2042, Feb. 2001.
- [401] J.-H. Park, C.-S. Kim, B.-C. Choi, and K.-Y. Ham, "The correlation of the complex dielectric constant and blood glucose at low frequency," *Biosensors Bioelectron.*, vol. 19, no. 4, pp. 321–324, Dec. 2003.
- [402] B. Potelon, C. Quendo, J.-L. Carré, A. Chevalier, C. Person, and P. Quéffélec, "Electromagnetic signature of glucose in aqueous solutions and human blood," in *Proc. MEMSWAVE Conf.*, Jun. 2014, pp. 4–7.
- [403] K. Shiraga, T. Suzuki, N. Kondo, T. Tajima, M. Nakamura, H. Togo, A. Hirata, K. Ajito, and Y. Ogawa, "Broadband dielectric spectroscopy of glucose aqueous solution: Analysis of the hydration state and the hydrogen bond network," *J. Chem. Phys.*, vol. 142, no. 23, Jun. 2015, Art. no. 234504.
- [404] T. Lin, S. Gu, and T. Lasri, "Highly sensitive characterization of glucose aqueous solution with low concentration: Application to broadband dielectric spectroscopy," Sens. Actuators A, Phys., vol. 267, pp. 318–326, Nov. 2017.
- [405] C. G. Juan, E. Bronchalo, G. Torregrosa, E. Ávila, N. García, and J. M. Sabater-Navarro, "Dielectric characterization of water glucose solutions using a transmission/reflection line method," *Biomed. Signal Process. Control*, vol. 31, pp. 139–147, Jan. 2017.
- [406] V. Turgul and I. Kale, "Permittivity extraction of glucose solutions through artificial neural networks and non-invasive microwave glucose sensing," Sens. Actuators A, Phys., vol. 277, pp. 65–72, Jul. 2018.
- [407] A. Weatherbee, I. Popov, and A. Vitkin, "Accurate viscosity measurements of flowing aqueous glucose solutions with suspended scatterers using a dynamic light scattering approach with optical coherence tomography," J. Biomed. Opt., vol. 22, no. 8, Aug. 2017, Art. no. 087003.

- [408] E. H. Grant, "Relationship between relaxation time and viscosity for water," J. Chem. Phys., vol. 26, no. 6, pp. 1575–1577, Jun. 1957.
- [409] E. Levy, A. Puzenko, U. Kaatze, P. B. Ishai, and Y. Feldman, "Dielectric spectra broadening as the signature of dipole-matrix interaction. I. water in nonionic solutions," *J. Chem. Phys.*, vol. 136, no. 11, Mar. 2012, Art. no. 114502.
- [410] B. R. Jean, E. C. Green, and M. J. McClung, "A microwave frequency sensor for non-invasive blood-glucose measurement," in *Proc. IEEE Sensors Appl. Symp.*, Atlanta, GA, USA, Feb. 2008, pp. 4–7.
- [411] T. Yilmaz, R. Foster, and Y. Hao, "Towards accurate dielectric property retrieval of biological tissues for blood glucose monitoring," *IEEE Trans. Microw. Theory Techn.*, vol. 62, no. 12, pp. 3193–3204, Dec. 2014.
- [412] H. Choi, S. Luzio, J. Beutler, and A. Porch, "Microwave noninvasive blood glucose monitoring sensor: Human clinical trial results," in *IEEE MTT-S Int. Microw. Symp. Dig.*, Jun. 2017, pp. 876–879.
- [413] V. Turgul and I. Kale, "Simulating the effects of skin thickness and fingerprints to highlight problems with non-invasive RF blood glucose sensing from fingertips," *IEEE Sensors J.*, vol. 17, no. 22, pp. 7553–7560, Nov. 2017.
- [414] R. Kumari, P. N. Patel, and R. Yadav, "An ENG resonator-based microwave sensor for the characterization of aqueous glucose," *J. Phys.* D, Appl. Phys., vol. 51, no. 7, Jan. 2018, Art. no. 075601.
- [415] A. K. Jha, Z. Akhter, N. Tiwari, K. T. M. Shafi, H. Samant, M. J. Akhtar, and M. Cifra, "Broadband wireless sensing system for non-invasive testing of biological samples," *IEEE J. Emerg. Sel. Topics Circuits Syst.*, vol. 8, no. 2, pp. 251–259, Jun. 2018.
- [416] A. Kandwal, L. W. Y. Liu, J. Li, Y. Liu, H. Tang, Z. Ju, T. Igbe, R. Jasrotia, and Z. Nie, "Designing highly sensitive microwave antenna sensor with novel model for noninvasive glucose measurements," *Prog. Electromagn. Res.*, vol. 176, pp. 129–141, Mar. 2023.
- [417] P. Mohammadi, A. Mohammadi, and A. Kara, "Dual-frequency microwave resonator for noninvasive detection of aqueous glucose," *IEEE Sensors J.*, vol. 23, no. 18, pp. 21246–21253, Sep. 2023.
- [418] S. Wang, W. Wang, and Y. Zheng, "Reconfigurable multimode microwave sensor with resonance and transmission sensing capabilities for noninvasive glucose monitoring," *IEEE Trans. Microw. Theory Techn.*, vol. 72, no. 5, pp. 3102–3117, May 2024.
- [419] M. Bazgir and A. Sheikhi, "High-accuracy microwave sensor for glucose detection using a slow-wave CRLH structure," *IEEE Sensors J.*, vol. 25, no. 1, pp. 468–475, Jan. 2025.
- [420] A. Kandwal, S. Dutt, L. W. Y. Liu, Z. Nie, R. Jasrotia, C. K. Chan, A. M. Almuhlafi, and H. Vettikalladi, "Frequency selective metasurface based radio frequency glucose sensor with a periodic array of meta cells," *Sci. Rep.*, vol. 14, no. 1, Oct. 2024, Art. no. 25716.
- [421] A. Kandwal, R. Jasrotia, S. Kumar, A. Kumari, R. Sharma, A. M. Almuhlafi, and H. Vettikalladi, "Flexible surface plasmon based coupled triple band UHF-microwave sensor for glucose sensing application," Sens. Actuators A, Phys., vol. 379, Dec. 2024, Art. no. 115864.
- [422] W. Liu and L. Xu, "Dual-band microwave sensor for sensing application of microfluidic based on transmission line loaded pair of SIR resonators," *IEEE Trans. Instrum. Meas.*, vol. 73, pp. 1–11, 2024.
- [423] W. Liu and Y. Yang, "Miniaturized multiband planar sensor based on transmission line loaded with pairs of improved resonators for glucoseaqueous solution sensing applications," *IEEE Sensors J.*, vol. 24, no. 14, pp. 22377–22386, Jul. 2024.
- [424] A. Ebrahimi, W. Withayachumnankul, S. F. Al-Sarawi, and D. Abbott, "Microwave microfluidic sensor for determination of glucose concentration in water," in *Proc. IEEE 15th Medit. Microw. Symp. (MMS)*, Lecce, Italy, Nov. 2015, pp. 1–3.
- [425] G. Govind and M. J. Akhtar, "Metamaterial-inspired microwave microfluidic sensor for glucose monitoring in aqueous solutions," *IEEE Sensors J.*, vol. 19, no. 24, pp. 11900–11907, Dec. 2019.
- [426] G. Govind and M. J. Akhtar, "Design of an ELC resonator-based reusable RF microfluidic sensor for blood glucose estimation," *Sci. Rep.*, vol. 10, no. 1, Nov. 2020, Art. no. 18842.
- [427] C. Li, H. Li, L. Wang, X. Fan, Y. Xiong, L. Qian, D. Li, L. Miao, J. Wang, H. Li, and M. Li, "Microwave microfluidic glucose sensor based on a single-port dumbbell defective ground structure," *IEEE Sensors J.*, vol. 24, no. 16, pp. 25670–25679, Aug. 2024.
- [428] S. Harnsoongnoen and A. Wanthong, "Coplanar waveguides loaded with a split ring resonator-based microwave sensor for aqueous sucrose solutions," *Meas. Sci. Technol.*, vol. 27, no. 1, Jan. 2016, Art. no. 015103.



- [429] S. Harnsoongnoen and A. Wanthong, "Coplanar waveguide transmission line loaded with electric-LC resonator for determination of glucose concentration sensing," *IEEE Sensors J.*, vol. 17, no. 6, pp. 1635–1640, Mar. 2017.
- [430] Z. Abedeen and P. Agarwal, "Microwave sensing technique based label-free and real-time planar glucose analyzer fabricated on FR4," Sens. Actuators A, Phys., vol. 279, pp. 132–139, Aug. 2018.
- [431] Omkar, W. Yu, and S. Y. Huang, "T-shaped patterned microstrip line for noninvasive continuous glucose sensing," *IEEE Microw. Wireless Compon. Lett.*, vol. 28, no. 10, pp. 942–944, Oct. 2018.
- [432] S. Y. Huang, Omkar, Y. Yoshida, A. J. G. Inda, C. X. Xavier, W. C. Mu, Y. S. Meng, and W. Yu, "Microstrip line-based glucose sensor for noninvasive continuous monitoring using the main field for sensing and multivariable crosschecking," *IEEE Sensors J.*, vol. 19, no. 2, pp. 535–547, Jan. 2019.
- [433] M. A. Zidane, A. Rouane, C. Hamouda, and H. Amar, "Hyper-sensitive microwave sensor based on split ring resonator (SRR) for glucose measurement in water," Sens. Actuators A, Phys., vol. 321, Apr. 2021, Art. no. 112601.
- [434] S. Harnsoongnoen and B. Buranrat, "Glucose concentration monitoring using microstrip spurline sensor," *Meas. Sci. Rev.*, vol. 23, no. 4, pp. 168–174, Aug. 2023.
- [435] P. Vélez, J. Mata-Contreras, D. Dubuc, K. Grenier, and F. Martín, "Solute concentration measurements in diluted solutions by means of split ring resonators," in *Proc. 48th Eur. Microw. Conf. (EuMC)*, Madrid, Spain, Sep. 2018, pp. 231–234.
- [436] C. Jang, J.-K. Park, H.-J. Lee, G.-H. Yun, and J.-G. Yook, "Temperature-corrected fluidic glucose sensor based on microwave resonator," *Sensors*, vol. 18, no. 11, p. 3850, Nov. 2018.
- [437] S. Mohammadi, B. Wiltshire, M. C. Jain, A. V. Nadaraja, A. Clements, K. Golovin, D. J. Roberts, T. Johnson, I. Foulds, and M. H. Zarifi, "Gold coplanar waveguide resonator integrated with a microfluidic channel for aqueous dielectric detection," *IEEE Sensors J.*, vol. 20, no. 17, pp. 9825–9833, Sep. 2020.
- [438] A. Tahmid, T. Rahman, S. M. A. Emam, S. M. Reza, M. I. Hosen, R. Inum, and A. Habib, "Low-cost and easy-to-fabricate microwave sensor for sensitive glucose monitoring: A step towards continuous glucose monitoring," *IEEE J. Electromagn.*, RF Microw. Med. Biol., vol. 9, no. 2, pp. 221–228, Jun. 2025, doi: 10.1109/JERM.2024.3477596.
- [439] U. Schwerthoeffer, R. Weigel, and D. Kissinger, "A highly sensitive glucose biosensor based on a microstrip ring resonator," in *IEEE MTT-S Int. Microw. Symp. Dig.*, Singapore, Singapore, Dec. 2013, pp. 1–3.
- [440] G. Guariti, M. Hofmann, R. Weigel, G. Fischer, and D. Kissinger, "Determination of sugar concentration in aqueous solutions using ultrawideband microwave impedance spectroscopy," in *IEEE MTT-S Int. Microw. Symp. Dig.*, Seattle, WA, USA, Jun. 2013, pp. 1–4.
- [441] J. A. Byford, K. Y. Park, and P. Chahal, "Metamaterial inspired periodic structure used for microfluidic sensing," in *Proc. IEEE 65th Electron. Compon. Technol. Conf. (ECTC)*, San Diego, CA, USA, May 2015, pp. 1997–2002.
- [442] M. Abdolrazzaghi, R. Genov, and G. V. Eleftheriades, "Microwave planar sensor antenna for glucose sensing in aqueous solutions," in Proc. IEEE Int. Symp. Antennas Propag. USNC-URSI Radio Sci. Meeting (APS/URSI), Dec. 2021, pp. 127–128.
- [443] H.-C. Chang, C.-T.-M. Wu, and C.-H. Tseng, "A 24-GHz frequency-locked loop-based microwave microfluidic sensor for concentration detection," *IEEE J. Sel. Areas Sensors*, vol. 1, pp. 20–28, 2024.
- [444] U. Kaatze, "Complex permittivity of water as a function of frequency and temperature," J. Chem. Eng. Data, vol. 34, no. 4, pp. 371–374, Oct. 1989.
- [445] W. J. Ellison, "Permittivity of pure water, at standard atmospheric pressure, over the frequency range-25THz and the temperature range—100°C," *J. Phys. Chem. Reference Data*, vol. 36, no. 1, pp. 1–18, Mar. 2007.
- [446] S. Harnsoongnoen, A. Wanthong, U. Charoen-In, and A. Siritaratiwat, "Planar microwave sensor for detection and discrimination of aqueous organic and inorganic solutions," *Sens. Actuators B, Chem.*, vol. 271, pp. 300–305, Oct. 2018.
- [447] C. G. Juan, E. Bronchalo, B. Potelon, C. Quendo, E. Ávila-Navarro, and J. M. Sabater-Navarro, "Concentration measurement of microliter-volume water-glucose solutions using Q factor of microwave sensors," *IEEE Trans. Instrum. Meas.*, vol. 68, no. 7, pp. 2621–2634, Jul. 2019.
- [448] W. L. Clarke, D. Cox, L. A. Gonder-Frederick, W. Carter, and S. L. Pohl, "Evaluating clinical accuracy of systems for self-monitoring of blood glucose," *Diabetes Care*, vol. 10, no. 5, pp. 622–628, Sep. 1987.

- [449] C. G. Juan, E. Bronchalo, B. Potelon, C. Quendo, and J. M. Sabater-Navarro, "Glucose concentration measurement in human blood plasma solutions with microwave sensors," *Sensors*, vol. 19, no. 17, p. 3779, Aug. 2019.
- [450] C. G. Juan, H. García, E. Ávila-Navarro, E. Bronchalo, V. Galiano, Ó. Moreno, D. Orozco, and J. M. Sabater-Navarro, "Feasibility study of portable microwave microstrip open-loop resonator for non-invasive blood glucose level sensing: Proof of concept," *Med. Biol. Eng. Comput.*, vol. 57, no. 11, pp. 2389–2405, Nov. 2019.
- [451] H. García, C. G. Juan, E. Ávila-Navarro, E. Bronchalo, and J. M. Sabater-Navarro, "Portable device based on microwave resonator for noninvasive blood glucose monitoring," in *Proc. 41st Annu. Int. Conf. IEEE Eng. Med. Biol. Soc. (EMBC)*, Jul. 2019, pp. 1115–1118.
- [452] C. G. Juan, E. Bronchalo, B. Potelon, J. Álvarez-Pastor, and J. M. Sabater-Navarro, "Use of coplanar quarter-wave resonators for glucose sensing in aqueous solutions," in *IEEE MTT-S Int. Microw. Symp. Dig.*, Toulouse, France, Dec. 2020, pp. 1–3.
- [453] C. G. Juan, E. Bronchalo, and J. M. Sabater-Navarro, "Influence of dry layers in solute concentration measurement with planar microwave sensors," in *Proc. IEEE Int. Instrum. Meas. Technol. Conf. (I2MTC)*, Glasgow, United Kingdom, May 2024, pp. 1–6.
- [454] E. Bronchalo and C. G. Juan, "Effect of dry layers in solute concentration sensing with planar resonant microwave sensors," in *Proc. 54th Eur. Microw. Conf. (EuMC)*, Paris, France, Sep. 2024, pp. 940–943.
- [455] H. Woo, H.-J. Lee, and J.-G. Yook, "Noninvasive detection of glucose and NaCl solutions with environment correction using a dual IDC-based microwave sensor," *IEEE Sensors J.*, vol. 24, no. 12, pp. 19039–19049, Jun. 2024.
- [456] A. E. Omer, G. Shaker, S. Safavi-Naeini, H. Kokabi, G. Alquié, F. Deshours, and R. M. Shubair, "Low-cost portable microwave sensor for non-invasive monitoring of blood glucose level: Novel design utilizing a four-cell CSRR hexagonal configuration," *Sci. Rep.*, vol. 10, no. 1, Sep. 2020, Art. no. 15200.
- [457] N. Kazemi, M. Abdolrazzaghi, P. E. Light, and P. Musilek, "Inhuman testing of a non-invasive continuous low-energy microwave glucose sensor with advanced machine learning capabilities," *Biosensors Bioelectron.*, vol. 241, Dec. 2023, Art. no. 115668.
- [458] G. Buonanno and S. Costanzo, "Machine learning approach to microwave sensing of glucose concentration: Method and preliminary results," in *Proc. 4th URSI Atlantic RadioScience Conf. (AT-RAS)*, Meloneras, Spain, May 2024, pp. 1–4.
- [459] N. Pandit, R. K. Jaiswal, and N. P. Pathak, "Plasmonic metamaterial-based label-free microfluidic microwave sensor for aqueous biological applications," *IEEE Sensors J.*, vol. 20, no. 18, pp. 10582–10590, Sep. 2020.
- [460] A. Kandwal, Z. Nie, T. Igbe, J. Li, Y. Liu, L. W. Liu, and Y. Hao, "Surface plasmonic feature microwave sensor with highly confined fields for aqueous-glucose and blood-glucose measurements," *IEEE Trans. Instrum. Meas.*, vol. 70, pp. 1–9, 2021.
- [461] F. Soltanian, M. Nosrati, S. Mobayen, C.-C. Li, T. Pan, M.-T. Ke, and P. Skruch, "On-body non-invasive glucose monitoring sensor based on high figure of merit (FoM) surface plasmonic microwave resonator," *Sci. Rep.*, vol. 13, no. 1, Oct. 2023, Art. no. 17527.
- [462] Z. Gong, B. Ren, and Y. Chen, "Microwave continuous blood glucose monitoring using microgels-based sensor," in *Proc. Pho*ton. Electromagn. Res. Symp. (PIERS), Chengdu, China, Apr. 2024, pp. 1–7.
- [463] A. Mason, O. Korostynska, J. Louis, L. E. Cordova-Lopez, B. Abdullah, J. Greene, R. Connell, and J. Hopkins, "Noninvasive in-situ measurement of blood lactate using microwave sensors," *IEEE Trans. Biomed. Eng.*, vol. 65, no. 3, pp. 698–705, Mar. 2018.
- [464] A. Mason, O. Korostynska, J. Dixon, and R. Connell, "Non-invasive real-time monitoring of blood lactate using a low-power microwave sensor," in *Proc. IEEE Sensors*, Kobe, Kobe, Japan, Oct. 2024, pp. 1–4.
- [465] M. Baghelani, Z. Abbasi, M. Daneshmand, and P. E. Light, "Non-invasive lactate monitoring system using wearable chipless microwave sensors with enhanced sensitivity and zero power consumption," *IEEE Trans. Biomed. Eng.*, vol. 69, no. 10, pp. 3175–3182, Oct. 2022.
- [466] P. D. Jensen, P. M. Meaney, N. R. Epstien, and K. D. Paulsen, "Cole-cole parameter characterization of urea and potassium for improving dialysis treatment assessment," *IEEE Antennas Wireless Propag. Lett.*, vol. 11, pp. 1598–1601, 2012.



- [467] S. Hosseinzadeh and M. Yousefi, "A permittivity and conductivity sensor based on microstrip transmission line with defective ground for detection of urea in saline," *IEEE Trans. Instrum. Meas.*, vol. 73, pp. 1–11, 2024.
- [468] S. R. Charvadeh, J. Ghalibafan, A. Abbasi, A. Haidary, and E. Salimi, "Utilization of the dialysate to characterize dialysis adequacy by using microwave urea biosensor based on complementary split-ring resonator (CSRR)," *Measurement*, vol. 241, Feb. 2025, Art. no. 115703.
- [469] S. Singh, M. Sharma, and G. Singh, "Recent advancements in urea biosensors for biomedical applications," *IET Nanobiotechnol.*, vol. 15, no. 4, pp. 358–379, Jun. 2021.
- [470] K. Zhao, Y. Liu, and Q. Zhang, "Dielectric behavior of adulterated milk with urea and water," J. Mol. Liquids, vol. 273, pp. 37–44, Jan. 2019.
- [471] Y. Khanna and Y. K. Awasthi, "Dual-band microwave sensor for investigation of liquid impurity concentration using a metamaterial complementary split-ring resonator," *J. Electron. Mater.*, vol. 49, no. 1, pp. 385–394, Jan. 2020.
- [472] S. Jain, N. K. Tiwari, and M. J. Akhtar, "CSIWC RFsensor for micro-fluidicnon-contactquality assessment of milk," *Int. J. RF Microw. Comput.-Aided Eng.*, vol. 32, no. 2, Feb. 2022, Art. no. e22962.
- [473] U. Salmaz, T. Islam, and S. Ibrahim, "Capacitive droplet sensing for milk quality analysis," in *Proc. IEEE Int. Instrum. Meas. Technol. Conf.* (12MTC), Kuala Lumpur, Malaysia, May 2023, pp. 1–5.
- [474] A. Karthikeyan, R. Anbazhagan, and R. Vijay, "Non-invasive detection of multiple analytes in dairy industry using heterogeneous ring resonating sensor," *Appl. Phys. A, Solids Surf.*, vol. 130, no. 1, Jan. 2024, Art. no. 71.
- [475] Y. Cui, Z. Zhang, S. Sui, and W. Zhu, "Microwave measurement of bovine serum albumin solutions based on high-Q/high-resolution resonator," *IEEE Trans. Microw. Theory Techn.*, vol. 70, no. 8, pp. 3954–3963, Aug. 2022.
- [476] M. Nakamura, T. Tajima, and M. Seyama, "Broadband dielectric spectroscopy for quantitative analysis of glucose and albumin in multicomponent aqueous solution," *IEEE J. Electromagn., RF Microw. Med. Biol.*, vol. 6, no. 1, pp. 86–93, Mar. 2022.
- [477] R. Gautam, K. Bhardwaj, A. Singh, P. N. Tripathi, P. Kumar, and R. Kumar, "Single split resonance sensor device for detection of bovine serum albumin using water soluble perylenediimide as probe," *IEEE Sensors J.*, vol. 23, no. 23, pp. 28579–28586, Dec. 2023.
- [478] E. Porter, H. Bahrami, A. Santorelli, B. Gosselin, L. A. Rusch, and M. Popovic, "A wearable microwave antenna array for time-domain breast tumor screening," *IEEE Trans. Med. Imag.*, vol. 35, no. 6, pp. 1501–1509, Jun. 2016.
- [479] N. AlSawaftah, S. El-Abed, S. Dhou, and A. Zakaria, "Microwave imaging for early breast cancer detection: Current state, challenges, and future directions," *J. Imag.*, vol. 8, no. 5, p. 123, Apr. 2022.
- [480] C. Blanco-Angulo, A. Martínez-Lozano, R. Gutiérrez-Mazón, C. G. Juan, H. García-Martínez, J. Arias-Rodríguez, J. M. Sabater-Navarro, and E. Ávila-Navarro, "Non-invasive microwave-based imaging system for early detection of breast tumours," *Biosensors*, vol. 12, no. 9, p. 752, Sep. 2022.
- [481] C. Blanco-Angulo, A. Martínez-Lozano, C. G. Juan, R. Gutiérrez-Mazón, J. Arias-Rodríguez, E. Ávila-Navarro, and J. M. Sabater-Navarro, "Validation of an RF image system for real-time tracking neurosurgical tools," *Sensors*, vol. 22, no. 10, p. 3845, May 2022.
- [482] A. Martínez-Lozano, C. Blanco-Angulo, A. Rodríguez-Martínez, C. G. Juan, H. García-Martínez, J. M. Sabater-Navarro, and E. Ávila-Navarro, "Toward intraoperative brain-shift detection through microwave imaging system," *IEEE Trans. Instrum. Meas.*, vol. 72, pp. 1–11, 2023.
- [483] A. Martínez-Lozano, R. Gutierrez, C. G. Juan, C. Blanco-Angulo, H. García-Martínez, G. Torregrosa, J. M. Sabater-Navarro, and E. Ávila-Navarro, "Microwave imaging system based on signal analysis in a planar environment for detection of abdominal aortic aneurysms," *Biosensors*, vol. 14, no. 3, p. 149, Mar. 2024.
- [484] M. Gugliermino, D. O. Rodriguez-Duarte, C. Origlia, J. A. T. Vasquez, R. Scapaticci, L. Crocco, and F. Vipiana, "Portable microwave (pMWI) system for brain stroke imaging using off-the-shelf components," in *Proc.* 54th Eur. Microw. Conf. (EuMC), Paris, France, Sep. 2024, pp. 485–488.
- [485] A. Mishra, W. McDonnell, J. Wang, D. Rodriguez, and C. Li, "Intermodulation-based nonlinear smart health sensing of human vital signs and location," *IEEE Access*, vol. 7, pp. 158284–158295, 2019.
- [486] A. S. A. El-Hameed, D. M. Elsheakh, G. M. Elashry, and E. A. Abdallah, "A comparative study of narrow/ultra-wideband microwave sensors for the continuous monitoring of vital signs and lung water level," *Sensors*, vol. 24, no. 5, p. 1658, Mar. 2024.

- [487] D. N. Elsheakh, A. S. A. El-Hameed, G. M. Elashry, O. M. Fahmy, and E. A. Abdallah, "Coupled and radiated microwave sensors for vital signs and lung water level monitoring," *Measurement*, vol. 240, Jan. 2025, Art. no. 115535.
- [488] S. Trabelsi and S. O. Nelson, "Microwave sensing of quality attributes of agricultural and food products," *IEEE Instrum. Meas. Mag.*, vol. 19, no. 1, pp. 36–41, Feb. 2016.
- [489] Z. Meng, Z. Wu, and J. Gray, "Microwave sensor technologies for food evaluation and analysis: Methods, challenges and solutions," *Trans. Inst. Meas. Control*, vol. 40, no. 12, pp. 3433–3448, Aug. 2018.
- [490] N. Javanbakht, G. Xiao, and R. E. Amaya, "A comprehensive review of portable microwave sensors for grains and mineral materials moisture content monitoring," *IEEE Access*, vol. 9, pp. 120176–120184, 2021.
- [491] N. Javanbakht, G. Xiao, and R. E. Amaya, "Portable microwave sensor based on frequency-selective surface for grain moisture content monitoring," *IEEE Sensors Lett.*, vol. 5, no. 11, pp. 1–4, Nov. 2021.
- [492] M. Li, T. Hou, C. Cai, Z. Lv, Y. Wu, and Y. Qin, "Nondestructive wheat moisture detection system with metasurface plane wave antenna and de-embedding algorithm," *IEEE Trans. Instrum. Meas.*, vol. 72, pp. 1–9, 2023.
- [493] L. Fan, Z. Chai, Y. Wang, Z. Wang, P. Zhao, J. Li, Q. Zhou, X. Qin, J. Yao, S. Yan, Z. Wang, and L. Huang, "A novel handheld device for intact corn ear moisture content measurement," *IEEE Trans. Instrum. Meas.*, vol. 69, no. 11, pp. 9157–9169, Nov. 2020.
- [494] N. Hosseini and M. Baghelani, "Selective real-time non-contact multivariable water-alcohol-sugar concentration analysis during fermentation process using microwave split-ring resonator based sensor," Sens. Actuators A, Phys., vol. 325, Jul. 2021, Art. no. 112695.
- [495] R. Keshavarz, J. Lipman, D. M. M.-P. Schreurs, and N. Shariati, "Highly sensitive differential microwave sensor for soil moisture measurement," *IEEE Sensors J.*, vol. 21, no. 24, pp. 27458–27464, Dec. 2021.
- [496] Y. Du, F. T. Ulaby, and M. C. Dobson, "Sensitivity to soil moisture by active and passive microwave sensors," *IEEE Trans. Geosci. Remote Sens.*, vol. 38, no. 1, pp. 105–114, Jan. 2000.
- [497] M. Martínez-Estrada, B. Moradi, R. Fernández-Garcia, and I. Gil, "Impact of conductive yarns on an embroidery textile moisture sensor," *Sensors*, vol. 19, no. 5, p. 1004, Feb. 2019.
- [498] O. Malyuskin, "Microplastic detection in soil and water using resonance microwave spectroscopy: A feasibility study," *IEEE Sensors J.*, vol. 20, no. 24, pp. 14817–14826, Dec. 2020.
- [499] K. Sarabandi and E. S. Li, "Microstrip ring resonator for soil moisture measurements," *IEEE Trans. Geosci. Remote Sens.*, vol. 35, no. 5, pp. 1223–1231, Sep. 1997.
- [500] H. Peng, X. Yang, X. Wu, and W. Peng, "A wireless temperature sensor applied to monitor and measure the high temperature of industrial devices," *IEEE Trans. Antennas Propag.*, vol. 72, no. 6, pp. 5273–5282, Jun. 2024.
- [501] H. Peng, X. Wang, J. Zou, T. Zhang, F. Gao, and X. Yang, "A noncontact feed microwave temperature sensor for industry device based on metamaterial," *IEEE Sensors J.*, vol. 24, no. 16, pp. 26397–26406, Aug. 2024.
- [502] B. Leier, R. Mirzavand, M. Baghelani, and A. K. Iyer, "A feasibility examination using microwave stripline resonators for low-temperature sensing," *IEEE Sensors J.*, vol. 24, no. 23, pp. 38558–38568, Dec. 2024.
- [503] B. Leier, M. Baghelani, and A. K. Iyer, "A microwave stripline ring resonator sensor exploiting the thermal coefficient of dielectric constant for high-temperature sensing," *IEEE Sensors J.*, vol. 22, no. 22, pp. 21666–21675, Nov. 2022.
- [504] K. Hossain, T. Cowen, and M. Cheffena, "Molecularly imprinted polymer based antenna sensor for methanol vapor sensing," *IEEE Microw. Wireless Technol. Lett.*, vol. 33, no. 9, pp. 1385–1388, Sep. 2023.
- [505] H.-L. Kao, Y.-C. Tsai, L.-C. Chang, and H.-C. Chiu, "Microwave resonators embedded with carbon nanotubes for real-time gas sensing," *IEEE Sensors J.*, vol. 24, no. 4, pp. 4325–4333, Feb. 2024.
- [506] T. R. Jones, M. H. Zarifi, and M. Daneshmand, "Miniaturized quarter-mode substrate integrated cavity resonators for humidity sensing," *IEEE Microw. Wireless Compon. Lett.*, vol. 27, no. 7, pp. 612–614, Jul. 2017.
- [507] M. S. ur Rahman, M. A. Abou-Khousa, and M. F. Akbar, "A review on microwave non-destructive testing (NDT) of composites," *Eng. Sci. Technol. Int. J.*, vol. 58, Oct. 2024, Art. no. 101848.
- [508] M. Sun, W. J. Staszewski, and R. N. Swamy, "Smart sensing technologies for structural health monitoring of civil engineering structures," Adv. Civil Eng., vol. 2010, pp. 1–13, Jun. 2010.



- [509] G.-D. Zhou and T.-H. Yi, "Recent developments on wireless sensor networks technology for bridge health monitoring," *Math. Problems Eng.*, vol. 2013, pp. 1–33, Dec. 2013.
- [510] K.-K. Duan and S.-Y. Cao, "Emerging RFID technology in structural engineering—A review," Structures, vol. 28, pp. 2404–2414, Dec. 2020.
- [511] P. Kalansuriya, R. Bhattacharyya, S. Sarma, and N. Karmakar, "Towards chipless RFID-based sensing for pervasive surface crack detection," in *Proc. IEEE Int. Conf. RFID-Technol. Appl. (RFID-TA)*, Nice, Nice, France, Nov. 2012, pp. 46–51.
- [512] S. Dey, P. Kalansuriya, and N. C. Karmakar, "Chipless RFID based high resolution crack sensing through SWB technology," in *Proc. IEEE Int. Microw. RF Conf. (IMaRC)*, Bengaluru, India, Dec. 2014, pp. 330–333.
- [513] A. M. J. Marindra and G. Y. Tian, "Multiresonance chipless RFID sensor tag for metal defect characterization using principal component analysis," *IEEE Sensors J.*, vol. 19, no. 18, pp. 8037–8046, Sep. 2019.
- [514] S. Deif and M. Daneshmand, "Multiresonant chipless RFID array system for coating defect detection and corrosion prediction," *IEEE Trans. Ind. Electron.*, vol. 67, no. 10, pp. 8868–8877, Oct. 2020.
- [515] A. M. J. Marindra and G. Y. Tian, "Chipless RFID sensor for corrosion characterization based on frequency selective surface and feature fusion," *Smart Mater. Struct.*, vol. 29, no. 12, Oct. 2020, Art. no. 125010.
- [516] E. DiGiampaolo, A. DiCarlofelice, and A. Gregori, "An RFID-enabled wireless strain gauge sensor for static and dynamic structural monitoring," *IEEE Sensors J.*, vol. 17, no. 2, pp. 286–294, Jan. 2017.
- [517] G. Liu, Q.-A. Wang, G. Jiao, P. Dang, G. Nie, Z. Liu, and J. Sun, "Review of wireless RFID strain sensing technology in structural health monitoring," *Sensors*, vol. 23, no. 15, p. 6925, Aug. 2023.
- [518] S.-H. Min, H.-J. Kim, Y.-J. Quan, H.-S. Kim, J.-H. Lyu, G.-Y. Lee, and S.-H. Ahn, "Stretchable chipless RFID multi-strain sensors using direct printing of aerosolised nanocomposite," Sens. Actuators A, Phys., vol. 313, Oct. 2020, Art. no. 112224.
- [519] K. Mc Gee, P. Anandarajah, and D. Collins, "Proof of concept novel configurable chipless RFID strain sensor," *Sensors*, vol. 21, no. 18, p. 6224, Sep. 2021.
- [520] H. Nesser, H. A. Mahmoud, and G. Lubineau, "High-sensitivity RFID sensor for structural health monitoring," Adv. Sci., vol. 10, no. 26, Jul. 2023, Art. no. 2301807.
- [521] X. Xie, L. Dong, H. Wang, Y. Di, W. Guo, P. Wang, and J. Zhang, "High-sensitivity RFID tag sensor with coupled ring resonators for multiposition crack monitoring," *IEEE Sensors J.*, vol. 24, no. 22, pp. 37869–37878, Nov. 2024.
- [522] X. Xie, L. Dong, H. Wang, Y. Song, Y. Di, W. Guo, and J. Zhang, "Passive wireless RFID strain sensor for directional-independent structural deformation monitoring," Sens. Actuators A, Phys., vol. 380, Dec. 2024, Art. no. 116025.
- [523] S. Taheri, "A review on five key sensors for monitoring of concrete structures," *Construction Building Mater.*, vol. 204, pp. 492–509, Apr. 2019.
- [524] E. Pittella, R. Schiavoni, G. Monti, A. Masciullo, M. Scarpetta, A. Cataldo, and E. Piuzzi, "Split ring resonator network and diffused sensing element embedded in a concrete beam for structural health monitoring," Sensors, vol. 22, no. 17, p. 6398, Aug. 2022.
- [525] C. Strangfeld, S. Johann, M. Müller, and M. Bartholmai, "Embedded passive RFID-based sensors for moisture monitoring in concrete," in *Proc. IEEE SENSORS*, Glasgow, U.K., Oct. 2017, pp. 1–3.
- [526] A. Ramos, D. Girbau, A. Lazaro, and R. Villarino, "Wireless concrete mixture composition sensor based on time-coded UWB RFID," *IEEE Microw. Wireless Compon. Lett.*, vol. 25, no. 10, pp. 681–683, Oct. 2015.
- [527] P. Vélez, F. Paredes, P. Casacuberta, X. Canalias, L. Su, and F. Martín, "A microwave sensor system for the unattended control of corrosion in urban metallic infrastructures," *IEEE Sensors J.*, vol. 25, no. 11, pp. 20455–20465, Jun. 2025, doi: 10.1109/JSEN.2025.3564003.
- [528] D. Kilani, F. Niknahad, A. Shah, S. Olsen, M. Meaker, and M. H. Zarifi, "Wireless microwave sensor network using split ring resonators for ice monitoring applications," *IEEE Internet Things J.*, vol. 11, no. 14, pp. 25316–25325, Jul. 2024.
- [529] A. Shah, O. Niksan, and M. H. Zarifi, "Planar microwave sensor for localized ice and snow sensing," SAE Tech. Paper 2023-01-1432, Jun. 2023.
- [530] F. Niknahad, O. Niksan, and M. H. Zarifi, "Tunable microwave waveguide probe for noncontact ice detection on metallic surfaces," *IEEE Sensors J.*, vol. 24, no. 17, pp. 27421–27428, Sep. 2024.

- [531] E. Eitel, "Basics of rotary encoders: Overview and new technologies," Mach. Des. Mag., vol. 4, no. 2, May 2014.
- [532] G. K. McMillan and D. M. Considine, Process/Industrial Instrument and Control Handbook, 5th ed., McGraw-Hill, 1999.
- [533] X. Li, J. Qi, Q. Zhang, and Y. Zhang, "Bias-tunable dual-mode ultraviolet photodetectors for photoelectric tachometer," *Appl. Phys. Lett.*, vol. 104, no. 4, Jan. 2014, Art. no. 041108.
- [534] G. Ye, H. Liu, Y. Wang, B. Lei, Y. Shi, L. Yin, and B. Lu, "Ratiometric-linearization-based high-precision electronic interpolator for sinusoidal optical encoders," *IEEE Trans. Ind. Electron.*, vol. 65, no. 10, pp. 8224–8231, Oct. 2018.
- [535] Y.-S. Chen, T.-H. Hsu, C.-W. Chen, and C.-C. Hsieh, "A current-mode differential sensing CMOS imager for optical linear encoder," in *Proc. Int. Symp. VLSI Design, Autom. Test (VLSI-DAT)*, Hsinchu, Taiwan, Apr. 2019, pp. 1–2.
- [536] E. Celik and A. H. Obdan, "A new absolute encoder design based on piecewise pseudo-linear signals," *IEEE Sensors J.*, vol. 24, no. 16, pp. 25590–25600, Aug. 2024.
- [537] Z. Zhang, Y. Dong, F. Ni, M. Jin, and H. Liu, "A method for measurement of absolute angular position and application in a novel electromagnetic encoder system," *J. Sensors*, vol. 2015, pp. 1–10, Jul. 2015.
- [538] Z. Zhang, F. Ni, Y. Dong, M. Jin, and H. Liu, "A novel absolute angular position sensor based on electromagnetism," *Sens. Actuators A, Phys.*, vol. 194, pp. 196–203, May 2013.
- [539] X. Yang, W. Zhao, and B. Song, "Thrust force calculation and analysis for the permanent magnet linear motor motion system considering the encoder errors," *IEEE Trans. Ind. Electron.*, vol. 69, no. 6, pp. 6069–6079, Jun. 2022.
- [540] B. Chen and J.-Y. Chang, "Effect of flattening cracked medium on positioning accuracy of a linear magnetic encoder," *IEEE Trans. Magn.*, vol. 56, no. 2, pp. 1–7, Feb. 2020.
- [541] K.-Y. Peng, H.-S. Hsiao, and J.-Y. Chang, "Length-adaptive linear position sensing system based on de-Bruijn sequence," in *Proc. IEEE Sensors*, Vienna, Austria, Oct. 2023, pp. 1–4.
- [542] K.-Y. Peng and J.-Y. Chang, "Generation of absolute patterns for magnetic encoders of arbitrary size with de Bruijn sequences," *IEEE Sensors Lett.*, vol. 8, no. 9, pp. 1–4, Sep. 2024.
- [543] P.-Y. Chen and P.-J. Wang, "Design and analysis of linear incremental encoder based on back magnetic TMR sensors," in *Proc. Photon. Electromagn. Res. Symp. (PIERS)*, Jul. 2023, pp. 2142–2148.
- [544] J. Jezný and M. Čurilla, "Position measurement with Hall effect sensors," Am. J. Mech. Eng., vol. 1, no. 7, pp. 231–235, Jan. 2013.
- [545] P. N. Granell, G. Wang, G. S. Cañon Bermudez, T. Kosub, F. Golmar, L. Steren, J. Fassbender, and D. Makarov, "Highly compliant planar Hall effect sensor with sub 200 nT sensitivity," *Npj Flexible Electron.*, vol. 3, no. 1, Feb. 2019, Art. no. 3.
- [546] A. Lidozzi, L. Solero, F. Crescimbini, and A. Di Napoli, "SVM PMSM drive with low resolution Hall-effect sensors," *IEEE Trans. Power Electron.*, vol. 22, no. 1, pp. 282–290, Jan. 2007.
- [547] G. Scelba, G. De Donato, G. Scarcella, F. G. Capponi, and F. Bonaccorso, "Fault-tolerant rotor position and velocity estimation using binary Halleffect sensors for low-cost vector control drives," *IEEE Trans. Ind. Appl.*, vol. 50, no. 5, pp. 3403–3413, Sep. 2014.
- [548] X. Zhang, M. Mehrtash, and M. B. Khamesee, "Dual-axial motion control of a magnetic levitation system using Hall-effect sensors," *IEEE/ASME Trans. Mechatronics*, vol. 21, no. 2, pp. 1129–1139, Apr. 2016.
- [549] G. Liu, B. Chen, and X. Song, "High-precision speed and position estimation based on Hall vector frequency tracking for PMSM with bipolar Hall-effect sensors," *IEEE Sensors J.*, vol. 19, no. 6, pp. 2347–2355, Mar. 2019.
- [550] F. Martín, C. Herrojo, J. Mata-Contreras, and F. Paredes, *Time-Domain Signature Barcodes for Chipless-RFID and Sensing Applications*, vol. 647. Cham, Switzerland: Springer, Feb. 2020.
- [551] G. Bailly, A. Harrabi, J. Rossignol, D. Stuerga, and P. Pribetich, "Microwave gas sensing with a microstrip interDigital capacitor: Detection of NH₃ with TiO₂ nanoparticles," Sens. Actuators B, Chem., vol. 236, pp. 554–564, Nov. 2016.
- [552] J. Sorocki, A. Rydosz, and K. Staszek, "Wideband microwave multiportbased system for low gas concentration sensing and its application for acetone detection," Sens. Actuators B, Chem., vol. 323, Nov. 2020, Art. no. 128710.



- [553] A. Rydosz, E. Maciak, K. Wincza, and S. Gruszczynski, "Microwave-based sensors with phthalocyanine films for acetone, ethanol and methanol detection," *Sens. Actuators B, Chem.*, vol. 237, pp. 876–886, Dec. 2016.
- [554] N. R. Tanguy, K. K. Kazemi, J. Hong, K.-C. Cheung, S. Mohammadi, P. Gnanasekar, S. S. Nair, M. H. Zarifi, and N. Yan, "Flexible, robust, and high-performance gas sensors based on lignocellulosic nanofibrils," *Carbohydrate Polym.*, vol. 278, Feb. 2022, Art. no. 118920.
- [555] Y. Seekaew, S. Lokavee, D. Phokharatkul, A. Wisitsoraat, T. Kerdcharoen, and C. Wongchoosuk, "Low-cost and flexible printed graphene-PEDOT:PSS gas sensor for ammonia detection," *Organic Electron.*, vol. 15, no. 11, pp. 2971–2981, Nov. 2014.
- [556] M. Moradpour, M. C. Jain, N. R. Tanguy, and M. H. Zarifi, "Investigating the potential of a PEDOT:PSS organic microwave resonator for gas sensing applications," in *Proc. IEEE Sensors*, Oct. 2021, pp. 1–4.
- [557] H. Mirzaei, J. McClelland, D. Sharma, M. Arjmand, and M. H. Zarifi, "A microwave voyage into swelling phenomenon: Investigation of polydimethylsiloxane and VOCs interaction," ACS Appl. Mater. Interfaces, vol. 15, no. 31, pp. 38008–38017, Aug. 2023.
- [558] S. Mohammadi and M. H. Zarifi, "Differential microwave resonator sensor for real-time monitoring of volatile organic compounds," *IEEE Sensors J.*, vol. 21, no. 5, pp. 6105–6114, Mar. 2021.



CARLOS G. JUAN (Senior Member, IEEE) was born in Petrer, Spain, in 1991. He received the M.Sc. degree in telecommunication engineering and the Ph.D. degree in electronic engineering from the Miguel Hernández University of Elche (UMH), Elche, Spain, in 2014 and 2019, respectively.

He joined the Neuroengineering Biomedical (nBio) Research Group, as a Research Fellow. He was a Visiting Researcher with the Lab-

STICC Group, Université de Bretagne Occidentale (UBO), Brest, France, from 2016 to 2018. From 2019 to 2020, he was with the Department of Materials Science, Optics and Electronic Technology, UMH, as an Adjunct Professor. He held research positions with various universities, including Lab-STICC Group, UBO, from 2020 to 2021; the Medical Robotics Group, University of Málaga, Málaga, Spain, in 2022; and the Technical University of Cartagena, Cartagena, Spain, from 2023 to 2024. Since 2024, he has been a "Ramón y Cajal" Senior Research Fellow with the Institute of Bioengineering, UMH. He has authored the book *Glucose Concentration Detection in Aqueous and Biological Solutions with Microwave Sensors: An Approach Towards Non-Invasive Glucose Sensing* (Springer, 2021) and over 50 scientific publications. His main research interests include microwave engineering, sensors, dielectric characterization techniques, and biomedical applications.

Dr. Juan was a recipient of the CEA-Springer Award to the Best Ph.D. Thesis in Bioengineering, in 2020; the Santander Bank Young Researchers Award, in 2022; and the IEEE Transactions on Instrumentation and Measurement Outstanding Associate Editor Award, in 2023 and 2024, among other awards and distinctions. He served as the Associate Technical Program Committee Chair for IEEE International Instrumentation and Measurement Technology Conference (I2MTC), in 2024. He currently serves as a Counselor for IEEE UMH Student Branch. He is an Associate Editor-in-Chief for IEEE Transactions on Instrumentation and Measurement. He is an IEEE I&M Distinguished Lecturer, from 2025 to 2027.



KATIA GRENIER (Senior Member, IEEE) received the M.S. and Ph.D. degrees in electrical engineering from the Université de Toulouse (UT), Toulouse, France, in 1997 and 2000, respectively.

After a postdoctoral fellowship with Agere Systems (Bell Labs), Murray Hill, NJ, USA, in 2001, she joined the Laboratory of Analysis and Architecture of System, National Scientific Research Center (LAAS-CNRS), Toulouse. She was engaged in the development of microwave

microelectromechanical systems (RF MEMS). From 2007 to 2009, she was with the Laboratory for Integrated Micromechatronic Systems CNRS (LIMMS-CNRS)/Institute of Industrial Science (IIS), The University of Tokyo, Tokyo, Japan, where she was engaged in launching research activities on miniature microwave-based biosensors. Since then, her research interests at LAAS-CNRS are focused on the interaction of RF electromagnetic waves with complex fluids. It involves the development of microwave systems based on dielectric spectroscopy for biological sensing and healthcare applications and in vitro exposure systems for evaluating electromagnetic waves effects on cells and microtissues. She has been the Head (and a Founder) of the High Frequency and Fluidic Micro-Nanosystems Group (MH2F Group), LAAS-CNRS, since 2019. She has authored or co-authored over 230 technical conference, letter, journal articles, and book chapters; and holds five patents. Sha has involved in the spreading of microwave techniques within industrial products. She is a member of the technical committee dedicated to Biological Effects and Medical Applications of the IEEE Microwave Theory and Techniques Society, European Microwave Association, and URSI, Commission K. She serves as a Program Committee Member for several conferences, including IEEE MTT-S International Microwave Symposium and European Microwave Week. She has chaired IEEE BioWireleSS 2015 and 2016 conferences. She was the General Chair of IEEE International Microwave Biomedical Conference 2020. She was also involved in Women in Microwave Events' Organization. She has acted as a Guest Editor in several special issues in IEEE Transactions on Microwave THEORY AND TECHNIQUES and IEEE JOURNAL OF ELECTROMAGNETICS, RFAND MICROWAVES IN MEDICINE AND BIOLOGY.



MOHAMMAD H. ZARIFI (Senior Member, IEEE) received the B.Sc., MSc., and Ph.D. degrees in electrical and computer engineering from the University of Tabriz, Iran, in 2004, 2006, and 2009, respectively.

He is currently an Associate Professor and the Tier II Principal's Research Chair (PRC) in sensors and microelectronics with the School of Engineering, The University of British Columbia (UBC); and the Director of Okanagan Micro

Electronics and Gigahertz Applications Laboratory (OMEGA Lab), Canada. Prior joining UBC, he was a postdoctoral fellow with the University of Alberta, Canada, from 2013 to 2017. He has authored or co-authored more than 150 papers in peer-reviewed journals and conference proceedings and holds six issued or pending patents. His research focuses on applied electromagnetics and circuits and systems for communications and sensing applications. He received the CMC-NRC First Place Award, on industrial collaboration for the innovative microwave sensors, in Canada, in 2015. He is the Chair and a member of IEEE MTT-S TC-26 "RFID, Wireless Sensor, and IoT." He is a member of IEEE MTT-S TC-4 "Microwave Passive Components and Transmission Line Structures." He is also a Senior Member of the IEEE Microwave Theory and Technology Society and the IEEE Circuits and Systems Society. He has received the Emerging Researcher Award and the Best Teaching Award at the School of Engineering, in 2020 and 2021, respectively. He has served as a Reviewer and an Associate Editor for several journals and conferences, such as IEEE Sensors Journal and IEEE OPEN JOURNAL OF ANTENNAS AND PROPAGATION. He is an IEEE MTT-S Distinguished Microwave Lecturer, from 2024 to 2027.





AMIR EBRAHIMI (Senior Member, IEEE) received the B.Sc. degree in electrical engineering and the M.Sc. and Ph.D. degrees in microelectronics from the University of Adelaide, Adelaide, Australia, in 2008, 2011, and 2016, respectively.

He is currently a Senior Research Fellow with the School of Engineering, RMIT University, Melbourne, Australia. He was a Visiting Research Fellow with Nanyang Technological University

(NTU), Singapore, from 2014 to 2015. His research interests include metamaterial inspired microwave devices, microwave circuit design, microwave filters, frequency-selective surfaces (FSSs) and nonlinear RF, and microwave circuits design and analysis.

Dr. Ebrahimi was a recipient of the Australian National Fabrication Facility (ANFF) Award, in 2013, the University of Adelaide D. R. Stranks Traveling Fellowship, in 2014; the Yarman-Carlin Best Student Paper Award at the Mediterranean Microwave Symposium, in 2015; the Simon Rockliff Scholarship, in 2016; the Best Paper Award at the Australian Microwave Symposium, in 2016; the Gertrude Rohan Memorial Prize, in 2017; the CASS Foundation Travel Award, in 2019, the Best Young Investigator Paper Award, MTT Section, Australian Microwave Symposium, in 2020; and the Best Paper Award at Asia Pacific Microwave Conference (APMC2024). Since 2023, he has been serving as an Associate Editor of IEEE Sensors IOUENAL



FERRAN MARTIN (Fellow, IEEE) was born in Barakaldo, Biscay, Spain, in 1965. He received the B.S. and Ph.D. degrees in physics from the Universitat Autònoma de Barcelona (UAB), in 1988 and 1992, respectively.

From 1994 to 2006, he was an Associate Professor in electronics with the Departament d'Enginyeria Electrònica (UAB). Since 2007, he has been a Full Professor of electronics. He is the Head (and a Founder) of the Microwave

Engineering, Metamaterials and Antennas Group (GEMMA Group), UAB; and the Director (and a Founder) of CIMITEC, a research and technology transfer center ascribed to the Departament d'Enginyeria Electrònica, UAB. Throughout his career, he has been very active in research fields as diverse as metamaterials and artificial transmission lines, microwave circuits and filters, antennas, chipless-RFID, and planar microwave sensors (his main research topic). He has authored or co-authored over 700 technical conferences, letters, journal articles, and book chapters. He is the co-author of the book on metamaterials titled Metamaterials With Negative Parameters: Theory, Design and Microwave Applications (John Wiley & Sons Inc.), Time-Domain Signature Barcodes for Chipless-RFID and Sensing Applications (Springer), and Planar Microwave Sensors (Wiley/IEEE Press); the author of the book Artificial Transmission Lines for RF and Microwave Applications (John Wiley & Sons Inc.); and a co-editor of the book Balanced Microwave Filters (Wiley/IEEE Press) and Coupled Structures for Microwave Sensing (Springer). He has generated 23 Ph.D.s, has filed several patents on metamaterials, chipless-RFID, and sensors, and has headed dozens of development contracts and collaborative projects with companies. He is a fellow of IET. He is a member of the IEEE Microwave Theory and Techniques Society (IEEE MTT-S). He is a member of the Technical Program Committee of European Microwave Conference (EuMC) and the Scientific Advisory Board of the International Congress on Advanced Electromagnetic Materials in Microwaves and Optics (Metamaterials). Among his distinctions, he has received the 2006 Duran Farell Prize for Technological Research, holds the Parc de Recerca UAB-Santander Technology Transfer Chair, and a recipient of four ICREA ACADEMIA Awards (calls 2008, 2013, 2018, and 2024). He has organized several international events related to metamaterials, chipless-RFID, and sensors, including Workshops at the IEEE International Microwave Symposium (2005 and 2007), European Microwave Conference (2009, 2015, 2017, 2018, and 2024), and Fifth International Congress on Advanced Electromagnetic Materials in Microwaves and Optics (Metamaterials 2011), where he acted as the Chair of the local organizing committee. He is a Reviewer of IEEE TRANSACTIONS ON MICROWAVE THEORY AND TECHNIQUES and IEEE MICROWAVE AND WIRELESS COMPONENTS LETTERS, among many other journals. He serves as an Editorial Board Member for IEEE Transactions on Microwave Theory AND TECHNIQUES, IET Microwaves, Antennas and Propagation, and Sensors. He has acted as a guest editor for seven special issues on metamaterials and sensors in various international journals.

• • •